

Surface Discharge of Cooling Water Effects of Distortion in Model Investigations

by

Steffen Häggström

AKADEMISK AVHANDLING,

som för avläggande av teknisk doktorsexamen
vid Chalmers tekniska högskola kommer att försvaras
offentligt den 10 november 1978 kl. 10.15 i Palmstedtsalen,
CTH, Sven Hultins gata 2, Göteborg.

Fakultetsopponent: Tekn.dr. Peter Larsen

Examinator: Professor Anders Sjöberg

SURFACE DISCHARGE OF COOLING WATER EFFECTS OF DISTORTION IN MODEL INVESTIGATIONS

Steffen H. Häggström, Department of Hydraulics,
Chalmers University of Technology, Fack, 402 20 Göteborg, Sweden

ABSTRACT

The investigation deals with the scaling effects that arise when the spread of cooling water is studied in a physical model with different horizontal and vertical length scale ratios. The investigation is limited to surface discharges under stationary conditions. Froude and Reynolds modelling practice is presumed.

Different physical processes of importance are studied and the effects of distortion are evaluated. The analyses show that two-dimensional jet diffusion, buoyancy spread, and convective heat transport can, under certain conditions, be accurately reproduced in a distorted model. A three-dimensional nonbuoyant jet will, however, have a centre-line excess temperature that is too great by a factor of $(\lambda_v/\lambda_h)^{1/2}$. (λ_v , λ_h being vertical and horizontal length scale ratios, respectively). For correct modelling of ambient diffusion special calibration is necessary.

Analytical solutions to the spread of a buoyant surface jet indicate that the centre-line excess temperature will be too great by a factor of $(\lambda_v/\lambda_h)^{1/3}$. Calculations using the Prych numerical model give similar results for discharges with high outlet densimetric Froude numbers but show also that a good agreement between model and prototype is achieved for discharges with a low densimetric Froude number. Analyses of laboratory experiments confirm these theoretical results.

For a distortion of eight, the areas within isotherms can be as much as 4-6 times too great. If the receiving body of water is shallow, then a better agreement between the model and the prototype can be achieved.

Model-prototype comparisons show that a good agreement between the model and the prototype often demands the model to be calibrated for ambient diffusion.

Key words: Cooling water, warm-water discharges, distortion, physical models, effects of distortion, jet diffusion, ambient diffusion.



Institutionen för vattenbyggnad
Chalmers Tekniska Högskola

Department of Hydraulics
Chalmers University of Technology

Surface Discharge of Cooling Water Effects of Distortion in Model Investigations

Steffen Häggström

Report
Series A:3
ISSN 0348-1050

Göteborg 1978

Address:	Institutionen för vattenbyggnad Chalmers Tekniska Högskola Fack S-402 20 Göteborg 5, Sweden
Telephone:	031/81 01 00

PREFACE

The purpose of this work has been to present results and ideas useful for designing as well as evaluating physical model investigations of the spread of cooling water from thermal power plants. Modelling of surface warm-water discharges is very complex, and a wide variety of physical processes have to be considered. Some of these processes have been treated rather from an engineering point of view than in a scientific way so that practicable results could be obtained with reasonable efforts.

The work was initiated by an investigation of cooling-water discharge from the Oskarshamn Nuclear Power Plant that was performed at the Department of Hydraulics, Chalmers University of Technology, by the late Professor Lennart Rahm and myself (Rahm and Häggström 1976). The physics of modelling warm-water discharges was not well known. Therefore, considerable effort was spent on transforming the results of the model investigation into prototype conditions. This part of the study was partly supported by the National Swedish Institute for Building Research (Häggström 1973).

Since then I have performed a more thorough study of the problems of distorted models, which gives more general information than was obtained in the first studies.

My present adviser, Professor Anders Sjöberg, gave valuable comments and encouragement during the late part of my work. Mrs. Göta Bengtsson and Mrs. Ann-Marie Holmdahl patiently typed my manuscripts during a period of several years, however, not continuously. Mrs. Alicja Janiszewska drew the figures and Mrs. Gerd Eng corrected the language. To those and to all others involved in my work I am very grateful.

SUMMARY

The present investigation deals with the scaling effects that arise when the spread of cooling water is studied in a distorted physical model, i.e. in a model with different horizontal and vertical length scales. The investigation is limited to surface discharges under stationary conditions. Common practice of modelling according to the Froude and Reynolds modelling laws is assumed.

The effects of distortion on the spread of warm water in a physical model are evaluated by means of the method of inspectional analysis based on the equations describing the studied phenomena in the model and the prototype, respectively. A comparison of the obtained expressions for the variables then gives the effects of the scaling.

In Chapter 2 different physical processes are studied and effects of distortion evaluated. The aim of this chapter is mainly to improve the understanding of the physical modelling of these processes. The analyses show that two-dimensional jet diffusion, buoyancy spread and convective transport in principle can be correctly modelled with independent vertical and horizontal length scales, that is in a distorted model. Three-dimensional jet diffusion will, however, give centre-line excess temperatures that are $\lambda_v^{1/2} \cdot \lambda_h^{-1/2}$ too great in a distorted model (λ_v and λ_h are vertical and horizontal length scales, respectively). Special calibration is necessary for correct modelling of ambient diffusion.

In Chapter 3 analytical solutions to warm-water discharges in a deep stagnant ambient body of water with no ambient diffusion are studied. The effects of distortion are evaluated using these solutions and the most reliable one give centre-line excess temperatures that are too great by a factor of $\lambda_v^{1/3} \cdot \lambda_h^{-1/3}$.

In Chapter 4 the PSD and the Prych models are used for calculation of the effects of distortion on warm-water spread in a deep receiving body of water. The results show that the discharges with a high densimetric Froude number are more affected by distortion than those with a low one and also that the outlet shape is an important parameter, giving the best agreement between model and prototype at large width to height ratios of the outlet.

In Chapters 5 and 6 laboratory experiments and model-prototype comparisons are employed for the estimation of scale effects. The laboratory experiments where no ambient diffusion was present show that the effects of distortion are negligible for discharges with low outlet densimetric Froude numbers ($F_{\Delta} \approx 1.4$) and that the effects as evaluated by Engelund's moderate Richardson number theory were of the right order for discharges with high outlet densimetric Froude numbers ($F_{\Delta} \geq 6$). The model-prototype comparisons show that special attention should be paid to the reproduction of ambient diffusion.

Effects of distortion will significantly affect the results of an investigation using a distorted model. For a distortion of eight the areas within isotherms can be as much as 4-6 times too great in a distorted model. With a shallow ambient body of water the modelling can be much better. The accuracy of physical models seems to be better than the accuracy of numerical models, but investigations using physical models should always be supplemented by numerical model calculations. An example of a transformation of model data into prototype conditions is given in Chapter 7.

LIST OF CONTENTS

Page

PREFACE	1
SUMMARY	3
LIST OF CONTENTS	5
1. COOLING WATER SPREAD	7
1.1 Background, purpose and limitations	7
1.2 Hydraulic features of warm water surface discharges	11
1.3 Mathematical models	15
1.4 Physical models	17
2. IMPORTANT PROCESSES. THEORY, REPRODUCIBILITY AND EFFECTS OF DISTORTION	23
2.1 Introduction	23
2.2 Three-dimensional jet diffusion	24
2.3 Two-dimensional jet diffusion	34
2.4 Vertical entrainment in stratified flow	40
2.5 Buoyancy spread	46
2.6 Convective heat transport by ambient flow	50
2.7 Horizontal ambient diffusion	59
2.8 Vertical ambient diffusion	69
2.9 Heat transfer to the atmosphere	72
3. EFFECTS OF DISTORTION EVALUATED BY MEANS OF ANALYTICAL SOLUTIONS OF SURFACE BUOYANT JET PROBLEMS	78
3.1 Introduction	78
3.2 Nonbuoyant surface discharge	80
3.3 Small Richardson number flow	82
3.4 Moderate Richardson number flow	86
3.5 Large Richardson number flow	90
3.6 Conclusions	91
4. EFFECTS OF DISTORTION CALCULATED BY MEANS OF NUMERICAL MODELS	93
4.1 Numerical models used in the calculation	93
4.2 The PSD model calculation	94
4.3 The Prych model calculation	101
4.4 Conclusions	107
5. EFFECTS OF DISTORTION DETERMINED BY MEANS OF LABORATORY EXPERIMENTS	110
5.1 Laboratory investigations of surface warm-water jets	110
5.2 Laboratory data for $F_{\Delta} \approx 1.4$	111
5.3 Laboratory data for $F_{\Delta} \approx 6$	112
5.4 Laboratory data for $F_{\Delta} \approx 10$	114
5.5 Laboratory data for $F_{\Delta} \approx 25$	116
5.6 Conclusions	117

6.	MODEL-PROTOTYPE COMPARISONS	119
6.1	Introduction	119
6.2	Model-prototype comparison for Berkeley Power Station	120
6.3	Model-prototype comparison for Ringsend and Pigeon House Power Stations, Dublin	123
6.4	Model-prototype comparison for Pacific Gas and Electric Company's Pittsburg Power Plant	126
6.5	Model-prototype comparison for Power Plant at the U.S. East Coast	128
6.6	Model-prototype comparison for Madison Gas and Electric Company Plant, Lake Monona	131
6.7	Model-prototype comparison for Ingå Power Plant	135
6.8	Model-prototype comparison for Oskarshamn Nuclear Power Plant, Sweden	135
7.	DISCUSSION OF RESULTS	141
7.1	Effects of distortion in summary	141
7.2	Recommendations for physical model investiga- tions	147
7.3	Further Research	151
	REFERENCES	153
	LIST OF FIGURES	161
	LIST OF TABLES	165
	LIST OF NOTATION	167

1. COOLING WATER SPREAD

1.1 Background, purpose and limitations of this study

The energy demand in the world has resulted in an average 10-year doubling time of the electricity consumption. At present, there is a trend towards a reduction of the increase in energy consumption in Sweden and other developed countries, but in spite of this, there will probably be a significant increase in the energy demand and consumption in the future, at least in the less advanced regions of the world.

A great deal of the energy used is electrical energy. This energy is mainly produced in water power plants and steam power plants. The latter can be nuclear power stations or stations fuelled by coal or oil. Steam power plants produce electric power and large amounts of cooling water at low temperature. The cooling water may be re-cycled after cooling in a cooling tower but is generally discharged into rivers, lakes, or coastal waters.

A fossil-fuelled plant has an electrical efficiency of about 40% which means that 60% of the input energy is discharged as waste heat. The corresponding figures for a nuclear power plant are approximately 33% and 67%, respectively. This means that 1.5 to 2 times more energy is discharged than is produced as electrical energy. Drastic changes of this situation are not expected during this century even if beneficial use of the cooling water is possible. By lowering the efficiency of the electric power generation, one can make the temperature of the cooling water high. This hot water can be used for heating buildings, but economic aspects limit this use.

Whether the waste heat is discharged into the atmosphere or into a receiving water body, environmental effects will occur. In this study, however, only discharge into water is considered.

Discharge of cooling water

The cooling water can be discharged into the water environment either by a single-port outlet or by a multi-port outlet also called a diffusor. The amount of cooling water is 40-50 m³/s with a temperature increase of 10°C for 1000 MW generated electric power. In

8.

principle, there are two ways of disposing of the warm water into a homogeneous water body:

By mixing of the warm water with the receiving water a large flow of water with low excess temperature is generated. A large surface area and water volume will have an increased temperature from which heat is transferred to the atmosphere which is the ultimate sink of the waste heat.

A gentle spread of the warm water as a surface layer reduces mixing. The surface layer will have a relatively high excess temperature, which makes the heat transfer to the atmosphere effective. The total area and volume influenced by increased temperature will be reduced, but it will at the same time have a significantly higher temperature.

Efficient mixing of the cooling water with the ambient water can be obtained by use of diffusors as has often been the case in the United States and also by single-port outlets in areas with good renewal of ambient water. To obtain an undisturbed surface layer of warm water, one must use a single-port outlet with very low discharge velocity. In this study only single-port outlets at the water surface will be considered.

Environmental effects

When designing an outlet for large amounts of cooling water, one must strive to keep the effects on the environment as small as possible with reasonable economic efforts. It is, however, very difficult to make an evaluation of environmental effects caused by the discharge of cooling water.

Data on reactions to increased temperatures are to some extent available for some species of fish and other animals as well as plants under more or less controlled conditions (Grimås 1974 and Nyman 1974). It is, however, much more difficult to foresee what will happen to a whole ecosystem, where there is a simultaneous competition from other species.

An evaluation of the environmental effects must be based on knowledge of the existing ecosystem, hydrological and physio-chemical

conditions of the receiving water body as well as a prediction of the spread and temperature distribution of the cooling water discharged into the receiving water body.

Mathematical and/or physical models can be used for predicting cooling-water spread from a single-port surface discharge. The models must be based on field investigations so the status is clear concerning currents, temperature, salinity, stratification, etc. of the receiving water body.

Mathematical models

An extensive evaluation of mathematical models for predicting cooling water spread has been done by Dunn et al. (1975). They have examined models of surface discharge of cooling water, and the computed temperature distributions have been compared with measurements of real discharges. The study shows an accuracy for the best models of five times too high or too low for an area having a given minimum excess temperature. In most mathematical models the ambient water is considered unlimited. If bottom or other boundaries influence the flow of warm water, the accuracy and the usefulness of the models are reduced. The poor agreement reported by Dunn et al. must to a great extent be caused by lack of coincidence between model assumptions and site conditions.

Advantages of mathematical models are that they are easy to handle and inexpensive to run. They give fast results and therefore allow an easy change of variables, e.g. outlet conditions.

Physical models

Physical models for prediction of cooling water spread from steam power plants have been used since the fifties. The investigations often employ two separate models. The spread of cooling water close to the outlet is normally studied in a physical model geometrically similar to the prototype. A so called distorted model, which is a physical model with different vertical and horizontal length scales, is used to study the spread of cooling water far from the outlet.

The reason for making a model distorted is that the conditions required for reproducing a current pattern in a model limit the choice of water depth in the model. The area that is covered by the warm-water spread is very large and for handling the model in a laboratory, the horizontal scale must be small, often 5-10 times smaller than the vertical scale. Another reason is that correct reproduction of heat transfer to the atmosphere requires a distorted model.

Physical models are more expensive and take longer time to run than mathematical models. The distortion of a physical model does also affect the results of an investigation. The most obvious advantages of the physical models compared with mathematical models are that the influence of topography on the spread of warm water is better simulated and that non-specialists feel more confident in results from physical models.

Purpose of this study

As already mentioned, the distortion of a physical model will affect the results of an investigation. This is a well-known fact, but very little has been done to evaluate in what way and how much it affects the results. It is therefore very difficult to estimate the accuracy of results from a distorted physical model.

The main purpose of this investigation is to evaluate effects of distortion in physical model tests of surface discharges of warm water. Such an evaluation will make it possible to estimate the accuracy of a proposed physical model so that one can determine if a mathematical or a physical model is the best way of predicting warm-water spread. It will also be possible to make a rough transformation of results of model investigations into prototype conditions. Thus the value of tests in physical models is increased. Hopefully the results and discussions presented here can also be used as an aid when designing new laboratory investigations.

Since the problem is very complex, this study is mainly limited to physical modelling of surface warm-water discharges under stationary conditions, where the receiving water body is homogeneous. However, the results can to some extent also be applied to surface discharges in tidal areas as well as to discharges through diffusors.

No consideration has been given to the special case where the ambient water has a temperature close to the freezing point and the discharged cooling water is first lighter and then when reaching the temperature of maximum density is heavier than the ambient water.

1.2 Hydraulic features of warm water surface discharges

The temperature of warm water discharged into a water body decreases as it flows from the outlet (see Figure 1.1). This is due to two different processes, mixing with the ambient water and heat transfer to the atmosphere. Mixing with the cold ambient water is the predominating process near the outlet but is usually important also far from the outlet. Heat transfer to the atmosphere is the process by which all heat discharged must leave the receiving body of water. For heat transfer to be of any importance compared with mixing, large areas must be available, and this can only be the case far from the outlet.

Close to a warm-water outlet the mixing is to a great extent due to jet diffusion, which is very much influenced by outlet conditions such as flow velocity, buoyancy, outlet dimensions, and bottom topography but also to the conditions in the receiving body of water such as currents and density stratification.

Jet diffusion reduces the temperature very fast if there is water available for the dilution of the warm water, which makes the bottom topography important for the process. The buoyancy decreases the vertical jet entrainment and makes thus the process less efficient. This effect is pronounced when the velocity is low and the buoyancy high, which is expressed by the densimetric Froude number for the outlet,

$$F_{\Delta} = u_o / \left(g H_o \frac{\Delta \rho_o}{\rho} \right)^{1/2}, \quad (1.1)$$

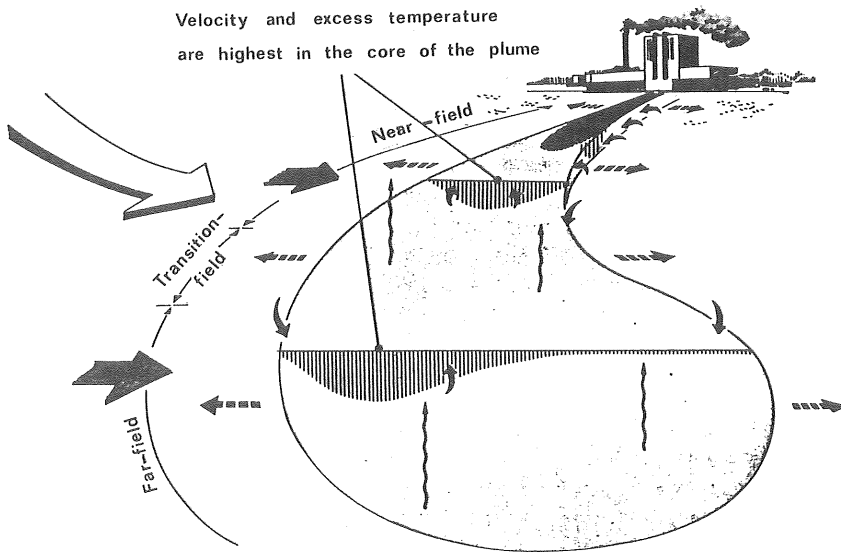
where u_o = discharge velocity,

g = gravitational acceleration

H_o = water depth of outlet (rectangular surface outlet),

$\Delta \rho_o$ = the density deficiency of the discharged water compared with the ambient water density

ρ = ambient water density








-  Radiation, evaporation, and heat conduction leading to heat transfer to the atmosphere and space.
-  The density deficit of the cooling water gives rise to gravitational flow, i.e. the cooling water flows out at the surface of the ambient water.
-  The ambient current bends the cooling water plume.
-  The wind deforms the cooling water plume and influences its direction.
-  Mixing with ambient water through the sides and from underneath decreases the temperature of the discharged cooling water.

Figure 1.1 Surface discharge of cooling water.
Adapted from Ehlin (1974).

For high values of F_{Δ} the jet diffusion is very important while buoyancy effects are negligible and for low F_{Δ} the jet diffusion is almost negligible. The buoyancy also gives rise to a lateral spread of the warm water flow, leading to a much larger lateral than vertical extension, which is shown in Figure 1.2 (Hayashi and Shuto, 1967).

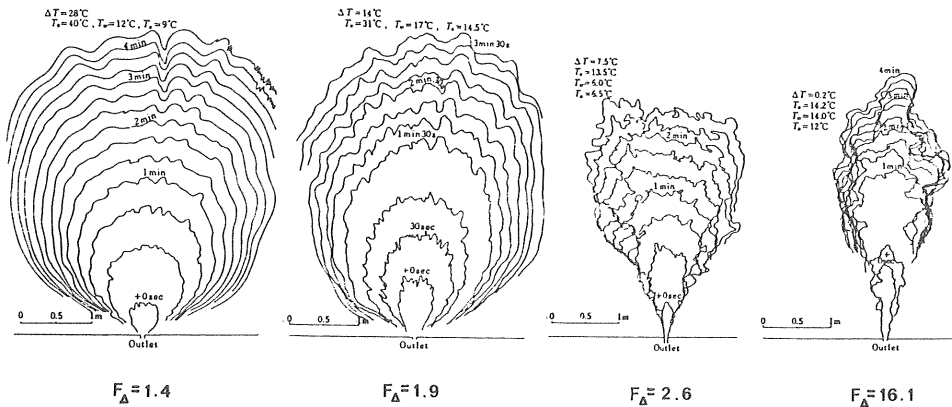


Figure 1.2 Spreading pattern of warm water discharge. The lines shown are dye patterns at different times after marking the flow at the outlet. The flow and outlet are the same, and the densimetric Froude number is changed by different heating, and thus different buoyancy is received. From Hayashi and Shuto (1967).

The dilution of the warm water decreases the velocity and the excess temperature. The magnitude and direction of the warm water current will successively approach that of the ambient current. As the velocity of the warm water flow decreases to the same order as that of the ambient current, the diffusive properties of the ambient water are becoming more important, while the jet diffusion effect will be less. The temperature decrease is much slower here than close to the outlet. Of course, the bottom topography is very important and can often reduce the mixing by ambient turbulence if the depth is shallow.

The increased temperature in the receiving water caused by a warm-water discharge leads to an increase of the heat transfer to the atmosphere. The excess heat transfer per square unit is approximately linearly dependent on the excess temperature. Close to an outlet, the areas with excess temperature normally are not large enough to give a noticeable temperature decrease. Further away, where buoyancy spread and diffusion have led to large areas with excess temperature and the mixing processes are slow, the heat transfer to the atmosphere is significant.

Many scientists divide the temperature-decreasing course into two or more zones. Ehlin (1974) like others described a near-field, where jet diffusion is most important; a far-field, where the turbulent diffusion of the ambient water gives the intensity of mixing; and a transition-field, where both processes are of importance. The main problem is, however, not to divide the warm water flow into several regions but to understand the different processes that decrease the temperature, their interaction, and the possibilities to control them as outlined above.

The most important processes affecting surface discharges of warm water are listed in the order they are treated in Chapter 2.

- Three-dimensional jet diffusion
- Two-dimensional jet diffusion
- Vertical entrainment in stratified flow
- Buoyancy spread
- Convective heat transport by ambient currents
- Horizontal ambient diffusion
- Vertical ambient diffusion
- Heat transfer to the atmosphere

There are phenomena not included separately here that also affect the warm-water spread and the temperature distribution. Thus the wind affects ambient currents as well as heat transfer to the atmosphere. These effects are, however, presumed to be included when representative data for currents and heat transfer are chosen. The natural stratification of the ambient water and the bottom configuration also affect the currents and diffusion of the ambient water. This is, however, to some extent treated in the discussion of the different processes in Chapter 2.

As mentioned earlier, it is possible to control some processes by the choice of outlet structures. Thus, the outlet velocity and density deficit affect the jet diffusion and buoyancy spread of the near-field as shown in Figure 1.2.

The processes of the far-field such as ambient turbulent diffusion, convection and heat transfer to the atmosphere can not be controlled. However, the resulting effects of the processes are, of course, highly influenced by the conditions when the warm-water flow enters the far-field.

1.3 Mathematical models

Theories earlier applied to submerged jets were first used to develop prediction models for warm-water surface discharges in the late sixties. The entrainment principle and Gaussian temperature and velocity profiles were applied to the warm-water flow. Hoopes et al. (1968) suggested that the warm-water flow is entirely two-dimensional with Gaussian temperature and velocity profile in the horizontal plane. Furthermore, they assumed that the warm-water layer has a constant thickness and is vertically homogeneous. The warm-water flow is deflected by entrained momentum from the ambient flow, and the temperature decrease is caused by mixing with entrained ambient fluid and heat loss to the atmosphere.

Motz and Benedict (1970) developed a model based on that of Hoopes et al. but with a modification concerning entrainment, adding a form drag force on the warm water and excluding the heat loss to the atmosphere.

Stolzenbach and Harleman (1971) improved the model technique by adding vertical entrainment under influence of a density gradient according to experiments by Ellison and Turner (1959), and the buoyancy spread was included by a momentum equation leading to a variable thickness of the warm-water layer. Heat loss to the atmosphere was included as well. In this analysis the bottom effect could also be considered, and it was initially included, but this part did not work satisfactorily so it was later abandoned (Adams and Stolzenbach, 1975).

Prych (1972 a) presented a numerical model based on the analysis made by Stolzenbach and Harleman. In this model no bottom interference is taken into account but mixing due to diffusion of the ambient water is included by a technique suggested by Prych (1972 b). The model has been verified with prototype data by Weil (1974).

Shirazi and Davis (1974) further improved Prych's model mostly by testing the model with laboratory data, which gave new values of model constants but also by making some minor changes in the program. They also made extensive calculations with the improved model for a wide range of input parameters and presented the results in diagram form. This model, called the PSD model, is considered as

the best available model and capable of correctly predicting general plume characteristics according to Dunn et al. (1975). (The predictions show, roughly a factor-of-two accuracy in the centre-line distance to a given isotherm, a factor-of-two accuracy in the centre-line and a factor-of-five accuracy in isotherm areas.)

The Prych model and the diagram results from the PSD model are used in this work for evaluating effects of distortion (Chapter 4). Therefore, the main principles of Prych's model, and thereby also of the PSD model are presented in this chapter.

Other analytical works using the jet entrainment principle have been presented by Engelund and Pedersen (1973), Engelund (1976), Ottesen Hansen (1973 a) and Pande and Rajaratnam (1975 a) for warm water discharged at the surface of a deep quiescent water body. Ottesen Hansen (1973 b), Carter (1969), and Barry and Hoffman (1972) studied warm-water discharges in shallow waters. These analytical models neglect ambient diffusion and ambient currents and are thus of limited practical value. Some of them have, however, been used here for evaluation of distortion effects, (Chapter 3).

All the models presented here are mainly based on the jet entrainment theory and are thus applicable to the near-field where jet diffusion is important.

The Prych and the PSD models

In this investigation the Prych and the PSD models are used for calculating effects of distortion, and the basic principles of the two models will be given here. No equations will, however, be included in the presentation. For a thorough study the works by Prych (1972 a) and Weil (1974) are recommended for the Prych model, the report by Shirazi and Davis (1974) is recommended for the PSD model. A good presentation and an analysis of these and other numerical models are given by Dunn et al. (1975).

The discharged cooling water is analysed as a buoyant surface jet in a uniform, flowing ambient fluid. The ambient water body is assumed to be infinitely deep and of infinite horizontal extent. The temperature of the water in the jet decreases because of dilution with

the cooler ambient water and because of heat transfer to the atmosphere. Jet mixing and turbulence of the ambient fluid are the diluting processes. In the analysis the diluting processes are separated into the horizontal and vertical directions, with buoyancy affecting the vertical mixing. Lateral spread due to buoyancy, together with increased volume flux in the jet, spreads the jet flow in the lateral direction. Velocity and temperature distributions within the jet are approximated by similarity functions, and equations are written for the rates of change along the jet trajectory of integral quantities such as volume, heat, and momentum fluxes.

The governing equations are solved numerically for the scaling parameters in the similarity distributions. These parameters include the velocity and temperature along the jet trajectory and the thickness and width of the jet. The coordinates of the jet trajectory are also computed.

1.4 Physical models

Physical models have for a long time been used to study flow phenomena where mathematical models have been insufficient. This has especially been the case when irregular, man-made or natural, boundaries have strongly influenced the flow, e.g. warm-water surface discharges in the coastal zone.

As will be shown later, many of the physical models for study of warm-water discharges must be made geometrically distorted, i.e. with different vertical and horizontal scales. Although in this way the geometry is changed, such models can be very useful and can serve the following main purposes of physical models as described by Silberman and Stefan (1970).

1. Qualitative visualization of the behaviour of the prototype is readily obtained. Gross omissions in the design of the work and over-refinement of details become apparent in the model, where changes can be made at a small fraction of the cost of corresponding changes in the prototype.
2. Quantitative estimates of some of the flow quantities such as velocities, depths and pressures can be obtained for use in

designing the prototype. If these estimates are carried out simultaneously with the design process, the feedback between model and calculation can produce a near optimum design. (Not all parameters lend themselves equally well to quantitative evaluation in a model, however.)

3. Observation in the model leads to better understanding of the physical phenomena influencing the behaviour of the prototype.
4. Visualization in a model leads to better understanding of a proposed project by a layman.

A single model of a given engineering work may not serve all these purposes simultaneously. Sometimes two or more models are used to emphasize different aspects of a project and different purposes.

In modelling of surface warm-water discharges many different physical phenomena must be reproduced. Modelling of all these processes is impossible in a single model, since different scaling is required for reproducing different physical phenomena, as will be seen in Chapter 2. The modelling technique for warm-water discharges has earlier been treated by Ackers (1969), Silberman and Stefan (1970), Stolzenbach and Harleman (1971 b) and Abraham (1975). The two former publications treated the aspects of modelling jet diffusion, ambient flow, density stratification, and heat transfer to the atmosphere, while Stolzenbach and Harleman and Abraham also included ambient diffusion. These works are limited to deriving model scales for correctly reproducing different phenomena and do not treat what happens if these scales are not present, which is often the case.

Derivation of model scales

As described by Abraham (1975), there are two different ways of deriving scale relationships: dimensional and inspectional analysis.

Dimensional analysis is a formal method to organize the parameters which describe a given flow in dimensionless groups. It relates the number of parameters and the number of dimensions of these parameters to the required number of dimensionless groups. Similarity

between the hydraulic model and the prototype is obtained if all dimensionless groups have the same value in model and prototype.

Inspectional analysis takes the basic equations as a starting point and is the method used in this work and earlier by Cederwall (1968) and Stolzenbach and Harleman (1971 b). By introducing the scale factors into the basic equations, one finds how the different phenomena are scaled.

Since different physical processes are of different importance close to and far from a warm-water outlet, often more than one model have to be employed. Therefore, commonly an undistorted model is used to predict velocity and temperature distribution in the near-field, where the final design of outlet construction is made. The far-field temperature distribution is studied in a distorted model with, if possible, near-field data from the undistorted model as input.

The choice of model scales must be based on representative data of the ambient water, and therefore, thorough field investigations of temperature, currents, winds, etc. must be made.

The prototype area covered by a physical model must be based on the extension of the warm-water flow. Therefore, numerical tests with a suitable mathematical model are very valuable when designing physical models.

Near-field physical models

As described earlier, the jet diffusion, influenced by density stratification and bottom topography, is of major importance to the dilution and spread of the warm water. This is a typical three-dimensional flow problem and correct reproduction demands nondistorted modelling. This is usually done for submerged discharges, but for surface discharges the near-field is so wide that nondistorted modelling is in many cases almost impossible for economic and practical reasons.

When modelling the near-field, one should consider the feed-back from the far-field as well as the effects of the model boundaries. The main purposes of a near-field model are:

To design outlet structures so as to obtain a desired warm water flow pattern close to the outlet

To obtain input conditions of distorted far-field models

To find the near-field spread of a warm-water discharge.

Model tests of the near-field must be made under turbulent flow conditions with correct reproduction of free surface flow as well as stratified flow. Since bottom topography is important, geometric similarity is required.

The outlet flow as well as ambient flow must be turbulent, i.e. the effects of molecular viscosity must be negligible. This is the case if the Reynolds number is greater than a critical number according to conditions given in Chapter 2.

The velocities in a free surface flow problem are modelled according to the Froude model condition, which states that the Froude number, F , should be equal in model, index M, and prototype, index P

$$F_M = F_P \quad (1.2)$$

$$F = \frac{u}{\sqrt{gh}}, \quad (1.3)$$

where u = velocity

g = acceleration of gravity

h = water depth.

The density differences of a stratified flow are modelled so that the densimetric Froude number, F_Δ , is the same in model and prototype

$$F_{\Delta M} = F_{\Delta P} \quad (1.4)$$

$$F_\Delta = \frac{u}{\sqrt{gh \frac{\Delta \rho}{\rho}}}, \quad (1.5)$$

where $\Delta \rho$ = the density deficiency of the warm water compared with the ambient water density.

The combination of the Froude and the densimetric Froude laws gives directly that the relative density difference, $\Delta \rho / \rho$, should be

the same in model and prototype. The Froude law also states that the velocity scale is the square root of the vertical length scale. For turbulent flow in a model the velocity and the vertical extension of the flow must be large enough. This requirement limits the vertical length scale, and thus also the horizontal length scale, because a near-field model is made geometrically similar to the prototype.

Large warm water surface discharges, hundreds of m^3/s , can have a near-field zone of large horizontal extension. Therefore, it can be practically and economically difficult to model this whole area in an undistorted model. The boundaries of the model will heavily influence the flow and temperature patterns because of the limited laboratory space available. In spite of this, an undistorted model can give much information, even if it often is of more qualitative than quantitative character.

Far-field physical models

In the far-field bottom topography, ambient diffusion, ambient currents, density stratification, and heat transfer to the atmosphere highly influence the decrease of the warm-water temperature. Often the flow in this zone is of a two-dimensional character and can be reproduced in a distorted model. However, a far-field model must have a correct input, which means that the near-field must be modelled in an undistorted model or maybe in an analytical model.

The model rules applied to the near-field modelling also hold for the far-field. It is more important in a model that turbulent conditions exist than that geometrical similarity exists. Therefore, far-field models are made in a horizontal scale smaller than the vertical scale so that the horizontal extension of the model is small enough to be placed in a laboratory; the model is distorted. This distortion is justified by the fact that Froude and Reynolds types of modelling do not include horizontal length parameters and thus do not limit the choice of the horizontal scale. The modelling of diffusion phenomena has earlier been treated very little and will be discussed in detail in Chapter 2. The heat transfer to the atmosphere can be very important and can take away more than half of the heat

input of the discharge within the modelled area. This phenomenon can be reproduced only in a distorted model. The temperature and humidity of the air must also be well controlled. A detailed analysis of the different processes will be given in Chapter 2.

Advantages and limitations of physical models

Although distorted models in some ways are questionable, they can give much information, especially in combination with undistorted near-field models. In contrast to mathematical models, bottom topography, irregular ambient flow field, as well as nonstationary flow can be handled. The construction and operation of the models are expensive, since special heating and measuring equipment is often required. Extensive calibration of the models must also be made.

One aspect of the discharge design can be whether to have one single or several outlets. This aspect can, so far, only be studied in physical models, since existing mathematical models do not take into account the interaction between separated outlets.

As will be seen later, the physical models, especially the distorted ones, cannot in a correct way reproduce all participating physical processes. Nevertheless, quite valuable results can come out of the physical models, especially when the limitations of the models are considered in a proper way. Qualitative rather than accurate quantitative results are, however, to be expected.

More quantitative results can be obtained if numerical models are applied together with the physical model tests. By doing so one can estimate the scale effects caused by distortion. Very little has been presented in literature concerning the evaluation of model tests even if some model-prototype comparisons are given. In this work an attempt is made to determine the effects of distortion in physical model tests, where it is assumed that the common practice of modelling with the Froude and Reynolds scaling is applied.

2. IMPORTANT PROCESSES. THEORY, REPRODUCIBILITY, AND EFFECTS OF DISTORTION

2.1 Introduction

As has been shown earlier, the spread and temperature decrease of a warm-water surface discharge is very complicated, since several different physical processes are involved. Correct reproduction of these processes in hydraulic models requires that different scaling criteria are simultaneously satisfied. Mainly due to limited laboratory space, physical models of the overall spread of cooling water generally have to be distorted, that is designed with exaggerated depths. Such a distortion will affect the model results in various ways. For different outlet conditions the effects of distortion will be evaluated in later chapters by means of analytical and numerical models as well as laboratory and field investigations of warm-water surface discharges.

Before entering into these analyses we will discuss separately each basic process involved and its reproducibility in distorted models. This will be done by inspectional analysis. As pointed out earlier, it is assumed that the modelling is done according to Reynolds, Froude, and densimetric Froude modelling criteria as is common practice. In the analyses the following notation is used:

λ = geometric scale (model length/prototype length)
 h = index indicating horizontal property
 v = index indicating vertical property
 r = index indicating model to prototype ratio of parameter

If λ_h and λ_v are the geometric scales in the horizontal and vertical direction, respectively, Froude and densimetric Froude scaling (Equations (1.2) - (1.5)) then gives:

$$u_r = h_r^{1/2} = \lambda_v^{1/2} \quad (\text{horizontal velocity relation}), \quad (2.1)$$

$$\Delta\rho_r = 1 \quad (\text{density deficit relation}), \quad (2.2)$$

$$q_r = u_r \cdot \lambda_v \cdot \lambda_h = \lambda_v^{3/2} \cdot \lambda_h \quad (\text{volume flux relation}). \quad (2.3)$$

Each basic process will here be treated in the following way:

Theories and equations describing the process are presented.

Scaling criteria for correct reproduction are developed.

Effects of distortion are estimated.

The processes treated are:

Three-dimensional jet diffusion

Two-dimensional jet diffusion

Vertical entrainment in stratified flow

Buoyancy spread

Convective heat transport by ambient flow

Horizontal ambient diffusion

Vertical ambient diffusion

Heat transfer to the atmosphere

The effects of distortion presented here are given for each process separately. In practice, several processes will simultaneously be involved. Nevertheless, the results will be valuable in the following ways:

They give a better understanding of the problem.

They may be used to evaluate results of investigations in distorted models where only one or a few processes are of significance.

They may serve as design tools for physical models of warm-water discharges.

They form a basis for checking whether effects of distortion are reasonable when estimated by other methods in this work.

2.2 Three-dimensional jet diffusion

In cases where the outlet velocity of a cooling-water discharge is high and the water depth large the cooling-water flow will be similar to a three-dimensional jet.

Submerged nonbuoyant jet

Submerged nonbuoyant three-dimensional jets in stagnant infinite ambient fluid have been thoroughly studied, both theoretically and

experimentally. The basic theories and references can be found in Abramovich (1963). For the present study, however, the well-established equations describing gross behaviour of the jet are sufficient. The following equations are taken from Abraham (1963).

$$\frac{u_m}{u_o} = 6.2 \frac{D_o}{s} \quad (2.4)$$

$$\frac{u}{u_m} = e^{-77 \left(\frac{r}{s}\right)^2} \quad (2.5)$$

$$\frac{c_m}{c_o} = 5.6 \frac{D_o}{s} \quad (2.6)$$

$$\frac{c}{c_m} = e^{-0.7 \cdot 77 \left(\frac{r}{s}\right)^2} \quad (2.7)$$

$$\frac{q}{q_o} = 0.32 \frac{s}{D_o}, \quad (2.8)$$

where

- D_o = diameter of outlet
- s = coordinate along jet centre-line from outlet
- r = radial coordinate perpendicular to centre-line
- u_m = centre-line velocity
- u = local velocity
- u_o = outlet velocity
- c_m = centre-line concentration (of tracer or discharge itself)
- c = local concentration
- c_o = outlet concentration
- q = jet volume flux
- q_o = discharge volume flux

The above equations are valid outside the zone of flow establishment i.e. at a distance greater than $6.2 D_o$ from the outlet (Figure 2.1). The zone of flow establishment is not treated here because of its slight interest in over-all modelling of warm-water flow.

The decrease of velocity and concentration along the centre-line is rapid close to the outlet and slow further away as seen in Figure 2.2.

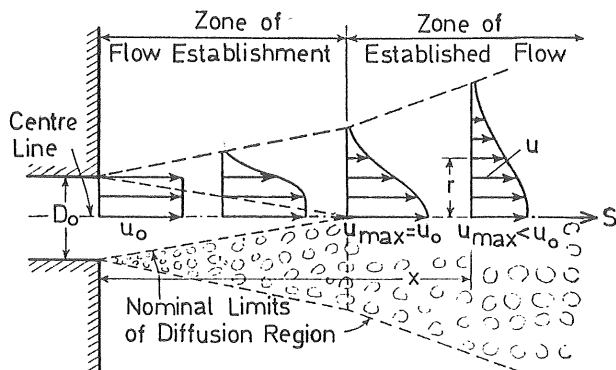


Figure 2.1 Definition sketch of three-dimensional jet.
The flow has a rotational symmetry.
After Albertson *et al.* (1950).

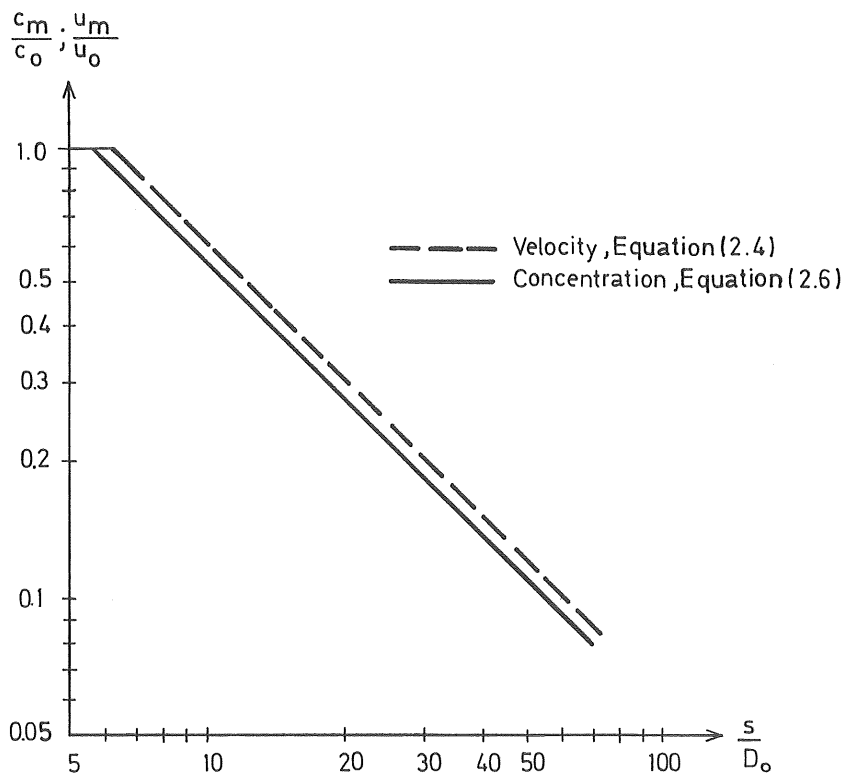


Figure 2.2 Velocity and concentration decay along centre-line of a three-dimensional jet.

The lateral distribution of the concentration, c , is given by Equation (2.7). In discussions of scale effects it is, however, more convenient to use the parameter A_{c/c_0} , defined as the area limited by a given isoconcentration line in a plane through the centre-line. By using Equations (2.6) and (2.7), one may develop the following expression for this area,

$$A_{c/c_0} = \frac{2}{D_0 \sqrt{0.7 \cdot 77}} \cdot \quad (2.9)$$

$$\cdot \int_0^{5.6 c_0/c} \sqrt{\ln \left(\frac{c_0}{c} \cdot 5.6 \right) - \ln \frac{s}{D_0}} \, d \left(\frac{s}{D_0} \right)$$

This equation has been solved numerically and is well approximated by the expression

$$\frac{A_{c/c_0}}{D_0^2} = 2.7 \left(\frac{c_0}{c} \right)^2 \quad (2.10)$$

Of course, this equation is not valid for values of c/c_0 close to 1.0, where the zone of flow establishment constitutes a great part of the area in question.

Jets with rectangular outlets

The presentation has so far been restricted to jets with circular outlets. Jets discharged through rectangular outlets are, however, of greater interest. As long as the width-to-height ratio does not differ too much from unity, the centre-line velocity decay is independent of outlet shape, which has been shown experimentally by Yevdjovich (1966) and theoretically by Stolzenbach and Harleman (1971 a).

Starting from the differential equations of continuity and momentum, Stolzenbach and Harleman developed the following equation for velocity decay far from a rectangular nonbuoyant submerged jet,

$$\frac{u_m}{u_o} = 7.2 \frac{\sqrt{H_o B_o}}{s}, \quad (2.11)$$

where

H_o = height of outlet

B_o = width of outlet.

This equation has been compared with the experimental data from Yevdjevich in Figure 2.3.

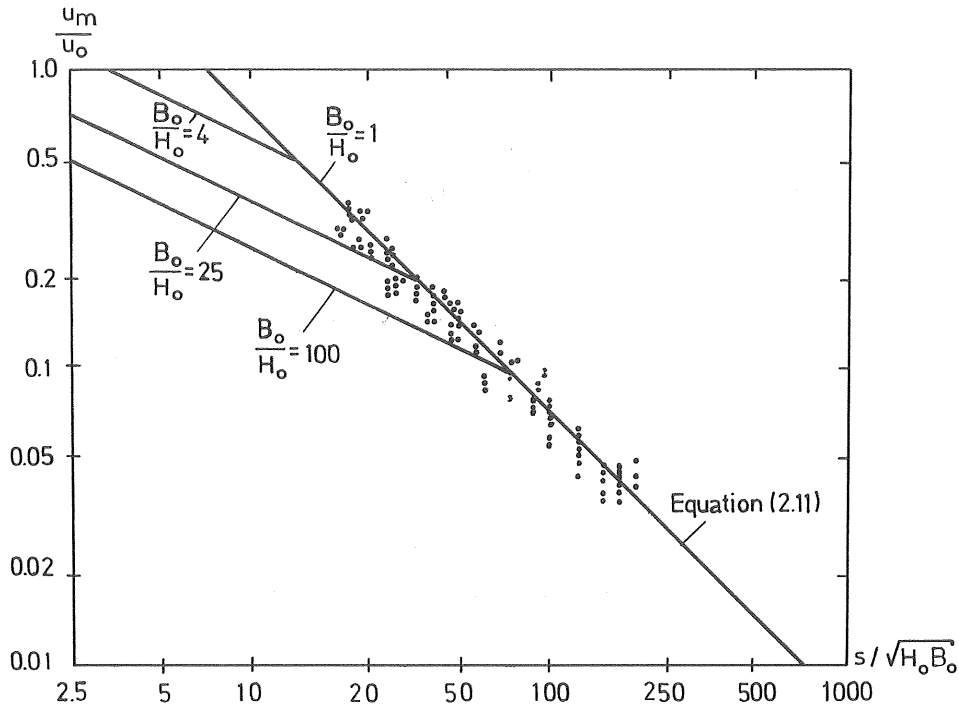


Figure 2.3 Centre-line velocity decrease for nonbuoyant jets with rectangular outlets, according to Stolzenbach and Harleman (1971a) with experimental data from Yevdjevich (1966), where $1.0 \leq B_o/H_o \leq 94$.

A simple way to develop almost the same equation as the one by Stolzenbach and Harleman is to replace the diameter in Equation (2.4) with an equivalent diameter, $D_{\text{equivalent}}$, giving the same circular area as the rectangular outlet area in question,

$$D_{\text{equivalent}} = 2 \sqrt{\frac{H_o B_o}{\pi}} \quad (2.12)$$

The centre-line velocity decay will then have the form

$$\frac{u_m}{u_o} = 7.0 \frac{\sqrt{H_o B_o}}{s} \quad (2.13)$$

In the analysis leading to Equations (2.11) and (2.13) different similarity profiles of velocity are assumed, which makes the constant differ. This slight difference is, however, of minor interest.

Since the centre-line velocity decay is insensitive to outlet shape, it seems reasonable to assume that this is also the case for the other parameters such as the centre-line concentration decay, volume flux, and lateral distribution of velocity and concentration. Replacing the diameter of Equations (2.6), (2.8), and (2.10) with expression (2.12) gives

$$\frac{c_m}{c_o} = 6.3 \frac{\sqrt{H_o B_o}}{s} \quad (2.14)$$

$$\frac{q}{q_o} = 0.28 \frac{s}{\sqrt{H_o B_o}} \quad (2.15)$$

$$\frac{A_c/c_o}{B_o^2} = 3.4 \left(\frac{c_o}{c}\right)^2 \cdot \frac{H_o}{B_o} \quad (2.16)$$

In Equation (2.16) the area, A_c/c_o , is divided by the outlet width, B_o , squared to make the equation dimensionless and well suited for inspectional analysis.

Surface nonbuoyant jets with rectangular outlets

The presented equations have so far little relevance to surface discharges. The equations can, however, easily be transformed to be valid for surface nonbuoyant jets. This is done by assuming an equivalent fictitious, discharge above the water surface and applying the equations for the combined discharge with the outlet dimensions $2H_o \cdot B_o$.

For a rectangular nonbuoyant surface discharge, the following equations are thus approximately valid,

$$\frac{u_m}{u_o} = 9.9 \frac{\sqrt{H_o B_o}}{s} \quad (2.17)$$

$$\frac{u}{u_m} = e^{-77 \left(\frac{r}{s}\right)^2} \quad (2.5)$$

$$\frac{c_m}{c_o} = 8.9 \frac{\sqrt{H_o B_o}}{s} \quad (2.18)$$

$$\frac{c}{c_m} = e^{-0.7 \cdot 77 \left(\frac{r}{s}\right)^2} \quad (2.7)$$

$$\frac{q}{q_o} = 0.2 \frac{s}{\sqrt{H_o B_o}} \quad (2.19)$$

$$\frac{A_{c/c_o}}{B_o^2} = 6.8 \left(\frac{c_o}{c}\right)^2 \cdot \frac{H_o}{B_o} \quad (2.20)$$

The equations given above are well suited for inspectional analysis. In their development, rough assumptions have been made, and the constants may be incorrect. This is, however, of no importance in this analysis as long as the relations between the different parameters and the outlet dimensions are correct in principle.

Reproducibility

Correct reproduction of a three-dimensional jet in a physical model requires that:

The flow is fully turbulent

Geometric similarity exists between the model and the prototype

The first condition has been studied by Pearce (1966) and Ungate (1974). Pearce found by visual observations that the jet obtained fully developed turbulence if

$$Re = \frac{u_o D_o}{\nu} > 3000 \quad (2.21)$$

Ungate measured the dilution of the jet and found that the gross behaviour of the jet was independent of Reynolds number if

$$\text{Re} > 1500 \quad (2.22)$$

These investigations were made for submerged jets with no boundary affecting the flow. Application of these criteria to warm-water discharges, where boundaries are affecting the flow, must be done carefully. Model tests of discharges from Forsmark Power Station (Swedish State Power Board, 1972) have shown that a small change in outflow direction can significantly change the whole flow pattern. If a jet flow in a model is not fully developed and therefore meandering, this can change the flow pattern in the same way as a change in the outflow direction. Therefore, physical models of warm-water discharges should be based on Equation (2.21).

The condition of geometric similarity means that the vertical and horizontal scales are identical. To illustrate this, we will use Equation (2.17). A transformation of this equation to model conditions gives with the vertical scale, λ_v , and the horizontal scale,

$$\lambda_h, \quad \left(\frac{u_m}{u_o} \right)_M = 9.6 \left(\frac{H_o B_o}{s} \right)_P \cdot \sqrt{\frac{\lambda_v}{\lambda_h}} \quad (2.23)$$

Thus, for equivalent points along the jet centre-line, the velocity decay is scaled according to

$$\left(\frac{u_m}{u_o} \right)_r = \lambda_v^{1/2} \cdot \lambda_h^{-1/2} \quad (2.24)$$

Of course, this expression has to be equal to unity for correct reproduction. This means that the geometric scaling has to fulfil the condition

$$\lambda_v \equiv \lambda_h \quad (2.25)$$

Effects of distortion

In a distorted model the depths and bottom slopes are exaggerated and thus $\lambda_v/\lambda_h > 1$. How such a distortion affects the reproduction of jet behaviour is treated here with the equations developed for a surface jet with rectangular outlet. As given above, the centre-

line velocity is scaled according to the relation

$$\left(\frac{u_m}{u_o}\right)_r = \lambda_v^{1/2} \cdot \lambda_h^{-1/2} \quad (\geq 1). \quad (2.24)$$

The velocity in a distorted model will be too great by a factor of $\lambda_v^{1/2} \cdot \lambda_h^{-1/2}$. By comparing Equations (2.17) and (2.18), we find that the same condition will hold for the centre-line concentration, which is thus too great by a factor of $\lambda_v^{1/2} \cdot \lambda_h^{-1/2}$.

The volume flux of a jet increases according to Equation (2.19), which will be scaled as

$$\left(\frac{q}{q_o}\right)_r = \lambda_h^{1/2} \cdot \lambda_v^{-1/2} \quad (\leq 1). \quad (2.25)$$

The jet volume flux in a distorted model will thus be too small and wrong by a factor of $\lambda_h^{1/2} \cdot \lambda_v^{-1/2}$.

For the dimensionless presentation of areas within isoconcentration lines, according to Equation (2.20), the following expression for the scaling will hold,

$$\left(\frac{A_{c/c_o}}{B_o^2}\right)_r = \lambda_v \cdot \lambda_h^{-1} \quad (\geq 1) \quad (2.26)$$

The area within a given isoconcentration line is in a distorted model too large by a factor of $\lambda_v \cdot \lambda_h^{-1}$.

The vertical penetration of the surface jet is studied by means of Equation (2.5), but Equation (2.7) could be used as well. Equation (2.5) can be written as

$$r = s \sqrt{\frac{\ln u_m/u}{77}} \quad (2.27)$$

The vertical penetration of the jet can be represented by the vertical distance, Z_p , from surface (centre-line) to a point having a velocity of a given fraction of the surface velocity, i. e. a given value of $\frac{u}{u_m}$. Defined in this way, the penetration is directly given by Equation (2.27). The equation is made dimensionless by being divided by the outlet height H_o , giving

$$\frac{Z_p}{H_o} = \frac{s}{H_o} \sqrt{\frac{\ln u_m/u}{77}} \quad (2.28)$$

In a distorted model this representation of the penetration gives the following scaling

$$\left(\frac{Z_p}{H_o}\right)_r = \lambda_h \cdot \lambda_v^{-1} \quad (\leq 1). \quad (2.29)$$

The vertical penetration is thus too small and wrong by a factor of $\lambda_h \cdot \lambda_v^{-1}$.

Summary

The jet characteristics are incorrectly reproduced in a distorted physical model. The theoretical effects of distortion are summarized in Table 2.1.

Table 2.1 Summary of effects of distortion on a nonbuoyant surface jet.

Parameter	Scaling factor	Comment
Centre-line velocity u_m/u_o	$\lambda_v^{1/2} \cdot \lambda_h^{-1/2}$	Too great
Centre-line concentration c_m/c_o	$\lambda_v^{1/2} \cdot \lambda_h^{-1/2}$	Too great
Volume flux q/q_o	$\lambda_h \cdot \lambda_v^{-1}$	Too small
Areas within given iso-concentration lines $A_c/c_o/B_o^2$	$\lambda_v \cdot \lambda_h^{-1}$	Too great
Vertical penetration Z_p/H_o	$\lambda_h \cdot \lambda_v^{-1}$	Too small

In the analysis it has been assumed that the jet characteristics have been studied far away from the outlet so as to avoid the zone of flow establishment. The main interest is thus concentrated on the overall spread of warm water. The temperature of the warm water can to some extent be considered a tracer and thus be evaluated as a concentration. This gives the deduction a more obvious connection

to warm-water surface discharges.

2.3 Two-dimensional jet diffusion

Two-dimensional jet diffusion can be an important diluting process for warm-water surface discharges. If the flow is limited by the water surface and a shallow bottom or a strong density interface, it can have the character of a two-dimensional jet.

Theory

The basic theories of the two-dimensional jet are found in Abramovich (1963). In this analysis, however, the well-established equations describing the gross features of a two-dimensional nonbuoyant jet in a stagnant ambient fluid are sufficient. The following equations are taken from Abraham (1963):

$$\frac{u_m}{u_o} = 2.37 \left(\frac{B_o}{s} \right)^{1/2} \quad (2.30)$$

$$\frac{u}{u_m} = e^{-50 (y/s)^2} \quad (2.31)$$

$$\frac{c_m}{c_o} = 2.06 \left(\frac{B_o}{s} \right)^{1/2} \quad (2.32)$$

$$\frac{c}{c_m} = e^{-50 \cdot \frac{1}{2} (y/s)^2} \quad (2.33)$$

$$\frac{q}{q_o} = 0.59 \left(\frac{s}{B_o} \right)^{1/2}, \quad (2.34)$$

where B_o = width of slot
 s = coordinate along jet centre-line
 y = coordinate perpendicular to centre-line
 u_m = centre-line velocity
 u = local velocity
 u_o = discharge velocity
 c_m = centre-line concentration
 c = local concentration
 c_o = discharge concentration

q = jet volume flux per unit height

q_0 = discharge volume flux per unit height

The flow is considered two-dimensional in the horizontal plane (ys-plane) with no changes in the vertical direction. (Figure 2.4).

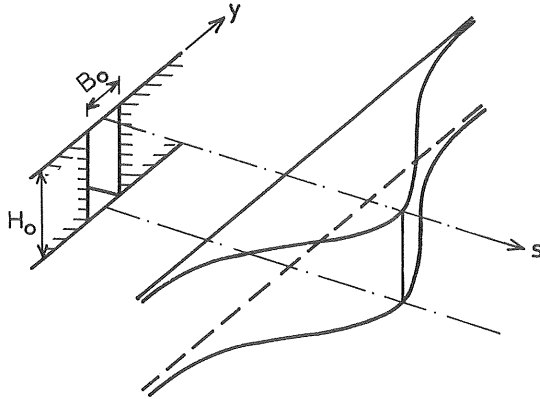


Figure 2.4 Velocity or concentration distribution of a two-dimensional jet.

The equations are valid at a distance greater than $5.6 B_0$ from outlet. Closer to the outlet there is a zone of flow establishment as for the three-dimensional jet. The velocity and concentration profiles are bell-shaped according to Equations (2.31) and (2.33). The centre-line velocity and concentration decay follow the inverse square root of the distance from the slot as seen from Equations (2.30) and (2.32). (Figure 2.5).

As for the three-dimensional jet, the area, A_{c/c_0} , limited by the isoconcentration line c/c_0 , has been formed. An approximate expression for this area has been obtained by numerical integration and has the form

$$\frac{A_{c/c_0}}{B_0^2} = 1.56 \left(\frac{c_0}{c} \right)^4 \quad (2.35)$$

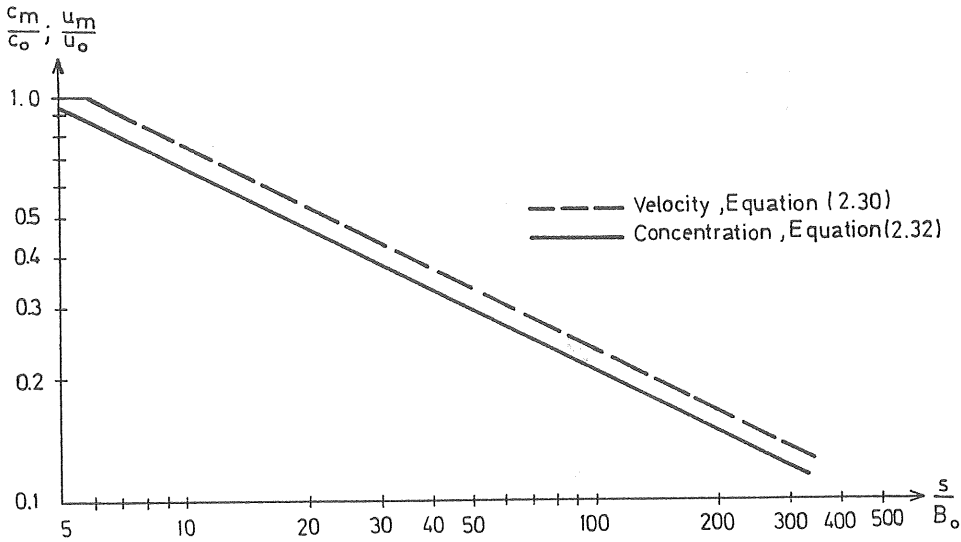


Figure 2.5 Velocity and concentration decay along centre-line of a two-dimensional jet.

Reattachment of two-dimensional jets

Influences of confined ambient fluid and ambient cross currents are more easily treated for two-dimensional jets than for three-dimensional jets and are therefore presented here.

The two-dimensional jet in an ambient fluid with an adjacent or an inclined wall has been studied by Borque and Newman (1960) and Sawyer (1963). The reattachment to an adjacent wall is shown in Figure 2.6. From Figure 2.7 it follows that the reattachment distance is a function of slot width and distance from slot to adjacent wall. The reattachment distance for a jet to an inclined wall is a function of angle and slot width.

Reattachment to a wall can also occur if there is a crossflow bending the jet as seen in Figure 2.8. Mikhail *et al.* (1975) have studied this problem and have shown the eddy height to be a function of the momentum flux ratio, (Figure 2.9).

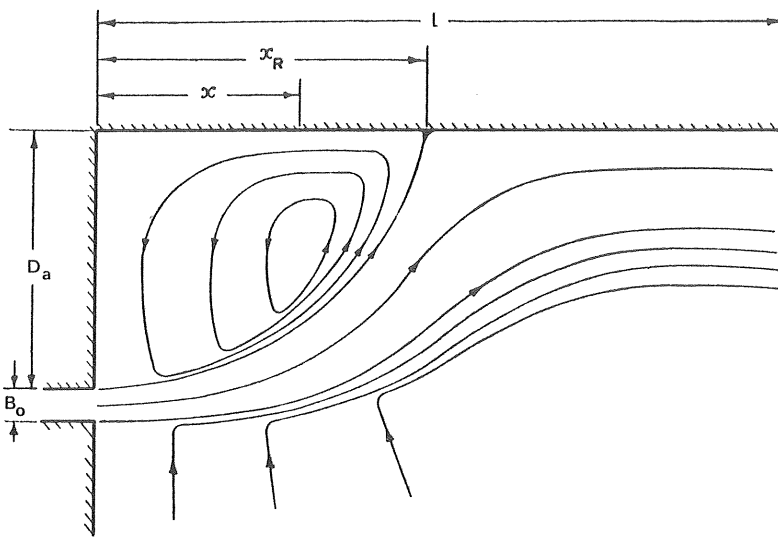


Figure 2.6 Definition sketch of reattachment of a two-dimensional jet to an adjacent wall, adapted from Borque and Newman (1960).

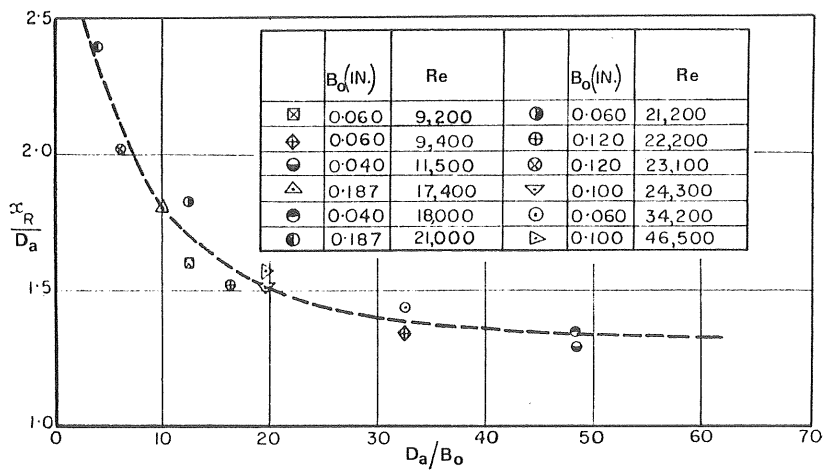


Figure 2.7 Reattachment distance for a two-dimensional jet reattaching to an adjacent wall, adapted from Borque and Newman (1960). Variables are defined by Figure 2.6.

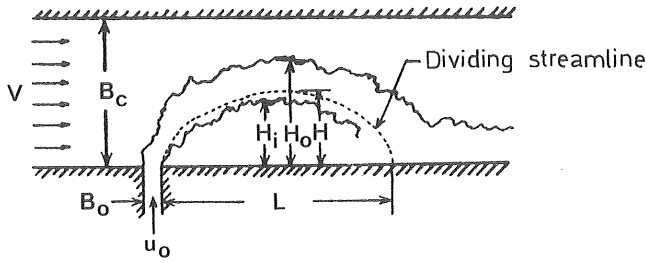


Figure 2.8 Definition sketch of reattachment of a two-dimensional jet caused by a crossflow, adapted from Mikhail *et al.* (1975).

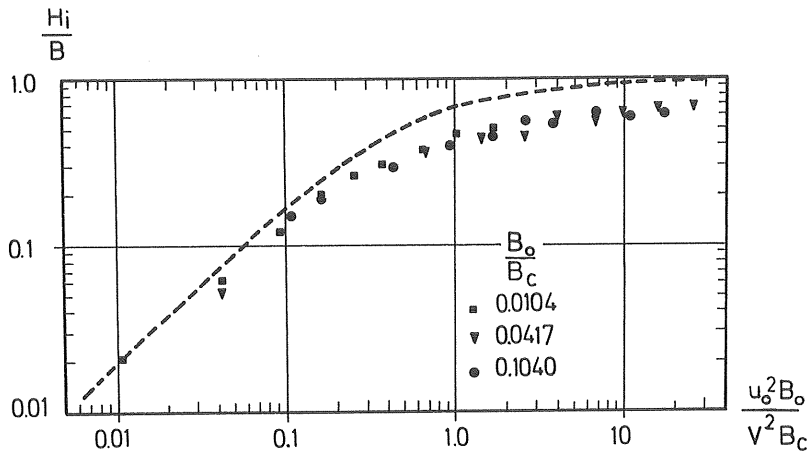


Figure 2.9 Eddy height as defined by Figure 2.8 for a two-dimensional jet in a crossflow, adapted from Mikhail *et al.* (1975).

Reproducibility

The two-dimensional jet can be reproduced in a physical model under the following conditions:

- The jet flow is fully turbulent
- Geometric similarity in the flow plane exists between prototype and model

As far as the author knows, there are no special investigations made concerning the critical Reynolds number for fully developed

turbulence in a two-dimensional jet. It is, however, reasonable to base the critical Reynolds number on the three-dimensional jet flow experiments. Thus, the following condition has to be fulfilled:

$$Re = \frac{u_o \cdot 4 R_h}{\nu} > 3000, \quad (2.36)$$

where R_h = hydraulic radius.

Equations (2.30) - (2.35) and Figures 2.7 and 2.9 show that the gross behaviour is the same in model and prototype as long as there is geometric similarity in the plane of flow between model and prototype. This is easily shown if one use Equation (2.30) as an example,

$$\frac{u_m}{u_o} = 2.37 \left(\frac{B_o}{s} \right)^{1/2} \quad (2.30)$$

Transformation to model scale is made by multiplying the length coordinates with the horizontal length scale giving the identical equation. Thus the velocity decays in a correct way in the model irrespective of the vertical length scale. Looking at Figure 2.7 and 2.9, one can see that all dimensionless parameters are identical for model and prototype conditions and thus give correct modelling.

Effects of distortion

The assumptions given earlier have been for a purely two-dimensional jet. A real warm-water discharge can, however, never be fully two-dimensional. But it can have a two-dimensional character if it is limited by the water surface and a shallow bottom. In such a flow the velocity will decrease towards the bottom because of the friction.

As long as the flow has the same two-dimensional character in model and prototype, it can be well reproduced in a distorted model. The distortion means, however, that all slopes are exaggerated. Therefore, there is a risk that the flow will separate from the bottom which would give the flow quite a different character in the distorted model than in the prototype (Figure 2.10).

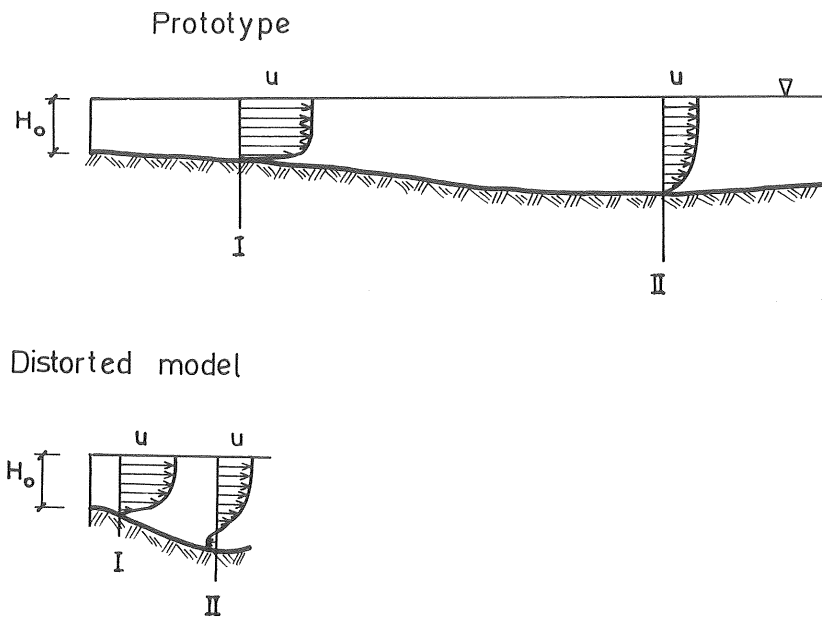


Figure 2.10 *The two-dimensional flow of the prototype can change character in a distorted model with exaggerated slopes.*

Reattachment to a wall is caused by low pressure between the jet and the wall. If the jet separates from the bottom, this low pressure will disappear, and the whole flow pattern becomes different. For the two-dimensional jet to be correctly reproduced, the bottom slopes of the model must be small enough to prevent separation of the jet flow. No rules of thumb can be given for this. It is, however, important to keep the bottom slopes of the model as small as possible.

2.4 Vertical entrainment in stratified flow

The increase of volume flux of turbulent jets is caused by inflow or entrainment of ambient water. For a warm-water surface jet the vertical entrainment of ambient water is affected by the density differences that reduce vertical entrainment. Even if there is a drastic reduction of entrainment because of density differences, the vertical entrainment is still important. The buoyancy of the surface flow leads to a much larger horizontal extension than verti-

cal extension of the flow, which makes the area available for vertical entrainment much larger than the area available for horizontal entrainment.

Theory

The vertical entrainment is here simplified to a two-dimensional flow in the vertical plane. The warm-water flow is limited by the water surface above and below by an infinite, denser fluid at rest (Figure 2.11).

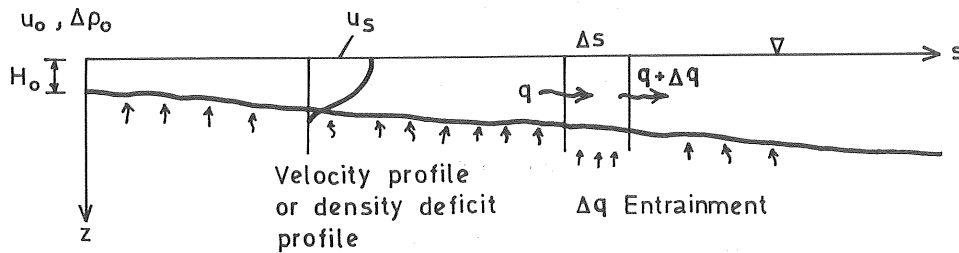


Figure 2.11 Definition sketch of vertical entrainment in stratified flow.

Under these conditions the entrainment is expressed in the following way:

$$\frac{dq}{ds} = \alpha \cdot u_s, \quad (2.37)$$

where

- q = volume flux per unit width
- s = length coordinate
- α = entrainment coefficient
- u_s = velocity at water surface

With a constant entrainment coefficient, Equation (2.37) is consistent with the equations for two-dimensional flow. Buoyancy, however, strongly influences the entrainment coefficient. The parameter normally used to describe this, is the gross Richardson number, Ri , giving the relation between buoyancy and inertia for-

ces.

$$Ri = \frac{g \frac{\Delta \rho}{\rho} \cdot h}{U^2}, \quad (2.38)$$

where h = height of upper layer

U = mean velocity of upper layer

$\Delta \rho$ = mean density deficit of upper layer

ρ = density of lower layer.

Ottesen Hansen (1975) has shown that the entrainment in a two-layered flow very much depends on how the turbulence is generated. The turbulence is generated at the interface between the upper and lower layer if the only external forces acting on the flow are due to pressure gradients. This case has been studied in the laboratory by Ellison and Turner (1959) for supercritical conditions of the upper flow and by Ottesen Hansen and Pedersen in Ottesen Hansen (1975) for subcritical conditions. (Supercritical, $F_{\Delta} > 1$, and subcritical, $F_{\Delta} < 1$, conditions in two-layered flow are analogous to the same terms of open channel flow, that is $F > 1$ and $F < 1$, respectively.)

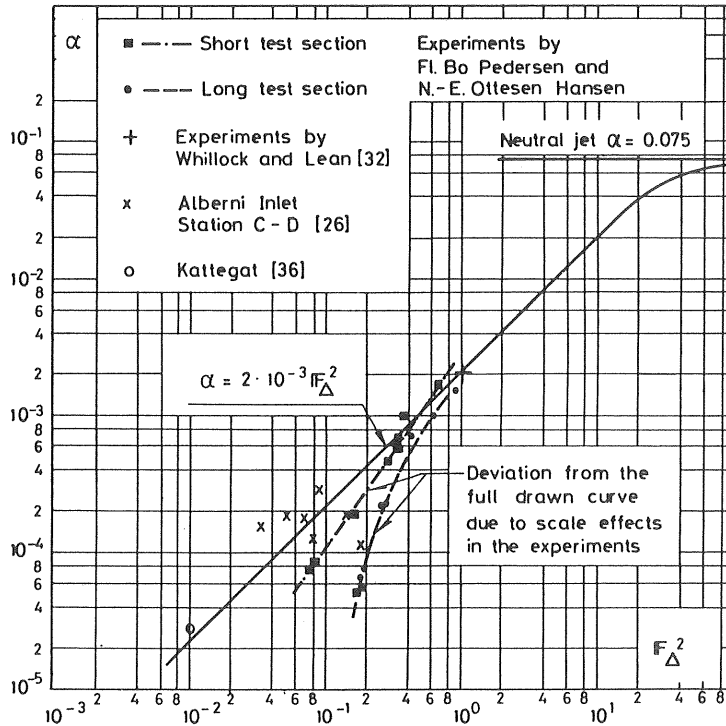


Figure 2.12 Entrainment coefficient as a function of $F_{\Delta}^2 = \frac{1}{Ri}$ from Ottesen Hansen (1975).

The experimental results by Ottesen Hansen and Pedersen are given in Figure 2.12. For high values of Ri , i.e. buoyancy being important, the following expression is given for the entrainment coefficient:

$$\alpha = 2 \cdot 10^{-3} Ri^{-1}. \quad (2.39)$$

The entrainment coefficient has a maximum value $\alpha = 0.075$ for nonbuoyant (neutral) conditions.

Reproducibility

As can be seen the entrainment coefficient is a function of the dimensionless parameter F_Δ (or Ri). The physical modelling is made so that the densimetric Froude number is equal in model and prototype and then also the Richardson number is equal. The entrainment coefficient will therefore be the same as long as the other parameters are correctly reproduced.

The main interest is, however, not the entrainment coefficient but the entrainment itself and how it is scaled in a physical model. The entrainment is given by Equation (2.37) and with the scales λ_h , λ_v and the scaling of entrainment coefficient $\alpha_r = 1.0$, the following expression for entrainment scaling is given

$$(dq)_r = \lambda_v^{1/2} \lambda_h. \quad (2.40)$$

According to Figure 2.11, the following condition must hold for correct scaling of volume flux per unit width,

$$\frac{q_M}{q_P} = \frac{q_M + \Delta q_M}{q_P + \Delta q_P} \quad (2.41)$$

This leads directly to the following condition for scaling of the entrainment,

$$(dq)_r = q_r. \quad (2.42)$$

The volume flux per unit width must be scaled as velocity times vertical distance giving the following scale condition for correct reproduction

$$(dq)_r = \lambda_v^{3/2} \quad (2.43)$$

Thus a correct reproduction of the vertical entrainment requires the horizontal and vertical scales to be equal.

Vertical entrainment in a distorted model

If all other parameters are assumed to be correctly scaled, the vertical entrainment in a distorted model will be wrong by a factor of $\lambda_h \cdot \lambda_v^{-1}$ according to Equations (2.40) and (2.43). Because the flow increase is incorrect, the velocities and the density deficit will be incorrect. The governing parameters for the entrainment will thus be changed and therefore also the entrainment. The problem is too complex to be solved generally, but two extremes can easily be calculated and these are:

Strongly stratified flow with an entrainment coefficient of practically zero.

Nonbuoyant flow with an entrainment coefficient equal to 0.075.

When the entrainment coefficient is equal to zero, there will be a constant flow, which will be correctly reproduced according to the scale laws used. It should be pointed out that this presumes the friction between the upper and lower layers to be negligible.

For the nonbuoyant case, where the entrainment coefficient is constant, the flow will be a two-dimensional jet in the vertical plane with the centre-line at the water surface. The volume flux can then be written as

$$\frac{q}{q_o} = 0.59 \sqrt{\frac{s}{2H_o}}, \quad (2.44)$$

where s = length coordinate

H_o = height of outlet

q = volume flux per unit width

q_o = outlet volume flux per unit width

According to this equation, the relative volume flux will be scaled as

$$\left(\frac{q}{q_0}\right)_r = \lambda_h^{1/2} \cdot \lambda_v^{-1/2} \quad (\leq 1) \quad (2.45)$$

Because of the dimensionless representation, Equation (2.40) should for correct reproduction be equal to unity. Far from the outlet, where Equation (2.44) is valid, the volume flux in a distorted model will be wrong by a factor of $\lambda_h^{1/2} \cdot \lambda_v^{-1/2}$. The entrainment is thus too small. The velocity and concentration at the water surface will be too small. The velocity and concentration at the water surface will be too great because of the reduced entrainment, while the vertical penetration, as for three-dimensional surface jets, will be too small. These effects can be deduced from the equations for velocity and concentration having the forms:

$$\frac{u_s}{u_0} = 2.37 \sqrt{2} \left(\frac{H_0}{s}\right)^{1/2}, \quad (2.46)$$

$$\frac{c_s}{c_0} = 2.06 \sqrt{2} \left(\frac{H_0}{s}\right)^{1/2}, \quad (2.47)$$

$$\frac{c}{c_s} = e^{-50 \cdot \frac{1}{2} \left(\frac{z}{s}\right)^2}. \quad (2.48)$$

If the same technique is used as before, these equations give the following effects of distortion:

Surface velocity is wrong by a factor of $\lambda_v^{1/2} \cdot \lambda_h^{-1/2} (\geq 1)$.

Surface concentration is wrong by a factor of $\lambda_v^{1/2} \cdot \lambda_h^{-1/2} (\geq 1)$.

Vertical penetration is wrong by a factor of $\lambda_h \cdot \lambda_v^{-1} (\leq 1)$.

It should be kept in mind that these calculations are made under the assumption of no density difference.

In the more realistic case, where density differences are present, there will be a better reproduction of vertical entrainment than the one given above. This can be seen from the Richardson number. With the assumption that depth, velocity, and concentration (the concentration is proportional to the density deficit) of the surface layer are scaled according to the given discussion, the scaling will have

the form

$$u_r = \lambda_v \cdot \lambda_h^{-1/2}, \quad (2.49)$$

$$\Delta\rho_r = \lambda_v^{1/2} \cdot \lambda_h^{-1/2}, \quad (2.50)$$

$$h_r = \lambda_h. \quad (2.51)$$

This leads to the following scaling of the Richardson number:

$$Ri_r = \lambda_h^{3/2} \cdot \lambda_v^{-3/2}. \quad (2.52)$$

This means that Ri will be too small, and thus the entrainment coefficient increases by the distortion. Because the vertical entrainment is too small in a distorted model, the increase of the entrainment makes the agreement between the distorted model and the prototype better when density differences are present.

Summary

The effects of distortion on vertical entrainment is given in Table 2.2.

Table 2.2 Summary of effects of distortion on vertical entrainment.

Parameter	Density effects dominating	Density effects negligible
Surface velocity	good agreement	$\lambda_v^{1/2} \lambda_h^{-1/2}$ (too great)
Surface concentration	good agreement	$\lambda_v^{1/2} \lambda_h^{-1/2}$ (too great)
Vertical penetration	good agreement	$\lambda_h \lambda_v^{-1}$ (too small)
Volume flux	good agreement	$\lambda_h \lambda_v^{-1/2}$ (too small)

2.5 Buoyancy spread

A warm-water surface jet spreads more laterally than vertically. This is mainly due to buoyancy spread. The importance of this pro-

cess depends on longitudinal velocity, density deficit, and geometric dimensions of the flow. The lateral extension can be 10-100 times larger than the vertical extension as found experimentally by Tamai *et al.* (1969) and Stefan and Schiebe (1970). The over-all spread of discharged warm water can thus significantly be affected by buoyancy spread.

Theory

The simplest case of buoyancy spread is when a buoyant homogeneous surface layer is spread unidirectionally over a quiescent fluid of large vertical extent (Figure 2.13).

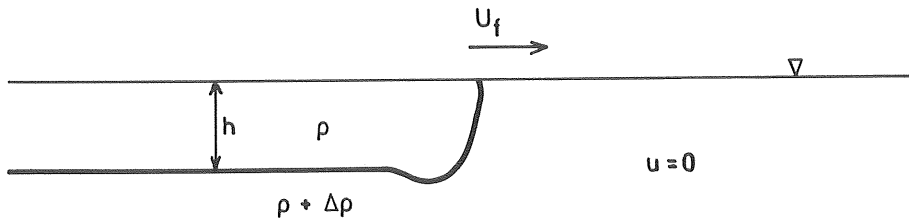


Figure 2.13 Definition sketch of unidirectional surface buoyant flow.

Excluding all shear stresses one can write the front velocity, U_f , as (Abbot 1961):

$$U_f = \left(g \cdot \frac{\Delta\rho}{\rho} \cdot h \right)^{1/2} \quad (2.53)$$

Larsen and Sørensen (1968) adopted this expression for calculating the spread of a buoyant surface layer passively transported by an ambient current. The increase in width was given by a vectorial addition of the ambient and the lateral (buoyant) velocities. A similar approach has been used in the numerical models by Prych (1972 a) and Odgaard (1975). Mean values have in these models been used for velocity, depth, and density deficit of the surface jet. Although the basic equation is written for a homogeneous layer, the applications seem reasonable.

Reproducibility

As seen from Equation (2.53), the scaling of buoyancy spread follows the basic scaling according to Froude densimetric scaling. However, viscosity must not influence the spread.

The influence of viscosity on buoyancy spread has been studied for lock exchange flow by Barr (1967) and Frazer et al. (1968). With the notation of Figure 2.14 the viscous effects can be estimated from Figure 2.15.

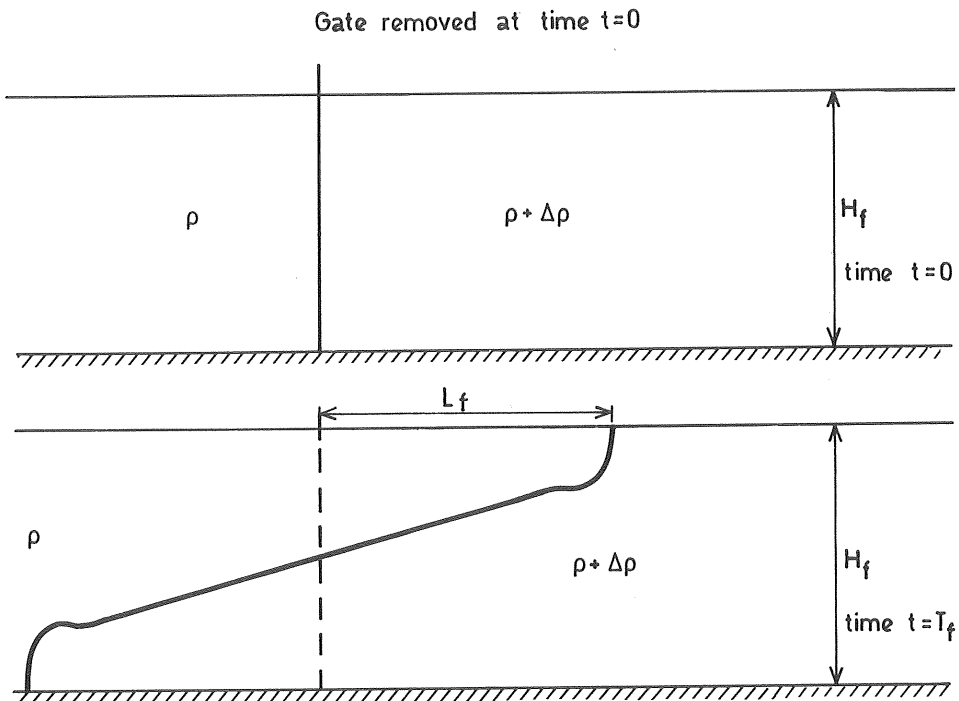


Figure 2.14 Definition sketch of lock exchange flow.

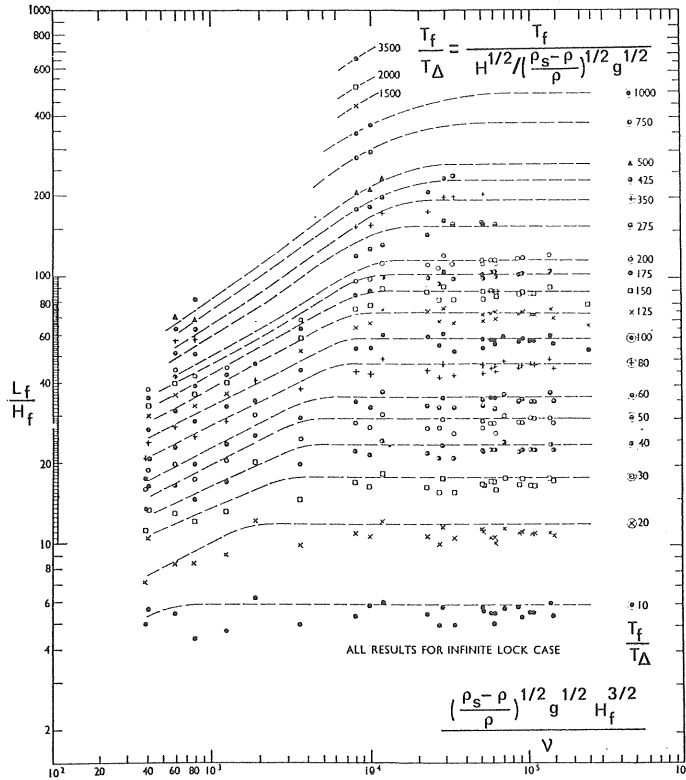


Figure 2.15 Spread of buoyant layer, with notation from Figure 2.14 after Frazer *et al.* (1968). The horizontal lines indicate a relationship $L_f/T_f = \text{constant} \cdot (H_f \cdot \frac{\rho_s - \rho}{\rho} \cdot g)^{1/2}$.

In the right hand part of the diagram the lines are horizontal, which means that the phenomenon is independent of viscosity. Here the mean velocity of the density front can be expressed as,

$$\frac{L_f}{T_f} = \text{constant} \cdot (g H_f \frac{\Delta \rho}{\rho})^{1/2}, \quad (2.54)$$

with the notation of Figure 2.14.

Ackers (1969) defined the zone where viscous effects are negligible by the expression

$$\frac{(g \cdot \frac{\Delta \rho}{\rho})^{1/2} \cdot H_f^{5/2}}{L_f \cdot v} > 150. \quad (2.55)$$

This expression should be satisfied in a physical model. Since it is derived for lock-exchange flow, it will be difficult to apply it to warm-water spread.

In summary:

Buoyancy spread can be modelled accurately in a distorted model.

Fully turbulent conditions must be present in model tests.

2.6 Convective heat transport by ambient flow

Warm water flowing into a moving ambient water body is diluted and receives successively the same velocity and direction of flow as the ambient water. This convective transport is of great importance for the temperature distribution of the far-field. Of course, convective transport of warm water is present also in the near-field, but it is included in the jet characteristics and therefore not treated separately.

The ambient currents must thus be properly reproduced in a model of the over-all spread of warm water. This is made by Froude modelling as will be seen later.

Theory

The spread of heat in a stationary ambient flow can be described by the equation of heat conservation (Ditmars 1971):

$$\begin{aligned} \frac{\partial H_t}{\partial t} + u \frac{\partial H_t}{\partial x} + v \frac{\partial H_t}{\partial y} + w \frac{\partial H_t}{\partial z} = \\ \frac{\partial}{\partial x} (K_x \frac{\partial H_t}{\partial x}) + \frac{\partial}{\partial y} (K_y \frac{\partial H_t}{\partial y}) + \frac{\partial}{\partial z} (K_z \frac{\partial H_t}{\partial z}), \end{aligned} \quad (2.56)$$

where H_t = heat content above some datum
 t = time coordinate
 x, y, z = Cartesian coordinates, z vertically upwards
 u, v, w = velocities in x, y , and z -directions, respectively
 K_x, K_y, K_z = eddy diffusion coefficients in x, y , and z -directions, respectively.

This equation can be transformed to express excess temperature. This is done by first writing a similar equation valid for ambient undisturbed conditions,

$$\frac{\partial H_a}{\partial t} + u \frac{\partial H_a}{\partial x} + v \frac{\partial H_a}{\partial y} + w \frac{\partial H_a}{\partial z} = \frac{\partial}{\partial x} (K_x \frac{\partial H_a}{\partial x}) + \frac{\partial}{\partial y} (K_y \frac{\partial H_a}{\partial y}) + \frac{\partial}{\partial z} (K_z \frac{\partial H_a}{\partial z}) \quad (2.57)$$

where H_a = heat content of undisturbed ambient fluid.

By subtracting this equation from (2.56), one obtains an equation expressing excess heat content, i.e. $H_t - H_a$ is given.

Within the small temperature ranges normally present, the excess heat can be expressed as a linear function of excess temperature:

$$H_t - H_a = \rho \cdot C_p \cdot T, \quad (2.58)$$

where C_p = specific heat of water
 T = excess temperature.

With ρ and C_p as constants an equation for excess heat content can be directly transformed to be valid for excess temperature,

$$\frac{\partial T}{\partial t} + u \frac{\partial T}{\partial x} + v \frac{\partial T}{\partial y} + w \frac{\partial T}{\partial z} = \frac{\partial}{\partial x} (K_x \frac{\partial T}{\partial x}) + \frac{\partial}{\partial y} (K_y \frac{\partial T}{\partial y}) + \frac{\partial}{\partial z} (K_z \frac{\partial T}{\partial z}) \quad (2.59)$$

The convective transport is governed by term two to four in this equation, while the terms to the right of the equal sign express diffusion.

It is obvious that the velocity field must be properly reproduced for the temperature spread to be modelled correctly. The basic governing equation for fluid movement is the Navier-Stokes equation. In a Cartesian coordinate system with the z-axis directed vertically upwards, it has the form (Daily and Harleman 1966),

$$\begin{aligned} \frac{\partial u}{\partial t} + u \frac{\partial u}{\partial x} + v \frac{\partial u}{\partial y} + w \frac{\partial u}{\partial z} = \\ = -\frac{1}{\rho} \frac{\partial p}{\partial x} + \frac{\eta}{\rho} \left(\frac{\partial^2 u}{\partial x^2} + \frac{\partial^2 u}{\partial y^2} + \frac{\partial^2 u}{\partial z^2} \right), \end{aligned} \quad (2.60 \text{ a})$$

$$\begin{aligned} \frac{\partial v}{\partial t} + u \frac{\partial v}{\partial x} + v \frac{\partial v}{\partial y} + w \frac{\partial v}{\partial z} = \\ = -\frac{1}{\rho} \frac{\partial p}{\partial y} + \frac{\eta}{\rho} \left(\frac{\partial^2 v}{\partial x^2} + \frac{\partial^2 v}{\partial y^2} + \frac{\partial^2 v}{\partial z^2} \right), \end{aligned} \quad (2.60 \text{ b})$$

$$\begin{aligned} \frac{\partial w}{\partial t} + u \frac{\partial w}{\partial x} + v \frac{\partial w}{\partial y} + w \frac{\partial w}{\partial z} = \\ = -g - \frac{1}{\rho} \frac{\partial p}{\partial z} + \frac{\eta}{\rho} \left(\frac{\partial^2 w}{\partial x^2} + \frac{\partial^2 w}{\partial y^2} + \frac{\partial^2 w}{\partial z^2} \right). \end{aligned} \quad (2.60 \text{ c})$$

where η = dynamic viscosity.

For free surface flow, where the pressure can be considered hydrostatic, the pressure terms can be expressed as,

$$\frac{\partial p}{\partial x} = \rho g \frac{\partial z_s}{\partial x}, \quad (2.61 \text{ a})$$

$$\frac{\partial p}{\partial y} = \rho g \frac{\partial z_s}{\partial y}, \quad (2.61 \text{ b})$$

$$\frac{\partial p}{\partial z} = -\rho g, \quad (2.61 \text{ c})$$

where z_s = elevation of the water surface.

The Navier-Stokes equation will then have the form,

$$\begin{aligned}
\frac{\partial u}{\partial t} + u \frac{\partial u}{\partial x} + v \frac{\partial u}{\partial y} + w \frac{\partial u}{\partial z} &= \\
&= -g \frac{\partial z_s}{\partial x} + \frac{\eta}{\rho} \left(\frac{\partial^2 u}{\partial x^2} + \frac{\partial^2 u}{\partial y^2} + \frac{\partial^2 u}{\partial z^2} \right),
\end{aligned}
\tag{2.62 a}$$

$$\begin{aligned}
\frac{\partial v}{\partial t} + u \frac{\partial v}{\partial x} + v \frac{\partial v}{\partial y} + w \frac{\partial v}{\partial z} &= \\
&= -g \frac{\partial z_s}{\partial y} + \frac{\eta}{\rho} \left(\frac{\partial^2 v}{\partial x^2} + \frac{\partial^2 v}{\partial y^2} + \frac{\partial^2 v}{\partial z^2} \right),
\end{aligned}
\tag{2.62 b}$$

$$\begin{aligned}
\frac{\partial w}{\partial t} + u \frac{\partial w}{\partial x} + v \frac{\partial w}{\partial y} + w \frac{\partial w}{\partial z} &= \\
&= \frac{\eta}{\rho} \left(\frac{\partial^2 w}{\partial x^2} + \frac{\partial^2 w}{\partial y^2} + \frac{\partial^2 w}{\partial z^2} \right).
\end{aligned}
\tag{2.62 c}$$

This equation has no general solution. For evaluating scaling criteria it is, however, very valuable.

Reproducibility

Froude and Reynolds scaling criteria are developed by making the Navier-Stokes equation dimensionless, and the following dimensionless parameters are used as in many textbooks:

$$\begin{aligned}
x_o &= \frac{x}{L} & y_o &= \frac{y}{L} & z_o &= \frac{z}{L} & z_{so} &= \frac{z_s}{L}, \\
u_o &= \frac{u}{U} & v_o &= \frac{v}{U} & w_o &= \frac{w}{U} & t_o &= \frac{t \cdot L}{U}
\end{aligned}
\tag{2.63}$$

where L = constant representative length
 U = constant representative velocity

With this notation Navier Stokes equation will have the form,

$$\begin{aligned}
\frac{\partial u_o}{\partial t_o} + u_o \frac{\partial u_o}{\partial x_o} + v_o \frac{\partial u_o}{\partial y_o} + w_o \frac{\partial u_o}{\partial z_o} &= \\
&= -\frac{gL}{U^2} \frac{\partial z_s}{\partial x_o} + \frac{\eta}{\rho LU} \left(\frac{\partial^2 u_o}{\partial x_o^2} + \frac{\partial^2 u_o}{\partial y_o^2} + \frac{\partial^2 u_o}{\partial z_o^2} \right),
\end{aligned}
\tag{2.64 a}$$

$$\begin{aligned}
\frac{\partial v_o}{\partial t_o} + u_o \frac{\partial v_o}{\partial x_o} + v_o \frac{\partial v_o}{\partial y_o} + w_o \frac{\partial v_o}{\partial z_o} = \\
= - \frac{gL}{U^2} \frac{\partial z_{so}}{\partial y_o} + \frac{\eta}{\rho LU} \left(\frac{\partial^2 v_o}{\partial x_o^2} + \frac{\partial^2 v_o}{\partial y_o^2} + \frac{\partial^2 v_o}{\partial z_o^2} \right),
\end{aligned} \tag{2.64 b}$$

$$\begin{aligned}
\frac{\partial w_o}{\partial t_o} + u_o \frac{\partial w_o}{\partial x_o} + v_o \frac{\partial w_o}{\partial y_o} + w_o \frac{\partial w_o}{\partial z_o} = \\
= \frac{\eta}{\rho LU} \left(\frac{\partial^2 w_o}{\partial x_o^2} + \frac{\partial^2 w_o}{\partial y_o^2} + \frac{\partial^2 w_o}{\partial z_o^2} \right).
\end{aligned} \tag{2.64 c}$$

For this equation to have the same solution for model conditions as well as prototype conditions the following well-known criteria must hold:

$$\left(\frac{gL}{U^2} \right)_M = \left(\frac{gL}{U^2} \right)_P \quad F_M = F_P \quad U_r = \lambda^{1/2} \tag{2.65}$$

$$\left(\frac{\eta}{\rho LU} \right)_M = \left(\frac{\eta}{\rho LU} \right)_P \quad Re_M = Re_P. \tag{2.66}$$

The last criterion is replaced by the normal criterion

$$Re_M > Re_{cr}, \tag{2.67}$$

Ackers (1969) gave the following value of the critical Reynolds number:

$$Re_{cr} \left(= \frac{\bar{U} \cdot 4 R_h}{\nu} \right) = 2400, \tag{2.68}$$

where \bar{U} = mean velocity of section

R_h = hydraulic radius (approximately equal to water depth).

As the equation is given here, the boundary condition of bottom geometry must be similar in model and thus the model must be undistorted. The boundary condition of bottom friction is also of interest. The head loss being approximately equal to friction loss can simply be described by the friction formula

$$S_f = f \cdot \frac{1}{4R_h} \frac{\overline{U}^2}{2g}, \quad (2.69)$$

where S_f = friction slope
 f = friction factor.

The friction slope must be the same in model as in prototype, which directly leads to

$$f_r = 1.0. \quad (2.70)$$

If the flow is a fully rough turbulent flow, the friction factor is a function of relative roughness alone, which gives the condition for modelling surface roughness:

$$k_r = \lambda_v \quad (2.71)$$

where k = equivalent sand roughness.

Effects of distortion

As before, the Navier-Stokes equation (2.62) is used for the analysis. Since the effect of distortion is sought, different representative parameters for velocity and length must be used in the vertical and horizontal directions. The parameters used for making the equation dimensionless are thus:

$$\begin{aligned} x_o &= \frac{x}{L} & y_o &= \frac{y}{L} & z_o &= \frac{z}{D} & z_{so} &= \frac{z_s}{D} \\ u_o &= \frac{u}{U} & v_o &= \frac{v}{U} & w_o &= \frac{w}{W} & t_o &= \frac{t \cdot U}{L}, \end{aligned} \quad (2.72)$$

where L = representative horizontal length
 D = representative vertical length
 U = representative horizontal velocity
 W = representative vertical velocity

The Navier-Stokes equation will then have the dimensionless form,

$$\begin{aligned}
\frac{\partial u_o}{\partial t_o} + u_o \frac{\partial u_o}{\partial x_o} + v_o \frac{\partial u_o}{\partial y_o} + \frac{W \cdot L}{U \cdot D} w_o \frac{\partial u_o}{\partial z_o} &= \\
= -\frac{gD}{U^2} \frac{\partial z_{so}}{\partial x_o} + \frac{\eta}{\rho \cdot U \cdot L} \left(\frac{\partial^2 u_o}{\partial x_o^2} + \frac{\partial^2 u_o}{\partial y_o^2} \right) + & \quad (2.73 \text{ a}) \\
+ \frac{\eta \cdot L}{\rho \cdot U \cdot D^2} \frac{\partial^2 u_o}{\partial z_o^2}, &
\end{aligned}$$

$$\begin{aligned}
\frac{\partial v_o}{\partial t_o} + u_o \frac{\partial v_o}{\partial x_o} + v_o \frac{\partial v_o}{\partial y_o} + \frac{W \cdot L}{U \cdot D} w_o \frac{\partial v_o}{\partial z_o} &= \\
= -\frac{gD}{U^2} \frac{\partial z_{so}}{\partial y_o} - \frac{\eta}{\rho \cdot U \cdot L} \left(\frac{\partial^2 v_o}{\partial x_o^2} + \frac{\partial^2 v_o}{\partial y_o^2} \right) + & \quad (2.73 \text{ b}) \\
+ \frac{\eta \cdot L}{\rho \cdot U \cdot D^2} \frac{\partial^2 v_o}{\partial z_o^2}, &
\end{aligned}$$

$$\begin{aligned}
\frac{\partial w_o}{\partial t_o} + u_o \frac{\partial w_o}{\partial x_o} + v_o \frac{\partial w_o}{\partial y_o} + \frac{W \cdot L}{U \cdot D} w_o \frac{\partial w_o}{\partial z_o} &= \\
= \frac{\eta}{\rho \cdot U \cdot L} \left(\frac{\partial^2 w_o}{\partial x_o^2} + \frac{\partial^2 w_o}{\partial y_o^2} \right) + \frac{\eta \cdot L}{\rho \cdot U \cdot D^2} \frac{\partial^2 w_o}{\partial z_o^2}. & \quad (2.73 \text{ c})
\end{aligned}$$

In the same way as before the Froude criterion is developed and also a slightly modified Reynolds criterion, however, being the same in principle:

$$\left(\frac{g \cdot D}{U^2} \right)_M = \left(\frac{gD}{U^2} \right)_P \quad F_M = F_P \quad U_r = \lambda_v^{1/2} \quad (2.74)$$

Horizontal velocities are thus scaled as the square root of vertical length scale. In addition to these criteria the following condition must hold,

$$\left(\frac{W \cdot L}{U \cdot D} \right)_M = \left(\frac{W \cdot L}{U \cdot D} \right)_P \quad (2.75)$$

With the given Froude modelling of horizontal velocities, the following modelling condition must hold for vertical velocities:

$$W_r = \lambda_v^{3/2} \cdot \lambda_h^{-1}. \quad (2.76)$$

Compared with horizontal velocities, the vertical velocities must be exaggerated by a factor equal to the distortion $\lambda_v \cdot \lambda_h^{-1}$.

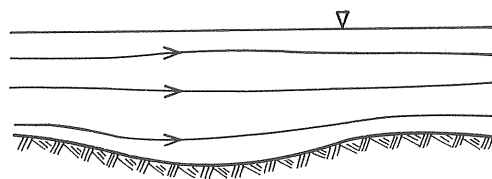
By studying the flow in a distorted model, one can find out if this condition is fulfilled. The following assumptions are made:

The main flow is horizontal and correctly reproduced.

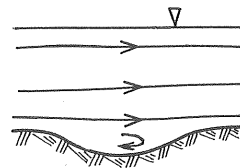
The vertical velocities are generated by the flow adapting to the bottom configuration.

If these assumptions hold, the vertical velocities will automatically be exaggerated in the same way as the bottom slope, that is by a factor of $\lambda_v \cdot \lambda_h^{-1}$.

The discussion above is based on oversimplified assumptions but shows that flow conditions can be properly reproduced in distorted models. This seems reasonable for the problems here, where the main velocities are horizontal. The exaggerated slopes can, however, give flow separation in a distorted model that is not present in an undistorted model or prototype (Figure 2.16).



Flow in undistorted model or prototype



Flow in distorted model

Figure 2.16 Flow separation can occur due to exaggerated slopes in distorted models.

Bottom friction is also important for the flow. The friction slope is again given by Equation (2.69):

$$S_f = f \cdot \frac{1}{4R_h} \cdot \frac{\bar{U}^2}{2g} \quad (2.69)$$

The energy slope of a distorted model must be exaggerated in the same way as the bottom slopes. The hydraulic radius, R_h , is assumed to be equal to or proportional to the water depth, i.e. a vertical length parameter. This leads to the following condition for the friction factor scaling,

$$f_r = S_{f_r} = \lambda_v \cdot \lambda_h^{-1} \quad (2.77)$$

The friction factor must thus be exaggerated in a distorted model compared with that of an undistorted model. The surface roughness must be increased, but there is no general way of doing it. In most cases the roughness of a distorted model is adjusted by trial and error until a good reproduction of the prototype flow field is generated.

The bottom surface that in prototype is mainly horizontal will be cause of distortion be more vertical in a distorted model. This change of geometry can significantly change the velocity distribution as shown in Figure 2.17 (Stolzenbach and Harleman 1971 b).

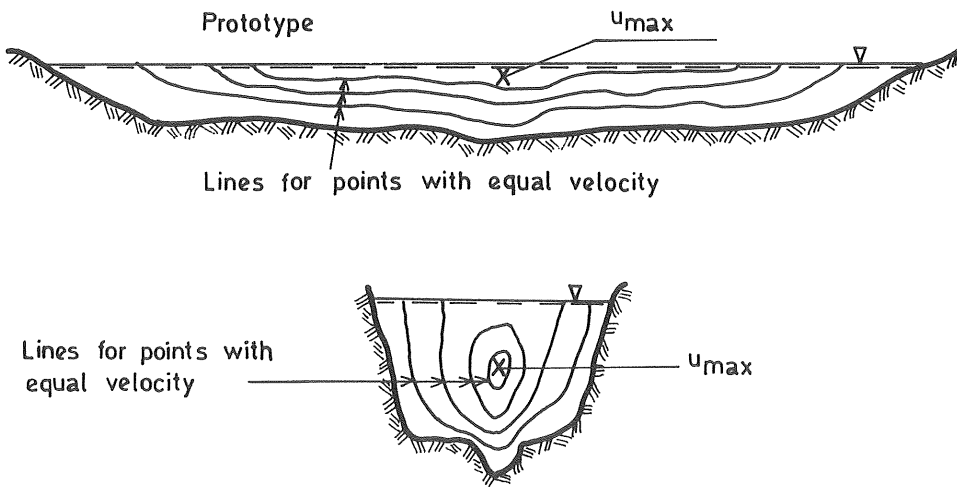


Figure 2.17 Velocity distribution in prototype and in a distorted model, after Stolzenbach and Harleman (1971b).

2.7 Horizontal ambient diffusion

In the far-field of a warm-water discharge, dilution of warm water is mainly due to ambient diffusion. In this chapter only horizontal diffusion will be discussed. The diffusion of a tracer (heat) passively transported by an ambient homogeneous current is treated, while effects of vertical diffusion and buoyancy spread are excluded.

The characteristics of diffusion are more or less unique to each receiving body of water. For open channels the diffusion is mainly caused by turbulence generated by bottom friction. The diffusion is then characterized by friction and water depth. In large lakes and open seas, however, the turbulence is to a great extent generated by energy input from the wind. This leads to quite another behaviour of the diffusion. The diffusion characteristics of a receiving body of water can thus vary and must be determined by field measurements if considered of great importance for the prediction of warm-water spread.

Governing equations

The governing equation for diffusion of excess temperature is given earlier by Equation (2.59):

$$\begin{aligned} \frac{\partial T}{\partial t} + u \frac{\partial T}{\partial x} + v \frac{\partial T}{\partial y} + w \frac{\partial T}{\partial z} = \\ = \frac{\partial}{\partial x} \left(K_x \frac{\partial T}{\partial x} \right) + \frac{\partial}{\partial y} \left(K_y \frac{\partial T}{\partial y} \right) + \frac{\partial}{\partial z} \left(K_z \frac{\partial T}{\partial z} \right). \end{aligned} \quad (2.59)$$

General solutions of this equation are so far not available. Some solutions to very simplified cases exist, and these are of great theoretical interest here even if for practical predictions of warm-water spread they are too simplified.

The following assumptions are made to get a simple governing equation:

The conditions are steady-state

The velocity U is homogeneous and unidirectional in the x -direction

Vertical diffusion is negligible

Longitudinal diffusion is negligible

Buoyant spread is negligible.

With these assumptions Equation (2.59) reduces to

$$U \frac{\partial T}{\partial x} = \frac{\partial}{\partial y} \left(K_y \frac{\partial T}{\partial y} \right). \quad (2.78)$$

The solution of this equation depends on the behaviour of the diffusion coefficient K_y . Therefore, this coefficient will be discussed before any solutions of the equation are given.

Horizontal diffusion coefficient

The diffusion coefficient in the horizontal direction depends on how the turbulence is generated. Uniform flow in prismatic channels is the simplest case. Bottom friction generates the turbulence giving a lateral diffusion coefficient as follows (see for instance Prych 1970):

$$K_y = \alpha_1 \cdot u_x \cdot d, \quad (2.79)$$

where α_1 = constant depending on channel shape

$$u_x = (g \cdot d \cdot S)^{1/2} = \text{shear velocity}$$

d = water depth

S = bottom slope in flow direction

The constant α_1 varies with the channel depth-to-width ratio, with α_1 decreasing for this ratio increasing (Okoye 1970) (Figure 2.18).

In a straight channel with groins, these are generating the main turbulence. The lateral diffusion coefficient can then be written as follows (Holley and Abraham 1973):

$$K_y = \alpha_2 \bar{U} d_1, \quad (2.80)$$

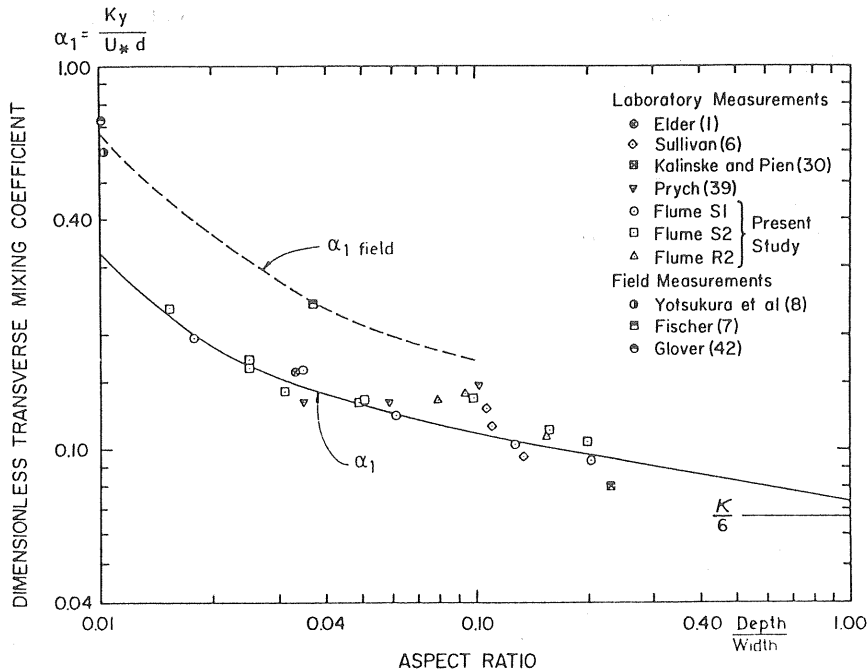


Figure 2.18 Dimensionless lateral mixing coefficient as a function of channel geometry (Okoye 1970).

where $\alpha_2 = \text{constant}$

$\overline{U} = \text{mean velocity}$

$d_1 = \text{local depth.}$

In other water environments, where the turbulence is generated by wind stress at the water surface, the lateral diffusion coefficient will behave in quite another way. Large lakes and open seas are examples of such water environments. Here the diffusion coefficient normally follows the 4/3 power law (see for instance Okubo and Ozmidov 1970):

$$K_y = \alpha_3 l^{4/3}, \quad (2.81)$$

where $\alpha_3 = \text{constant}$

$l = \text{dimension of the studied plume or marked cloud}$

Okubo (1971) found by studying field measurements that the $4/3$ power law holds within some ranges of magnitude of cloud dimensions (Figure 2.19).

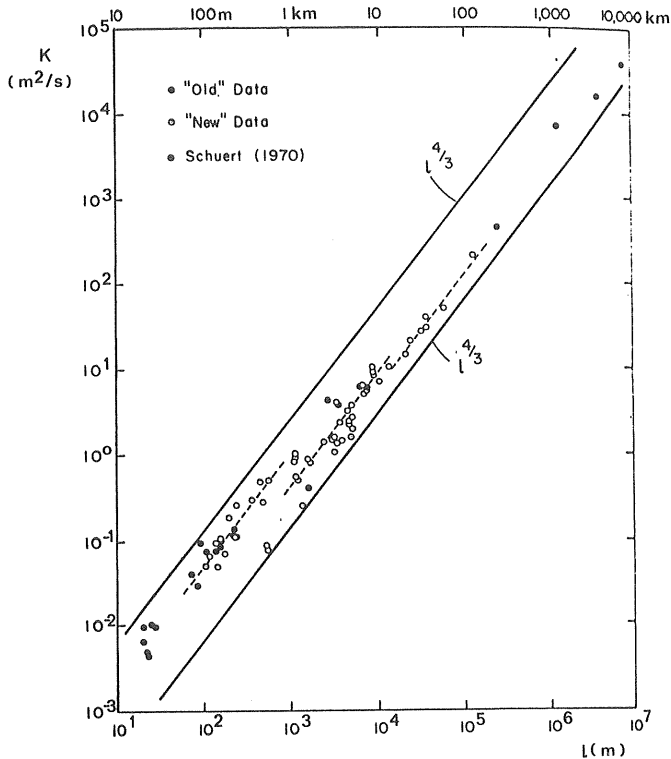


Figure 2.19 Horizontal diffusion coefficient for large lakes and oceans as a function of scale of diffusion (Okubo 1971).

Kullenberg (1974) found the $4/3$ power law to hold as a mean value. The power could, however, vary between 1.1 and 1.6 for individual measurements. It should also be pointed out that the size of the plume or cloud must be smaller than the largest eddies for the $4/3$ power law to be valid. As seen by the scatter of data, the diffusion characteristics can not be determined from literature with any con-

fidence. Therefore, prototype measurements must be made so that the diffusion coefficient of a receiving water body can be determined.

Solutions of the simplified diffusion equation

Solutions of Equation (2.78) exist for some initial conditions and characteristic behaviour of the diffusion coefficient. Brooks (1960) has presented solutions with initial conditions, making the problem well suited for this model scale analysis. The assumptions are that (see also Figure 2.20):

The concentration or heat represented by the temperature is conservative, which means no heat transfer to the atmosphere.

The surface layer has a vertically constant temperature.

The surface layer has a constant thickness, that is no buoyancy or vertical diffusion affects the temperature distribution.

The current velocity is unidirectional and constant at all depths (\bar{U} m/s in x-direction).

The source at $x = 0$ has a constant temperature T_0 over the whole height and width of the surface layer.

The release is continuous and steady-state conditions are present, prescribed for Equation (2.78) to be valid.

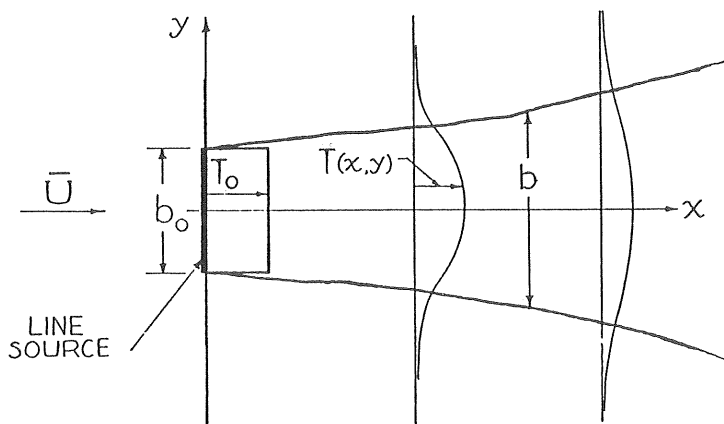


Figure 2.20 Definition sketch of the lateral diffusion problem solved by Brooks (1960) - plan view.

The solutions for excess temperature and plume width are as follows for different characteristic behaviour of the diffusion coefficient:

$$\frac{K_y = K_{y0}}{\frac{T_m}{T_o}} = \operatorname{erf} \left(\frac{\bar{U} b_o^2}{16 K_{y0} \cdot x} \right)^{1/2} \quad (2.82)$$

$$\frac{b}{b_o} = \left(1 + \frac{24 K_{y0} \cdot x}{\bar{U} b_o^2} \right)^{1/2} \quad (2.83)$$

$$\frac{K_y = K_{y0} \cdot \left(\frac{b}{b_o} \right)^{4/3}}{\frac{T_m}{T_o}} = \operatorname{erf} \left(\frac{3/2}{\frac{8 K_{y0} \cdot x}{\bar{U} b_o^2} + 1} \right)^{1/2} \quad (2.84)$$

$$\frac{b}{b_o} = \left(1 + \frac{8 K_{y0} \cdot x}{\bar{U} b_o^2} \right)^{3/2}, \quad (2.85)$$

where b_o = width of line source

$b = 2 \cdot \sqrt{3} \sigma_y$ with σ_y as the variance of lateral temperature distribution

K_{y0} = lateral diffusion coefficient at source.

The temperature decay as a function of distance according to Equations (2.82) and (2.84) is given in Figure 2.21, while plume width according to Equations (2.83) and (2.85) is given in Figure 2.22.

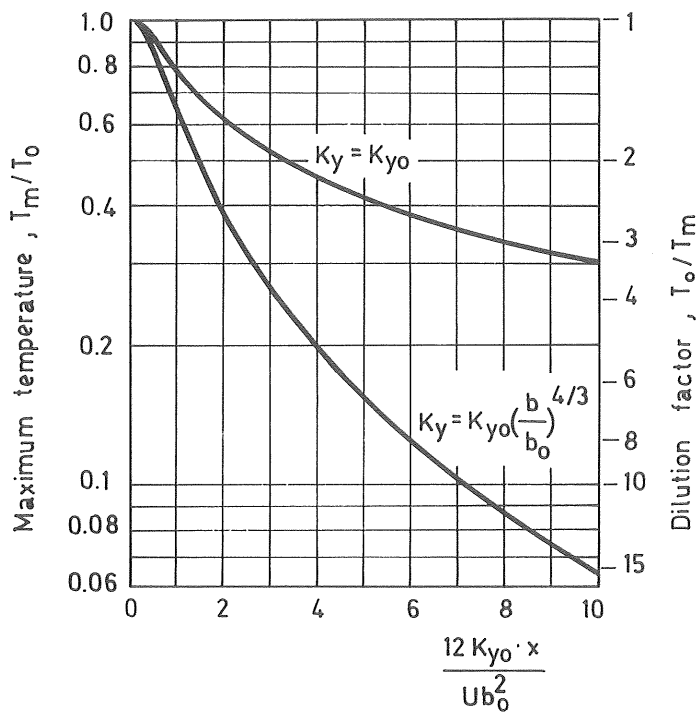


Figure 2.21 Temperature decay according to Equations (2.82), $K_y = K_{y0}$ and (2.84), $K_y = K_{y0} \cdot (b/b_0)^{4/3}$ (Brooks 1960).

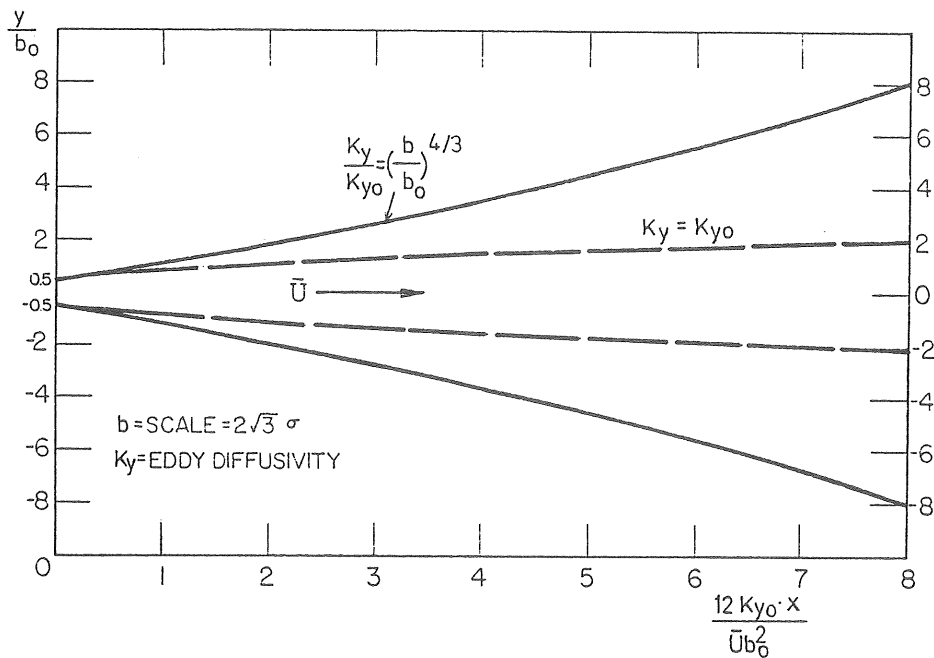


Figure 2.22 Lateral plume spread according to Equations (2.83), $K_y = K_{y0}$, and (2.85), $K_y = K_{y0} (b/b_0)^{4/3}$ (Brooks 1960).

Reproducibility

For a correct reproduction of lateral diffusion the following conditions must be fulfilled as can be seen directly from Equations (2.82) - (2.85), which are presumed to be valid:

The lateral diffusion coefficient at the source must be scaled to give $\left(\frac{K_{y0} x}{U b_o^2} \right)_r = 1$.

The lateral diffusion coefficient is related to the scale of diffusion in the same way in model and prototype.

The first condition gives the following scale condition for the diffusion coefficient:

$$(K_{y0})_r = \lambda_v^{1/2} \cdot \lambda_h. \quad (2.86)$$

The second condition can be fulfilled when the turbulence is generated in the same way in model and prototype. This is the case for open channel flow, which will be discussed here. The wind stress generating turbulence in large lakes and open seas is, on the other hand, almost impossible to reproduce in a model. Therefore, the scaling in that case is not discussed here. Models for such receiving water bodies must be carefully calibrated against prototype data to give good reproduction of lateral diffusion.

The diffusion coefficients for flow in prismatic channels and in channels with groins have been given by Equations (2.79) and (2.80). According to these equations, the ordinary model technique gives the following scaling of the lateral diffusion coefficient for a prismatic channel:

$$(K_y)_r = (\alpha_1)_r \cdot \lambda_v^2 \cdot \lambda_h^{-1/2} \quad (2.87)$$

and for a channel with groins:

$$(K_y)_r = (\alpha_2)_r \cdot \lambda_v^{3/2}. \quad (2.88)$$

These scalings and the prescribed scaling condition of Equation (2.86) give directly that the model must be undistorted for a correct reproduction of lateral diffusion.

Lateral diffusion in distorted models

As above, the lateral diffusion in prismatic channels and in channels with groins will be discussed. These problems are directly solvable concerning effects of distortion and as before, the scaling condition described by Equation (2.86) is presumed to hold.

At first we look at prismatic channels, where the scaling of lateral diffusion is given by Equation (2.87). In a distorted model the lateral diffusion coefficient is thus $(\alpha_1)_r \cdot \lambda_v^{3/2} \cdot \lambda_h^{-3/2}$ too great. As can be seen from Figure 2.19, $(\alpha_1)_r$ is of the order of unity but decreases slightly when distortion increases. The diffusion coefficient will thus be of the order of $\lambda_v^{3/2} \cdot \lambda_h^{-3/2}$ too great.

It is, however, not the constant itself that is of interest but the dilution and lateral spread caused by the lateral diffusion. These effects in a distorted model can be studied by means of Equations (2.82) and (2.83). The temperature decay will be scaled as follows:

$$\left(\frac{T_m}{T_o}\right)_r = \frac{\overline{U} b_o^2 \frac{1}{2} \operatorname{erf}\left(\frac{1}{16 K_{yo} x}\right) M}{\overline{U} b_o^2 \frac{1}{2} \operatorname{erf}\left(\frac{1}{16 K_{yo} x}\right) P} \quad (2.89)$$

For small values of the argument of the error function, the function is approximately equal to the argument. Thus for large values of x , Equation (2.89) can be replaced by the following expression

$$\left(\frac{T_m}{T_o}\right)_r = \frac{\overline{U}_r^{1/2} (b_o)_r}{(K_{yo})_r^{1/2} x_r^{1/2}} \quad (2.90)$$

With the scaling of the diffusion coefficient according to Equation (2.87) the following expression will hold for centre-line temperature far from the source:

$$\left(\frac{T_m}{T_o}\right)_r = (\alpha_1)_r^{-1/2} \cdot \lambda_v^{-3/4} \cdot \lambda_h^{3/4} \quad (2.91)$$

With $(\alpha_1)_r$ being close to unity the centre-line temperature in a distorted model is wrong by approximately $\lambda_v^{-3/4} \cdot \lambda_h^{3/4}$ and thus too small.

The width of the plume is according to Equation (2.83) modelled as follows:

$$\left(\frac{b}{b_o}\right)_r = \left(1 + \frac{24 K_{yo} \cdot x}{\bar{U} b_o^2}\right)_r^{1/2} \quad (2.92)$$

Far from the source, that is for large values of x , the following approximate expression holds:

$$\left(\frac{b}{b_o}\right)_r = \frac{(K_{yo})_r^{1/2} x_r^{1/2}}{\bar{U}_r^{1/2} (b_o)_r} \quad (2.93)$$

Again using Equation (2.87), one may develop the following scaling for lateral spread:

$$\left(\frac{b}{b_o}\right)_r = (\alpha_1)_r^{1/2} \cdot \lambda_v^{3/4} \cdot \lambda_h^{-3/4} \quad (2.94)$$

Thus the width of the plume will be too large by approximately $\lambda_v^{3/4} \lambda_h^{-3/4}$ if $(\alpha_1)_r$ is assumed equal to unity.

For a channel with groins the diffusion coefficient is scaled according to Equation (2.88). With the same arguments as above the following scaling will hold for centre-line temperature and plume width:

$$\left(\frac{T_m}{T_o}\right)_r = (\alpha_2)_r^{-1/2} \lambda_v^{-1/2} \lambda_h^{1/2} \quad (2.95)$$

$$\left(\frac{b}{b_o}\right)_r = (\alpha_2)_r^{1/2} \cdot \lambda_v^{1/2} \cdot \lambda_h^{-1/2} \quad (2.96)$$

Holley and Karelse (1974) have reported a model investigation where lateral diffusion for flow in a channel with groins was studied. The model tests were performed in one undistorted model and one distorted model. Comparisons of prototype and model measurements gave the result that lateral diffusion was well reproduced in the undistorted model, while scale effects occurred in the distorted model. This latter model had a horizontal scale of 1:100 and a vertical scale of 1:40. The model results showed a lateral spread of 1.5 to 2.0 times greater than the prototype results. These numbers agree well with the distortion effects as given by Equation (2.96):

$$\left(\frac{b}{b_o}\right)_r = (\alpha_2)_r \cdot 40^{-1/2} \cdot 100^{1/2} \approx 1.6 (\alpha_2)_r^{1/2}, \quad (2.97)$$

where $(\alpha_2)_r$ can be expected to be close to unity.

Summary

The effects of distortion on lateral diffusion have been discussed. This discussion has been limited to uniform flow in prismatic channels and channels with groins since these are the only cases, where it is possible to treat the problem theoretically. The derived effects are as follows:

	Prismatic channel	Channel with groins
Excess temperature $\left(\frac{T_m}{T_o}\right)_r$ far from source	$(\alpha_1)_r^{-1/2} \cdot \lambda_v^{-3/4} \cdot \lambda_h^{3/4}$ (too small)	$(\alpha_2)_r^{-1/2} \cdot \lambda_v^{-1/2} \cdot \lambda_h^{1/2}$ (too small)
Plume width $(b/b_o)_r$ far from source	$(\alpha_1)_r^{1/2} \cdot \lambda_v^{3/4} \cdot \lambda_h^{-3/4}$ (too great)	$(\alpha_2)_r^{1/2} \cdot \lambda_v^{1/2} \cdot \lambda_h^{-1/2}$ (too great)

2.8 Vertical ambient diffusion

Vertical diffusion as well as horizontal diffusion is an important mixing process in the far-field of a warm-water discharge. The vertical diffusion is, as a rule, less effective than the horizontal diffusion. In the ocean for a nonbuoyant tracer this leads to a horizontal extension that is of the order of 30 times greater than the vertical one (Csanady 1973). For channel flow this difference is, however, much less.

Theory

The basic governing equation is Equation (2.56), which for a tracer has the form:

$$\begin{aligned} \frac{\partial c}{\partial t} + u \frac{\partial c}{\partial x} + v \frac{\partial c}{\partial y} + w \frac{\partial c}{\partial z} = \\ = \frac{\partial}{\partial x} \left(K_x \frac{\partial c}{\partial x} \right) + \frac{\partial}{\partial y} \left(K_y \frac{\partial c}{\partial y} \right) + \frac{\partial}{\partial z} \left(K_z \frac{\partial c}{\partial z} \right) \end{aligned} \quad (2.98)$$

70.

This equation can be simplified under the following conditions:

Uniform flow velocity

Coordinate system moving with the flow velocity

Concentration is integrated over the horizontal plane

which defines $\bar{c} = \int_{-\infty}^{\infty} \int_{-\infty}^{\infty} c \, dx \, dy$

No sink or source of tracer.

If these assumptions are made Equation (2.98) can be written as follows:

$$\frac{\partial \bar{c}}{\partial t} = \frac{\partial}{\partial z} \left(K_z \frac{\partial \bar{c}}{\partial z} \right). \quad (2.99)$$

For an instantaneous point release at the water surface and a constant diffusion coefficient the solution has the form

$$\bar{c} = \frac{1}{(4 \pi K_z t)^{1/2}} \cdot \exp - \left(\frac{z^2}{4 K_z t} \right), \quad (2.100)$$

with the initial conditions

$$c = 0 \text{ for } z \neq 0$$

$$c \rightarrow \infty \text{ for } z = 0$$

$$\int_{-\infty}^0 \bar{c} \, dz = 1/2$$

$$\bar{c}(z) = \Delta(0)$$

($\Delta(0)$ is a Dirac function.)

This solution will form the basis upon which effects of distortion on vertical diffusion will be determined. First, however, the vertical diffusion coefficient, K_z , will be discussed.

Vertical diffusion coefficient

The vertical diffusion characteristics depend on the characteristics of the receiving water body, especially density stratification and

generation of turbulence.

Stratification reduces the vertical diffusion as well as the vertical entrainment discussed earlier. Modelling of stratification in estuaries is as a rule done by introducing obstacles into the flow to increase friction and diffusion until good agreement is reached between model and prototype. This is not possible to treat theoretically and is therefore not included in this analysis.

In large lakes and in the open sea the turbulence is mainly generated by wind stress at the surface. This gives a diffusion coefficient that decreases significantly with depth. Csanady reported a typical number of $3 \cdot 10^{-3} \text{ m}^2/\text{s}$ for the diffusion coefficient at the depth of 0 - 0.3 m and a number of $5 \cdot 10^{-4} \text{ m}^2/\text{s}$ for a depth of several meters. Such a phenomenon can not be reproduced in a model and will therefore not be treated here.

The vertical diffusion coefficient for flow in prismatic channels can be considered constant over depth and has the form (Ditmars 1971),

$$K_z = \alpha_3 u_x d, \quad (2.101)$$

where $\alpha_3 = \text{constant}$.

In this case the turbulence is generated by bottom friction. Effects of distortion will be studied on the basis of the diffusion coefficient following Equation (2.101).

Reproducibility

Modelling of vertical diffusion in a correct way requires that Equation (2.100) has the same form in model and prototype. The exponent of the equation must be identical for both prototype and model conditions, which leads to the following relation

$$\frac{z_r^2}{(K_z)_r t_r} = 1 \quad (2.102)$$

This gives the scale condition

$$(K_z)_r = \lambda_v^{5/2} \cdot \lambda_h^{-1}. \quad (2.103)$$

The vertical diffusion for flow in prismatic channels will according to Equation (2.101) be scaled as follows:

$$(K_z)_r = (\alpha_3)_r \cdot \lambda_v^2 \cdot \lambda_h^{-1/2}. \quad (2.104)$$

For the two expressions (2.103) and (2.104) to be equal, an undistorted model is required.

Vertical diffusion in distorted models

In a distorted model the distortion leads to a vertical diffusion coefficient that is wrong by a factor $(\alpha_3)_r \cdot \lambda_v^{-1/2} \cdot \lambda_h^{1/2}$ as can be seen from Equations (2.103) and (2.104). This means that the vertical penetration $(Z_p)_r$ defined as the depth of a given fraction of surface concentration is modelled as follows:

$$(Z_p)_r = \lambda_v \cdot (\alpha_3)_r \cdot \lambda_v^{-1/4} \cdot \lambda_h^{1/4}. \quad (2.105)$$

The vertical penetration defined in this way should for correct reproduction be scaled as the vertical scale and is thus wrong by a factor of $(\alpha_3)_r \cdot \lambda_v^{-1/4} \cdot \lambda_h^{1/4}$, where $(\alpha_3)_r$ could be expected to be close to unity.

The vertical penetration will thus be too small in a distorted model of flow in prismatic channels. This can also be expected in other water environments where bottom friction generates turbulence as can be the case in shallow coastal areas. It should be pointed out that the effects of distortion in this case are small compared to effects of other phenomena such as three-dimensional jet diffusion and horizontal ambient diffusion.

2.9 Heat transfer to the atmosphere

Heat transfer to the atmosphere is the ultimate sink of the heat added to the water environment by a cooling-water discharge. The importance of this process to the physical modelling varies from case to case. If mixing between warm water and ambient water is efficient, the heat loss within the area of interest for modelling may be small, 10% or less of the discharged heat. In such a case the process is of minor interest for the modelling. If, however, mixing is poor, the heat loss may be significant, because the surface temperatures will be high, leading to heat loss to the atmosphere that significantly de-

creases temperature. In this case heat loss must be considered in the choice of model scales.

The equations describing heat transfer to the atmosphere are complicated but can within a limited surface temperature range be linearized and are then well suited for describing the heat loss due to excess temperature of the water surface.

Theory

Several different physical processes are participating in the heat transfer through the water surface. Syntheses and simplifications of these processes have been presented by Milanov (1969), Stolzenbach (1971), and Paily et al. (1974). In the following presentation the outline of Paily et al. is followed.

The heat transport between the atmosphere and a water surface can be divided into incoming and reflected short-and-long-wave radiation and heat loss due to evaporation and conduction (see Figure 2.23).

The heat transfer to the atmosphere can be written as follows:

$$\phi^x = -\phi_{ri} + \phi_{rr} - \phi_{ba} + \phi_{br} + \phi_{bw} + \phi_E + \phi_H, \quad (2.106)$$

where ϕ^x = net heat loss to the atmosphere

ϕ_{ri} = incoming short-wave radiation

ϕ_{rr} = reflected short-wave radiation

ϕ_{ba} = atmospheric long-wave radiation

ϕ_{br} = reflected long-wave radiation

ϕ_{bw} = long-wave radiation emitted by water surface

ϕ_E = heat loss due to evaporation

ϕ_H = heat loss due to conduction (or heat gain).

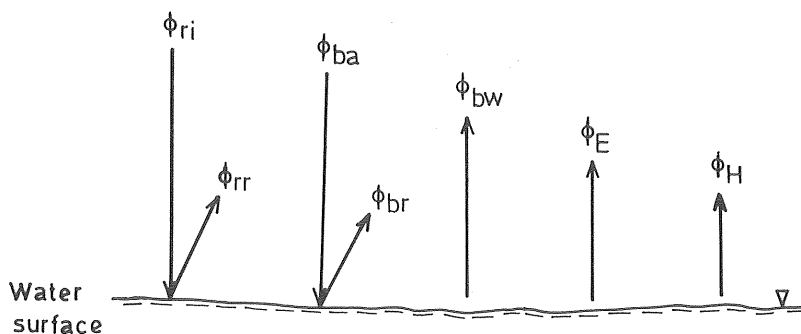


Figure 2.23 Rate of heat exchange between a water surface and the atmosphere.

Here, as in many other works, the meaning of heat loss is the rate of heat transfer per unit area from the water surface to the atmosphere. In the actual application the process is estimated as a mean value over a period of weeks or months.

Only the last three terms of Equation (2.106) are functions of water-surface temperature, while the terms describing incoming and reflected radiation depend on atmospheric conditions. Since the interest is concentrated to heat loss due to excess temperatures alone, the radiation terms will be excluded in the following presentation.

The long wave emission of the water surface, ϕ_{bw} , follows the law of Stefan-Bolzman:

$$\phi_{bw} = \epsilon_w \sigma (T_s + 273)^4, \quad (2.107)$$

where ϵ_w = the emissivity of water surface
 σ = Stefan-Bolzman constant
 T_s = temperature at water surface ($^{\circ}\text{C}$).

The heat loss due to evaporation, ϕ_E , is a function of water temperature, air temperature, vapour pressure of air, and wind velocity. In a simplified form it can be written as

$$\phi_E = \rho L (T_s) \cdot E, \quad (2.108)$$

where ρ = density of water
 $L(T_s)$ = latent heat of vapourization
 E = volumetric evaporation rate per unit area.

The flux of heat advected by the evaporated mass of water is considered negligible compared to the heat loss by evaporation. Within a limited range of temperature the latent heat of vapourization $L(T_s)$ can be considered constant.

The evaporation, E , depends on air vapour pressure and saturation vapour pressure corresponding to the water surface temperature as well as the turbulent diffusion transport above the water surface

$$E = N \cdot V_{az} (e_s - e_{az}), \quad (2.109)$$

where N = evaporation coefficient (can be a function of wind velocity)

V_{az} = wind velocity at level z above water surface

e_{az} = air vapour pressure at level z

e_s = saturation vapour pressure corresponding to water surface temperature, T_s .

The evaporation heat loss can then be written in the following way:

$$\phi_E = \rho L(T_s) \cdot N \cdot V_{az} (e_s - e_{az}). \quad (2.110)$$

The conductive heat transport is considered to be a fixed ratio of the heat transport by evaporation:

$$\phi_H = R \cdot \phi_E, \quad (2.111)$$

where $R = C \frac{p_a}{1000} \left(\frac{T_s - T_{air}}{e_s - e_a} \right)$ (Bowen's ratio)

C = Bowen's constant

p_a = air pressure in mb

T_{air} = air temperature

e_s = saturation vapour pressure corresponding to T_s in mb

e_a = vapour pressure of air corresponding to T_{air} and relative humidity.

Several models have been developed to reduce Equation (2.106) to a constant term and a term linearly increasing with the water surface temperature.

The constants of the equations vary with water surface temperature, wind velocity, relative humidity, and air temperature. The greatest influence on the heat exchange coefficient is the wind velocity. The most popular model seems to be the Edinger-Duttweiler-Geyer model, also called the equilibrium temperature model

$$\phi^x = K (T_s - T_E), \quad (2.112)$$

where K = heat exchange coefficient

T_S = water surface temperature

T_E = equilibrium temperature that is the water surface temperature giving zero net heat transport.

According to this equation, the excess heat causes an increase of heat transfer to the atmosphere that linearly depends on the excess temperature of the water surface.

The given equations are determined for prototype conditions. The heat losses under laboratory conditions are of great interest as well. Stolzenbach and Harleman (1971 b) give a typical number for K of 20-30 kcal/m²h °C for laboratory conditions. This number should be compared with a typical number of 30-50 kcal/m²h °C for prototype conditions.

Reproducibility

For correct reproduction of surface heat loss, a distorted model is as a rule required. The scale condition for the heat exchange coefficient is developed by comparing advective heat transport with surface heat loss. If there is correct scaling of temperature and velocity distribution, the following scaling of advective heat transport holds:

$$\begin{aligned} (\text{Advective heat transport})_r &= \\ &= T_r \cdot u_r \lambda_v \cdot \lambda_h = |\lambda_v|^{3/2} \cdot \lambda_h. \end{aligned} \quad (2.113)$$

The heat loss to the atmosphere will with the same assumptions be scaled as follows:

$$\begin{aligned} (\text{Surface heat loss})_r &= \\ &= K_r \cdot T_r \cdot \lambda_h^2 = K_r \cdot \lambda_h^2. \end{aligned} \quad (2.114)$$

Correct reproduction of surface heat loss requires that surface heat loss constitutes the same rate of the advective heat transport in both model and prototype. This means that surface heat loss and advective heat transport are scaled in the same way, which gives the following

scale condition:

$$K_r = \lambda_v^{3/2} \lambda_h^{-1} \quad (2.115)$$

As stated earlier, typical values of the heat exchange coefficient K are in the prototype 30-50 (kcal/m²h °C) and in the model 20-30 (kcal/m²h °C), which gives the following normal conditions for the heat exchange coefficient:

$$0.4 < K_r < 1 \quad (2.116)$$

If K_r is within these limits, a distorted model is as a rule required for correct reproduction of heat transfer to the atmosphere.

3. EFFECTS OF DISTORTION EVALUATED BY MEANS OF ANALYTICAL SOLUTIONS OF SURFACE BUOYANT JET PROBLEMS

3.1 Introduction

Analytical solutions of surface warm-water discharge problems are rare compared with the number of numerical models developed during the last 5-10 years. The analytical solutions reported by Stolzenbach and Harleman (1971 a), Engelund and Pedersen (1973), Pande and Rajaratnam (1975 a), and Engelund (1976) are presented here for the evaluation of the effects of distortion. The different theories include buoyancy effects in different ways, in which a large Richardson number indicates great influence of buoyancy. These solutions are schematized in Table 3.1.

Stolzenbach and Harleman have made an analytical solution of a non-buoyant surface jet discharged through a rectangular outlet. The solution is in accordance with the solutions of submerged jets as shown in Section 2.2. Pande and Rajaratnam achieved the same results, using a similarity analysis for what they call "small" Richardson number flow. However, they neglect all effects of buoyancy and are thus treating the nonbuoyant case.

Engelund and Pedersen have made a similarity analysis for small Richardson number flow where they include buoyancy effect in the lateral momentum equation. So do Pande and Rajaratnam for what they call "moderate" Richardson number flow. As can be seen from Table 3.1 their analysis give exponents in the dependence of distance from outlet that are indefinite. If, however, the entrainment principle with a constant entrainment coefficient, is added to their analysis, their results will be similar to the solution given by Engelund and Pedersen.

Both Engelund for moderate and Pande and Rajaratnam for "large" Richardson number flow include in their analyses buoyancy in the lateral and the longitudinal momentum equation. Engelund directly and Pande and Rajaratnam indirectly include buoyancy effects on the entrainment in the vertical direction. Also in this case Pande and Rajaratnam end up with results that are indefinite.

Table 3.1 Analytical solutions of warm-water flow problems

Source	Richardson number	Buoyancy influence taken into account			Dependence of distance from discharge for			
		Lateral spread	Longitudinal spread	Vertical entrainment	$\frac{U_m}{U_o}$	$\frac{\Delta \rho}{\Delta \rho_o}$ or $(\frac{\Delta T}{\Delta T_o})$	$\frac{B}{B_o}$	$\frac{H}{H_o}$
Stolzenbach Harleman 1971 a	Non-buoyant (= 0)	No	No	No	x^{-1}	x^{-1}	x	x
Pande-Rajaratnam 1975 a	"Small" (= 0)	No	No	---	x^{-1}	x^{-1}	x	x
Engelund-Pedersen 1973	Small	Yes	No	No	$x^{-5/3}$	$x^{-5/3}$	$x^{7/3}$	x
Pande-Rajaratnam 1975 a	Moderate	Yes	No	---	$x^{-(2/3+c)}$	$x^{-(2/3+c)}$	$x^{(4/3+c)}$	x^c
		Adding the entrainment principle with constant entrainment coefficient gives			$x^{-5/3}$	$x^{-5/3}$	$x^{7/3}$	x
Engelund 1976	Moderate	Yes	Yes	Yes	$x^{-7/9}$	$x^{-7/9}$	$x^{13/9}$	$x^{1/9}$
Pande-Rajaratnam 1975 a	Large	Yes	Yes	Yes	$x^{-1/3}$	$x^{-(2/3+c)}$	x	x^c

Adding the entrainment principle with constant entrainment coefficient gives

To use the given solutions for evaluating scale effects in distorted models, we must know the influence of the shape and dimensions of the outlet. This is earlier analysed and discussed only for the non-buoyant case and in a rough way by data fitting for theories of Pande and Rajaratnam. For the other cases we must add some reasonable assumptions to be able to evaluate the effects of distortion.

It must also be considered that these evaluations are valid only as long as the model and discharge conditions are similar to those on which the analyses are based. That means that the receiving water bodies should be quiescent, homogeneous, and "infinite" with negligible influence of the bottom on the flow of warm water. This is, however, seldom the case in practical applications. Still the analyses are valuable for comparisons with scale effects calculated by means of numerical models.

3.2 Nonbuoyant surface discharge

The theory developed by Stolzenbach and Harleman (1971 a) for non-buoyant surface jets discharged through rectangular outlets has partly been presented earlier in Section 2.2. Based on experimental data, they state that the theory is valid for discharges with densimetric Froude numbers greater than 15, which means that the Richardson number must be of the order $1/200$ or less. The results of Pande and Rajaratnam are in principle similar to those of Stolzenbach and Harleman but are without any information concerning the influence of outlet shape or range of validity.

Far from the outlet the equations for centre-line velocity and temperature have the form

$$\frac{u_m}{u_o} = 9.9 \frac{\sqrt{H_o B_o}}{x} \quad (3.1)$$

$$\frac{T_m}{T_o} = 9.5 \frac{\sqrt{H_o B_o}}{x} \quad (3.2)$$

where T_m = centre-line excess temperature
 T_o = outlet excess temperature.

The width B and thickness H vary linearly with distance from outlet:

$$B = C_1 \cdot x \quad (3.3)$$

$$H = C_2 \cdot x, \quad (3.4)$$

where C_1 and C_2 are constants.

The effects of distortion are evaluated in the same way as in Chapter 2, which leads to the same results as given in Section 2.2.

$$\left(\frac{u_m}{u_{or}}\right) = \lambda_v^{1/2} \cdot \lambda_h^{-1/2} \quad (3.5)$$

$$\left(\frac{T_m}{T_{or}}\right) = \lambda_v^{1/2} \cdot \lambda_h^{-1/2} \quad (3.6)$$

$$B_r = \lambda_h \quad (3.7)$$

$$H_r = \lambda_h. \quad (3.8)$$

Equations (3.5) and (3.6) directly give the result that centre-line velocity and excess temperature in a distorted model are too great by a factor of $\lambda_v^{1/2} \lambda_h^{-1/2}$. The width is modelled correctly. A correct modelling of thickness should be the same as the vertical scale so the thickness is modelled wrong by a factor of $\lambda_v^{-1} \lambda_h$, and thus it is too small.

A summary of the scale effects for a nonbuoyant surface discharge in a distorted model is thus as follows:

The centre-line velocity is too great by a factor of $\lambda_v^{1/2} \lambda_h^{-1/2}$

The centre-line temperature is too great by a factor of $\lambda_v^{1/2} \lambda_h^{-1/2}$

The width is correct

The thickness is too small and wrong by a factor of $\lambda_v^{-1} \lambda_h$.

The scale effects are valid far from the outlet, where effects of the zone of flow establishment are negligible as described in Section 2.2.

3.3 Small Richardson number flow

Engelund and Pedersen (1973) presented a similarity analysis of a buoyant surface jet at small Richardson numbers. In their analysis they include buoyancy effects in the lateral momentum equation but neglect them in the other governing equations. For the entrainment coefficient to be independent of buoyancy, the local bulk Richardson number should be less than 0.1. The analysis results in the following equations:

$$\frac{u_m}{u_o} = \left(\frac{x}{L}\right)^{-5/3} \quad (3.9)$$

$$\frac{T_m}{T_o} = \left(\frac{x}{L}\right)^{-5/3} \quad (3.10)$$

$$\frac{H}{D} = \frac{x}{L} \quad (3.11)$$

$$\frac{B}{L} = Ri_o^{1/2} \left(\frac{x}{L}\right)^{7/3}, \quad (3.12)$$

and as an additional result they get

$$\frac{3 e \cdot L}{5 D} = 1, \quad (3.13)$$

where L = a horizontal characteristic length.

D = a vertical characteristic length.

e = entrainment factor.

Here it is not possible to introduce any model scales into the equations since the horizontal and vertical lengths L and D are unknown functions of velocity, volume flux, and density deficiency. We instead introduce a control section in the flow as a reference section, thus giving the following equations.

$$\frac{u_m}{(u_m)_c} = \left(\frac{x}{x_c}\right)^{-5/3} \quad (3.14)$$

$$\frac{T_m}{(T_m)_c} = \left(\frac{x}{x_c}\right)^{-5/3} \quad (3.15)$$

$$\frac{H}{H_c} = \frac{x}{x_c} \quad (3.16)$$

$$\frac{B}{B_c} = \left(\frac{x}{x_c}\right)^{7/3}, \quad (3.17)$$

where index c indicates values of the control section.

It should be pointed out here that for a given warm-water flow with a given density deficit and a given velocity, there only exists one pair of B and H that satisfies the given equations. In a model the flux, the density deficit (temperature), and the velocity are modelled according to the Froude scaling. After an initial zone close to the outlet the flow will theoretically follow Equations (3.9) - (3.13) and more or less be independent of outlet shape. The control section is thus supposed to be outside the initial zone.

By using Equations (3.9) - (3.17) together with the relationships

$$\frac{Ri_c}{Ri_o} = \frac{\frac{(T_m)_c}{T_o} \frac{H_c}{D}}{\frac{(u_m)_c^2}{(u_o)_c^2}} \quad (3.18)$$

$$q \sim H \cdot B \cdot u_m, \quad (3.19)$$

one can write the following equations for H_c , B_c and x_c :

$$H_c = C_3 \cdot q_c^{2/3} (T_m)_c^{-1/5} \quad (3.20)$$

$$B_c = C_4 \cdot q_c^{3/5} (u_m)_c^{-1} (T_m)_c^{1/5} \quad (3.21)$$

$$x_c = C_5 \cdot q_c^{2/5} (T_m)_c^{-1/5} \quad (3.22)$$

By using the expressions for volume flux, temperature (density deficit), and centreline velocity of a given section in the developed flow, one can describe the flow parameters as functions of x , where origo

is defined by the given section and Equation (3.22). Equations (3.14) - (3.17) thus give

$$\frac{u_m}{(u_m)_c} = C_6 q_c^{2/3} (T_m)_c^{-1/3} x^{-5/3} \quad (3.23)$$

$$\frac{T_m}{(T_m)_c} = C_7 q_c^{2/3} (T_m)_c^{-1/3} x^{-5/3} \quad (3.24)$$

$$B = C_8 (T_m)_c^{2/3} q_c^{-1/3} (u_m)_c^{-1/3} x^{7/3} \quad (3.25)$$

$$H = \frac{3 e_o}{5} \cdot x. \quad (3.26)$$

Now we can develop the effects of distortion after making the following assumptions:

In model and prototype the flow is developed in the sense that the flow follows Equations (3.9) - (3.13).

The centreline velocity and temperature together with volume flux of the control section are correctly modelled with respect to Froude modelling.

Density difference is a linear function of temperature and scaled 1:1.

Effects of distortion are studied far from the control section so that the difference in the location of origo in model and in prototype is negligible.

With these assumptions the scaling according to Equations (3.23) - (3.26) is as follows:

$$\left(\frac{u_m}{(u_m)_c}\right)_r = \lambda_v \cdot \lambda_h^{-1} \quad (3.27)$$

$$\left(\frac{T_m}{(T_m)_c}\right)_r = \lambda_v \cdot \lambda_h^{-1} \quad (3.28)$$

$$B_r = \lambda_v^{-1} \cdot \lambda_h^2 \quad (3.29)$$

$$H_r = \lambda_h \quad (3.30)$$

Equations (3.27) and (3.28) directly give the result that centre-line velocity and excess temperature in a distorted model are too great by a factor of $\lambda_v \cdot \lambda_h^{-1}$. The width and thickness are underestimated and wrong by a factor of $\lambda_v^{-1} \cdot \lambda_h$, as can be seen from Equations (3.29) and (3.30).

The results given above show that, according to this theory, the effects of distortion are greater than for a nonbuoyant jet. This is in conflict with the results of scale effects for nonbuoyant jets, buoyancy spread, and buoyancy effects on vertical entrainment as presented in Chapter 2. According to these analyses buoyancy spread is correctly reproduced and the vertical entrainment in a distorted model is also better reproduced than for the nonbuoyant case.

The theory seems doubtful in the assumption that buoyancy is affecting lateral spread and not the vertical entrainment. This has resulted in a width that increases with the 7/3 power of distance compared to 1 st power for the nonbuoyant case, which seems too great.

The authors give a local bulk Richardson number of 0.1 as an upper limit for the theory to be valid. Stolzenbach and Harleman give an outlet densimetric Froude number of 15 as the lower limit for the nonbuoyant theory to be valid, which is equivalent to a Richardson number of 1/200. This number could be expected to be the lower value for small Richardson number theory to be valid, giving the range of validity as $0.005 < Ri < 0.1$. As can be calculated from Equation (3.18), the Richardson number increases with the 8/3 power of the distance from origo. If this fact is taken into account, the theory seems to have a very small range of application.

In spite of the doubts and limitations given above, the theory and evaluation of distortion effects are presented because of lack of other representative theories.

3.4 Moderate Richardson number flow

Both Pande and Rajaratnam (1975 a) and Engelund (1976) use a similarity analysis to develop the equations describing the flow for discharges of warm water at a moderate Richardson number.

In his analysis Engelund includes effects of buoyancy in the equations of lateral and longitudinal momentum as well as in the expression for vertical entrainment, while Pande and Rajaratman in their analysis include the effect of buoyancy in only the lateral momentum equation. However, they fit their theory to experimental data (Pande and Rajaratnam 1975 b), and this can indirectly add other buoyancy effects to the results.

Pande and Rajaratnam in their theory end up with the following set of equations

$$\frac{u_m}{u_o} \sim \left(\frac{x}{L}\right)^{-(2/3 + c_1)} \quad (3.31)$$

$$\frac{T_m}{T_o} \sim \left(\frac{x}{L}\right)^{-(2/3 + c_1)} \quad (3.32)$$

$$\frac{B}{B_o} \sim \left(\frac{x}{L}\right)^{(4/3 + c_1)} \quad (3.33)$$

$$\frac{H}{H_o} \sim \left(\frac{x}{L}\right)^{c_1}, \quad (3.34)$$

where $c_1 = \text{constant}$.

As can be seen, their results are indefinite but by comparing their theory with experimental data they found the following equations to be valid:

$$\frac{u_m}{u_o} \sim \left(\frac{x}{\sqrt{H_o B_o}}\right)^{-2/3} \quad (3.35)$$

$$\frac{T_m}{T_o} \sim \left(\frac{x}{\sqrt{H_o B_o}}\right)^{-2/3} \quad (3.36)$$

$$\frac{B}{B_o} \sim \left(\frac{x}{B_o}\right)^{4/3} \quad (3.37)$$

$$\frac{H}{H_o} = \text{constant.} \quad (3.38)$$

In their comparison Pande and Rajaratnam use a set of data from only 5 tests where the Richardson number at the outlet varies from 0.15 to 1.14 and the aspect ratio (B_o/H_o) is 1 and 3. This set of data is used for both moderate Richardson number flow, $Ri = 0.15$, 0.35, and 0.56 and large Richardson number flow, $Ri = 0.79$ and 1.14. The data set is too small to confirm the theories. Therefore the theory of Engelund is used in the further analysis. His first order theory results in the following set of equations: (His second order theory is not presented here, since the results are not suited for the analysis of scale effects.)

$$\frac{u_m}{u_o} = \left(\frac{x}{L}\right)^{-7/9} \quad (3.39)$$

$$\frac{T_m}{T_o} = \left(\frac{x}{L}\right)^{-7/9} \quad (3.40)$$

$$\frac{B}{L} \sim \sqrt{Ri_o} \left(\frac{x}{L}\right)^{13/9} \quad (3.41)$$

$$\frac{H}{D} = \left(\frac{x}{L}\right)^{1/9} \quad (3.42)$$

and as an additional condition

$$\frac{7}{9} \frac{e_o L}{D} = 1, \quad (3.43)$$

where e_o = entrainment factor corresponding to a Richardson number of one.

As can be seen the equation of Pande and Rajaratnam are comparable with the equations of Engelund. As in the theory of Engelund and Pedersen, there exists only one pair of B and H that for a given set of data for flow, temperature, and velocity satisfies the theory, i. e. Equations (3.39) - (3.43). A control section is therefore introduced.

The equations describing the flow will then have the following form:

$$\frac{u_m}{(u_m)_c} = \left(\frac{x}{x_c}\right)^{-7/9} \quad (3.44)$$

$$\frac{T_m}{(T_m)_c} = \left(\frac{x}{x_c}\right)^{-7/9} \quad (3.45)$$

$$\frac{B}{B_c} = \left(\frac{x}{x_c}\right)^{13/9} \quad (3.46)$$

$$\frac{H}{H_c} = \left(\frac{x}{x_c}\right)^{1/9} \quad (3.47)$$

The parameters B_c , H_c and x_c can be obtained as functions of $(T_m)_c$, $(u_m)_c$ and q_c if we use equations (3.39) - (3.43) together with the relation of the Richardson number of the control section Ri_c and of the section where $x = L \cdot Ri_o$, respectively:

$$\frac{Ri_c}{Ri_o} = \frac{\frac{(T_m)_c}{T_o} \cdot \frac{H_c}{H_o}}{\frac{(u_m)_c^2}{u_o^2}} \quad (3.48)$$

$$q \sim B \cdot H \cdot u_m. \quad (3.49)$$

Then the parameters of the control section will have the form

$$B_c = C_9 \cdot q_c^{5/7} (u_m)_c^{-11/7} (T_m)_c^{3/7} \quad (3.50)$$

$$H_c = C_{10} \cdot q_c^{2/7} (u_m)_c^{4/7} (T_m)_c^{-3/7} \quad (3.51)$$

$$x_c = C_{11} \cdot q_c^{4/7} (u_m)_c^{-6/7} (T_m)_c^{1/7}. \quad (3.52)$$

Introducing these expressions into Equations (3.44) - (3.47), one obtains the following expressions for velocity, temperature, width, and thickness of the flow:

$$\frac{u_m}{(u_m)_c} = C_{12} \cdot q_c^{4/9} (u_m)_c^{-2/3} (T_m)_c^{1/9} x^{-7/9} \quad (3.53)$$

$$\frac{T_m}{(T_m)_c} = C_{13} \cdot q_c^{4/9} (u_m)_c^{-2/3} (T_m)_c^{1/9} x^{-7/9} \quad (3.54)$$

$$B = C_{14} \cdot q_c^{-1/9} (u_m)_c^{-1/3} (T_m)_c^{2/9} x^{13/9} \quad (3.55)$$

$$H = C_{15} \cdot q_c^{2/9} (u_m)_c^{2/3} (T_m)_c^{-29/63} x^{1/9} \quad (3.56)$$

Now we can develop the effects of distortion after making the following assumptions:

In model and prototype the flow is developed in the sense that the flow follows Equations (3.39) - (3.43).

The centreline velocity and temperature together with volume flux of the control section are correctly modelled with respect to Froude modelling.

Density difference is a linear function of temperature and scaled 1:1.

Effects of distortion are studied far from the control section so that the difference in the location of origo in model and prototype is negligible.

With these assumptions the following scaling will be present in a distorted model:

$$\left(\frac{u_m}{(u_m)_c}\right)_r = \lambda_v^{1/3} \cdot \lambda_h^{-1/3} \quad (3.57)$$

$$\left(\frac{T_m}{(T_m)_c}\right)_r = \lambda_v^{1/3} \cdot \lambda_h^{-1/3} \quad (3.58)$$

$$B_r = \lambda_v^{-1/3} \cdot \lambda_h^{4/3} \quad (3.59)$$

$$H_r = \lambda_v^{2/3} \cdot \lambda_h^{1/3}. \quad (3.60)$$

From these equations it can be seen that the effects of distortion are as follows.

The centre-line velocity is wrong by a factor of $\lambda_v^{1/3} \cdot \lambda_h^{-1/3}$ (too great)

The centre-line temperature is wrong by a factor of $\lambda_v^{1/3} \cdot \lambda_h^{-1/3}$ (too great)

The flow width is wrong by a factor of $\lambda_v^{-1/3} \cdot \lambda_h^{1/3}$ (too small)

The thickness of flow is wrong by a factor of $\lambda_v^{-1/3} \cdot \lambda_h^{1/3}$ (too small).

This evaluation is valid only as long as the theory is valid, which according to Engelund is for a Richardson number greater than 0.1. An upper limit is not given.

3.5 Large Richardson number flow

Pande and Rajaratnam (1975 a) presented an analysis for large Richardson number flow. Their theoretical results are as follows

$$\frac{u_m}{u_o} \sim \left(\frac{x}{L}\right)^{-1/3} \quad (3.61)$$

$$\frac{T_m}{T_o} \sim \left(\frac{x}{L}\right)^{-(2/3 + c_2)} \quad (3.62)$$

$$\frac{B}{B_o} \sim \frac{x}{L} \quad (3.63)$$

$$\frac{H}{H_o} \sim \left(\frac{x}{L}\right)^{c_2} \quad (3.64)$$

where $c_2 = \text{constant}$.

Their comparison with experimental data gives the following result:

$$\frac{u_m}{u_o} \sim \left(\frac{x}{\sqrt{H_o B_o}} \right)^{-1/3} \quad (3.65)$$

$$\frac{T_m}{T_o} \sim \left(\frac{x}{\sqrt{H_o B_o}} \right)^{-2/3} \quad (3.66)$$

$$\frac{B}{B_o} \sim \frac{x}{B_o} \quad (3.67)$$

$$\frac{H}{H_o} = \text{constant.} \quad (3.68)$$

As pointed out in Section 3.4 the results have not been properly verified by experiments. Therefore, it is of little value to use their results for further analysis.

3.6 Conclusions

Scale effects have been evaluated by means of different theories with different influence of buoyancy. In the theories the ambient water has been presumed to be quiescent, infinite, and homogeneous with no ambient diffusion. The theory of Stolzenbach and Harleman for nonbuoyant flow and the theory of Engelund for moderate Richardson number flow both seem to be based on a good theoretical ground. The other theories seem to include too rough assumptions to give a good basis for evaluation of distortion effects.

The effects of distortion that can be used with any confidence are thus as follows:

	Nonbuoyant flow	Moderate Richardson number flow
Centre-line velocity	$\lambda_v^{1/2} \cdot \lambda_h^{-1/2}$ (too great)	$\lambda_v^{1/3} \cdot \lambda_h^{-1/3}$ (too great)
Centre-line temperature	$\lambda_v^{1/2} \cdot \lambda_h^{-1/2}$ (too great)	$\lambda_v^{1/3} \cdot \lambda_h^{-1/3}$ (too great)

Flow width	1 (correct)	$\lambda_v^{-1/3} \cdot \lambda_h^{1/3}$ (too small)
Thickness of flow	$\lambda_v^{-1} \cdot \lambda_h$ (too small)	$\lambda_v^{-1/3} \cdot \lambda_h^{1/3}$ (too small)

4. EFFECTS OF DISTORTION CALCULATED BY MEANS OF NUMERICAL MODELS

4.1 Numerical models used in the calculation

Effects of distortion in physical models are in this chapter calculated by numerical experiments using the PSD model (Shirazi and Davis 1974) and the Prych model (Prych 1972 a). These numerical models have been chosen in correspondence with an evaluation of mathematical models made by Dunn et al. (1975). They found that the PSD model was one of the two best models in predicting the general plume characteristics of warm-water discharges and also that the Prych model was best in calculating plume characteristics for laboratory conditions.

Method of calculation

The calculation has been made by using the models with input data simulating distortion. Since this is done numerically, no general expressions for effects of distortion can be given as was done in Chapters 2 and 3. The simulation of distortion is done by comparing two calculations where all input parameters, except outlet width, are identical and using outlet width as horizontal parameter and outlet height as vertical length parameter. Here a distortion of two is chosen, and the effects are obtained by dividing the results from one calculation by the results from another having twice as large outlet width. If no effects of distortion are present, this is given by the number one in this representation.

Effects of distortion for other distortions than two are simply obtained by taking the effects for a distortion of two raised to the power of the second logarithm of the actual distortion. Thus the effects of a distortion of 8 are obtained by taking the third power of the effects of a distortion of two.

The parameters that are studied here for effects of distortion are

- Areas within isotherms
- Centre-line excess temperature
- Thickness of warm-water flow.

4.2 The PSD model calculation

Together with the theoretical concepts and the program listing, Shirazi and Davis also present an extensive amount of calculations in diagram form. The diagram parameters are dimensionless with the following notation employed in this chapter

$$A = B_o/H_o = \text{aspect ratio of outlet}$$

$$K^x = \frac{K}{\rho c_p u_o} = \text{dimensionless surface heat exchange coefficient}$$

$$R = \frac{V}{u_o} = \text{relative ambient velocity}$$

$$V = \text{velocity of ambient flow.}$$

In the diagrams of Shirazi and Davis the horizontal length parameter is $s/\sqrt{H_o B_o}$, which made it necessary to transform the data to the more convenient parameter s/B_o . The diagram presentation was originally for the aspect ratios 1, 5, 10, and 15. Here the effects of distortion are studied by comparing results from aspect ratios 1-2, 3-6, and 8-16, making inter- and extrapolations necessary.

The effects of distortion are examined for areas within isotherms, centre-line excess temperature, and depth of warm-water flow. The different discharge conditions are

Ambient velocity perpendicular to ambient current
($R = 0.01, 0.1, \text{ and } 0.3$)

Outlet densimetric Froude number $F_\Delta = 2, 4, 6, \text{ and } 10$

Effects of distortion on areas within given isotherms

The calculation is here made for areas within isotherms, with the areas measured in the unit outlet width squared. In Figures 4.1a-c the effects of distortion on varying isotherms of excess temperature and different Froude numbers are given. No significant influence of having small or large aspect ratios could be seen from the data, so these are not represented in the figures.

Figure 4.1 a has data for an almost quiescent ambient fluid, $R = 0.01$, while Figure 4.1 b and c represent data for $R = 0.1$ and 0.3 .

In the figures the effects of a distortion of two according to the non-buoyant theory (Section 2.2) are presented, i.e. $\lambda_v \cdot \lambda_h^{-1} = 2$.

The general impression of these figures is that the effects of distortion are greater for high than for low densimetric Froude numbers, as could be expected from the discussions of Chapters 2 and 3. The more jet-type the warm-water flow is, i.e. high densimetric Froude number and close to the outlet, the greater the effects of distortion are. For the low densimetric Froude numbers the effects of distortion are even less than one. This is probably due to the influence of ambient diffusion that in the PSD model gives principally the same kind of effects of distortion as in channels with groins, as presented in Section 2.7, i.e. an overestimation of horizontal ambient diffusion. These effects are, as pointed out in Section 2.7, not general, and the given results should thus be used with care.

Effects of distortion on centreline excess temperature

A calculation of effects of distortion on centreline excess temperature is given in Figures 4.2 a-c. In the figures the effects of distortion according to Engelund's moderate Richardson number theory (Section 3.4) are given, i.e. $\lambda_v^{1/3} \cdot \lambda_h^{-1/3} = 2^{1/3} = 1.26$. The corresponding number for nonbuoyant jet theory is $\lambda_v^{1/2} \cdot \lambda_h^{-1/2} = 2^{1/2} = 1.4$.

For low densimetric Froude numbers the distortion seems to have very small effects. For high densimetric Froude numbers the effects of distortion are greater, especially for high ambient velocity and far from the outlet. In Figure 4.2 c data for $F_\Delta = 10$ and $s/B_o > 20$ is not present because this information was not available in the diagram presentation of Shirazi and Davis. The effects of distortion could, however, be expected to be greater with $F_\Delta = 10$ than $F_\Delta = 6$ as in the other figures.

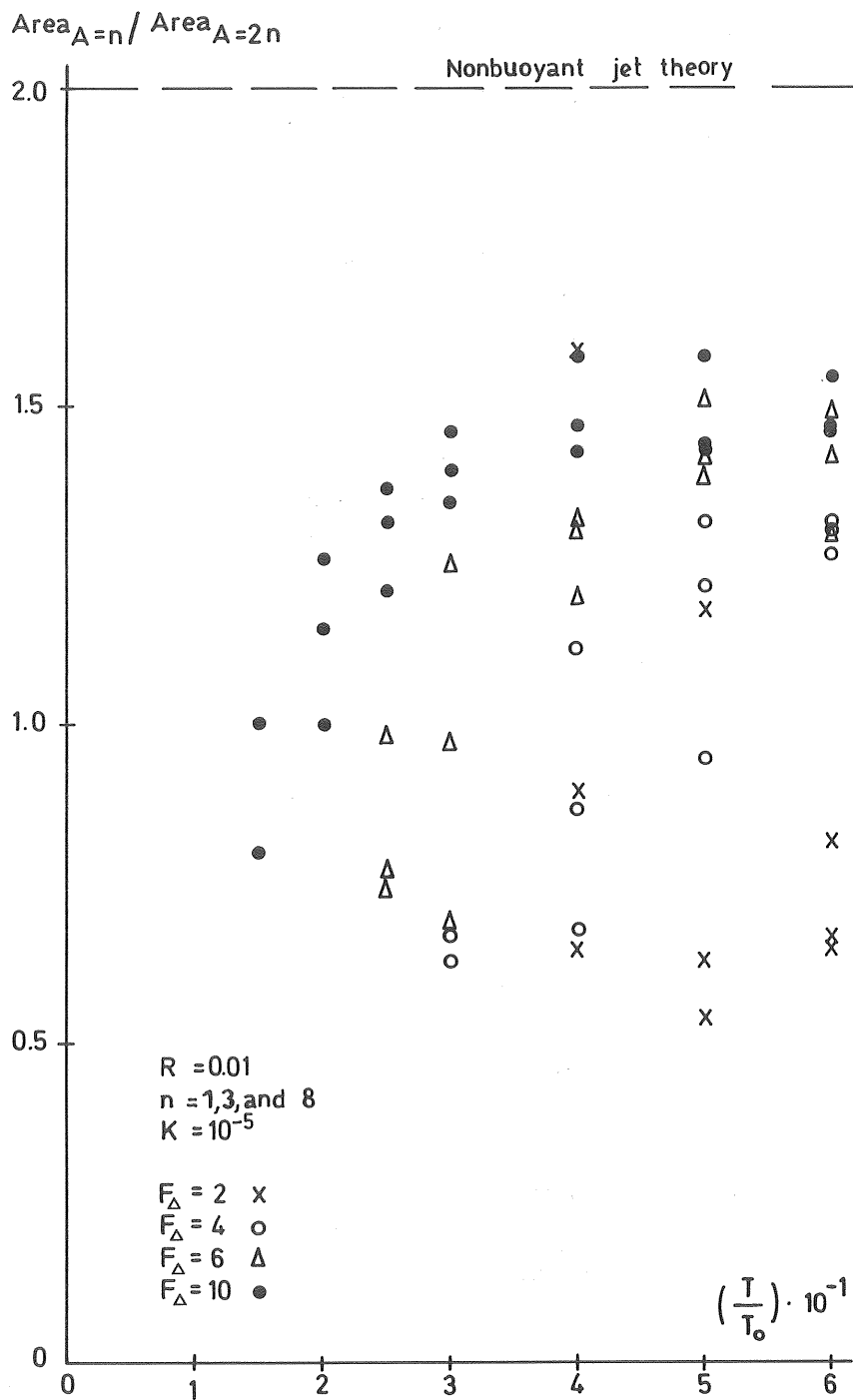


Figure 4.1a

Effects of a distortion of two on areas within isotherms. Calculation made with the PSD model data. The corresponding effects according to nonbuoyant jet theory are also given.

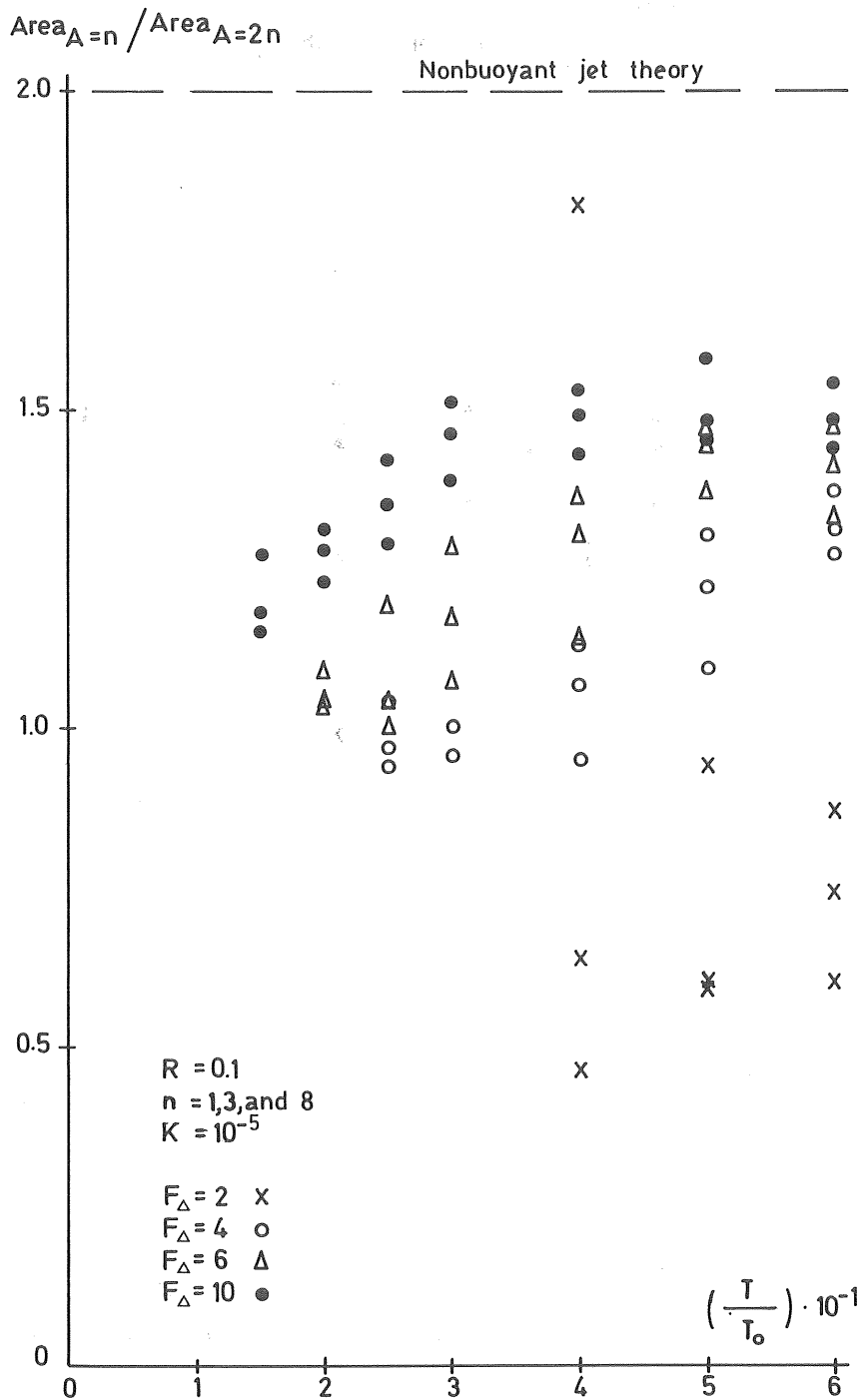


Figure 4.1b Effects of a distortion of two on areas within isotherms. Calculation made with the PSD model data. The corresponding effects according to nonbuoyant jet theory are also given.

$$\text{Area}_{A=n} / \text{Area}_{A=2n}$$

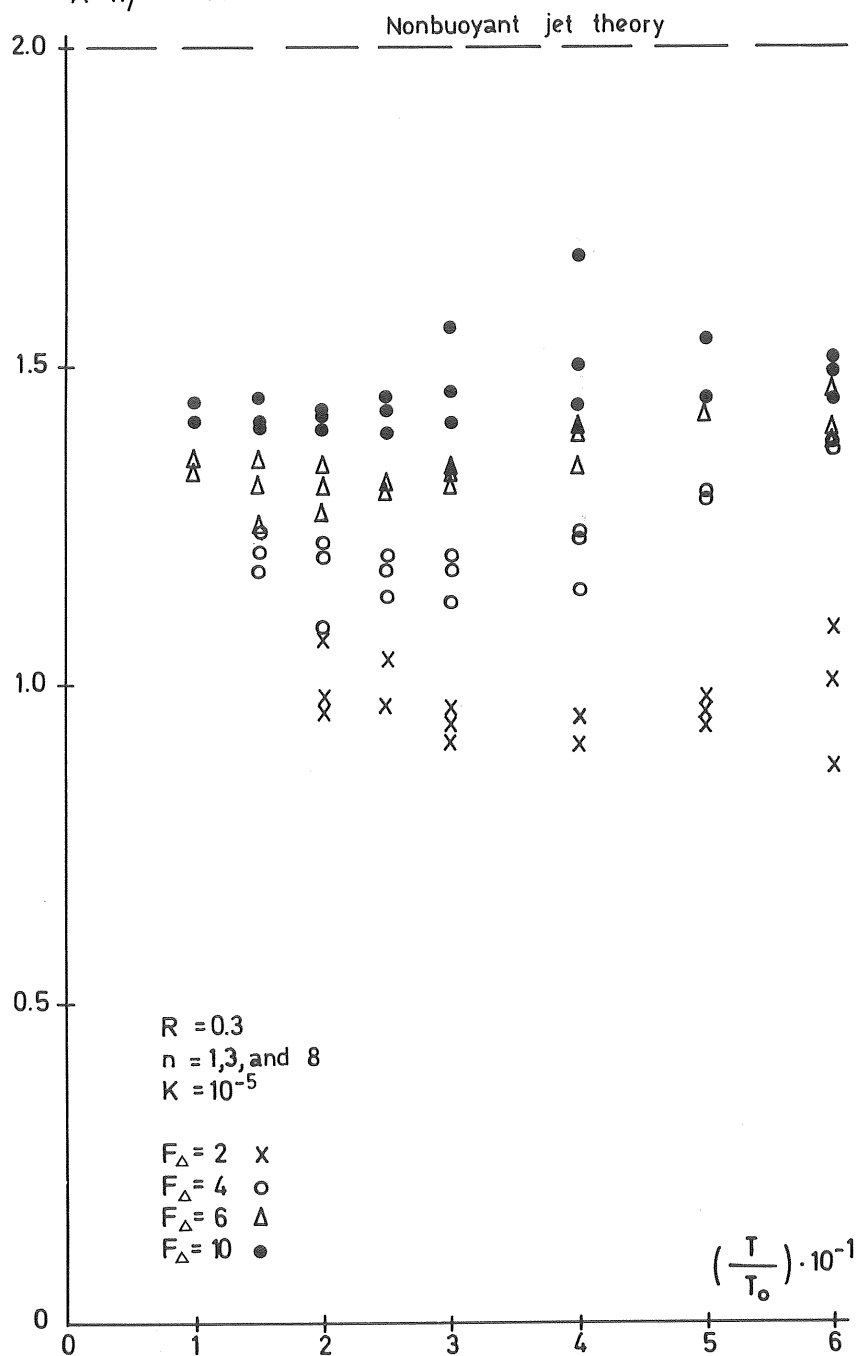


Figure 4.1c

Effects of a distortion of two on areas within isotherms. Calculation made with the PSD model data. The corresponding effects according to nonbuoyant jet theory are also given.

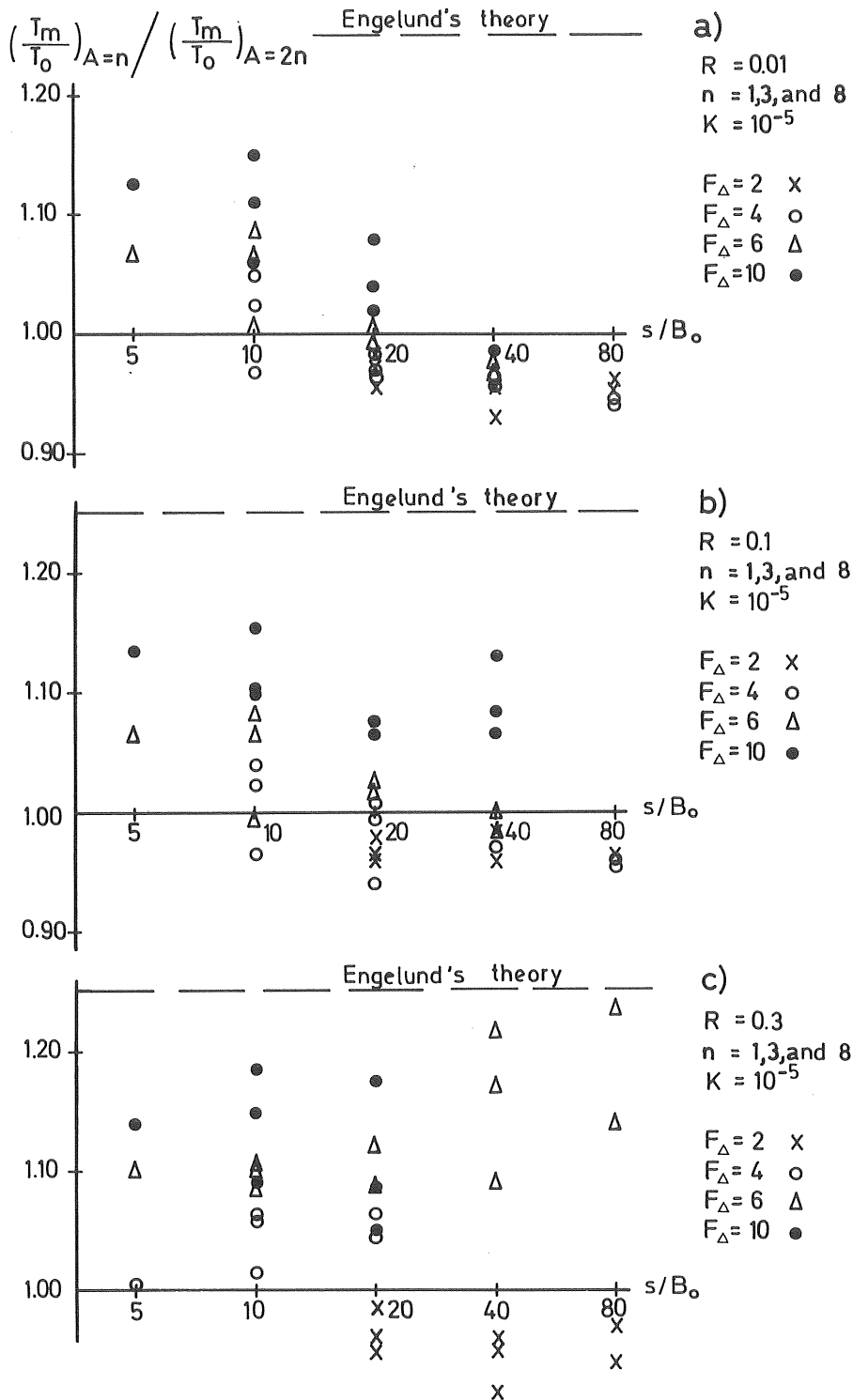


Figure 4.2 a-c Effects of a distortion of two on centre-line excess temperature at given distances from discharge. Calculation made with the PSD model data. The corresponding effects according to Engelund's moderate Richardson number theory are also given.

Effects of distortion on thickness of warm water flow

An examination of the effects of distortion on thickness of warm-water flow showed that the effects varied very little with distance from the outlet and also with outlet shape. The data presentation of Figure 4.3 is therefore based on mean values of effects of distortion for distances from the outlet of 10 to 40 B_o and for the aspect ratios $A = 1-2, 3-6$, and $8-16$. For low densimetric Froude numbers the effects of distortion are less than for high ones, where the correspondence with Engelund's moderate Richardson number theory is good. As can be seen, the thickness of the warm-water flow in a distorted model will be too small.

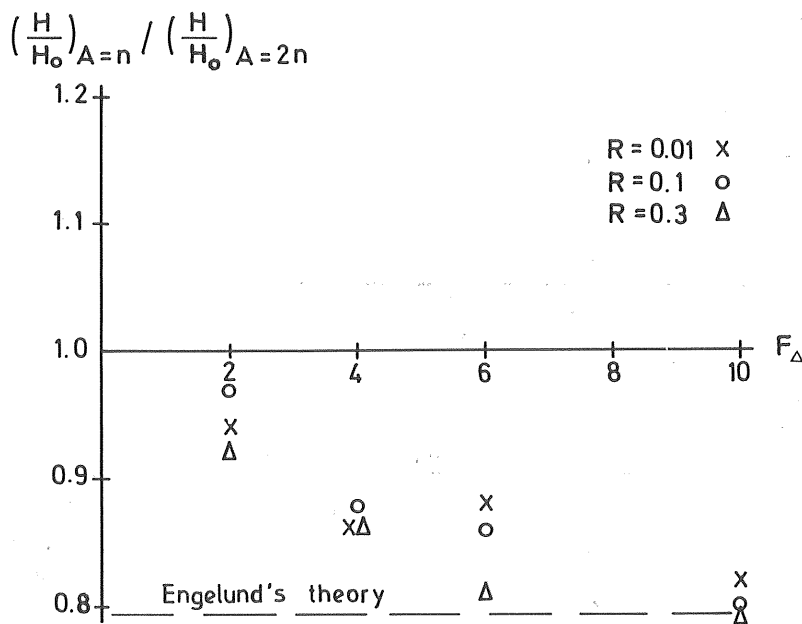


Figure 4.3

Effects of distortion of two on thickness of warm-water flow. Calculation made with the PSD model data. The corresponding effects according to Engelund's moderate Richardson number theory are also given.

Remarks

The PSD model is basically a jet-type integral model but also ambient diffusion is included. Discharges with as low densimetric Froude numbers as two are hardly considered as jet-type discharges and therefore the corresponding results are unreliable. Far from the outlet the flow becomes less and less jet-type even when the outlet densimetric Froude number is high. The ambient diffusion becomes more and more important the further away from the outlet the flow is studied. As discussed in Sections 2.7 and 2.8, there is no general way of treating ambient diffusion.

The PSD model works well for high ambient velocities, but problems occur for low ambient velocities. Therefore, Shirazi and Davis partly based their diagram presentation on extrapolated data. If the given remarks are taken into account, the results of the evaluation using the PSD model must be considered as just a rough guideline of what the effects of distortion are like for different parameters. Especially for low densimetric Froude numbers of the outlet, low ambient velocities, and locations far from the outlet, the results must be considered uncertain.

4.3 The Prych model calculation

The Prych model has been chosen partly because it reproduces laboratory data well and partly to avoid the difficulties that arise when ambient diffusion is included. To treat ambient diffusion correctly, one must have prototype data as discussed in Sections 2.7 and 2.8. No general way of treating ambient diffusion is thus available. Therefore, it is better to exclude it in the numerical model, which is done here. The data chosen for this calculation are for a discharge of 4 m height and outlet widths of 1, 2, 4, 8, 16, and 32 m corresponding to aspect ratios $1/4 - 8$. Initial density deficit is 2 kg/m^3 and Froude densimetric numbers are 2, 4, 8, and 16, corresponding to outlet velocities of 0.56 to 4.5 m/s. Ambient velocity was 0.2 m/s and perpendicular to the outlet velocity. Heat transfer to the atmosphere and ambient diffusion were zero.

The input data cover realistic discharge data for real plants under summer conditions in Sweden. No transformation to model scale has to be done since the Prych model with the given input data works

in accordance with the Froude modelling law.

The effects of distortion are obtained for a distortion of two by comparing results for aspect ratio $1/4$ with $1/2$, $1/2$ with 1 ... to 4 with 8 . All horizontal distances are measured in the unit outlet width and all vertical distances in the unit outlet height as in the analysis using the PSD model.

Effects of distortion on areas within isotherms

Areas within isotherms measured with the unit outlet width squared are studied, and effects of distortion have been calculated.

In Figure 4.4 the effects of distortion are given as mean values for distortion with aspect ratios varying from $1/4$ to 8 . The effects are given as a function of excess temperature for different outlet densimetric Froude numbers. The effects of distortion are greater for high densimetric Froude numbers than for low ones and decrease also with decreasing excess temperature.

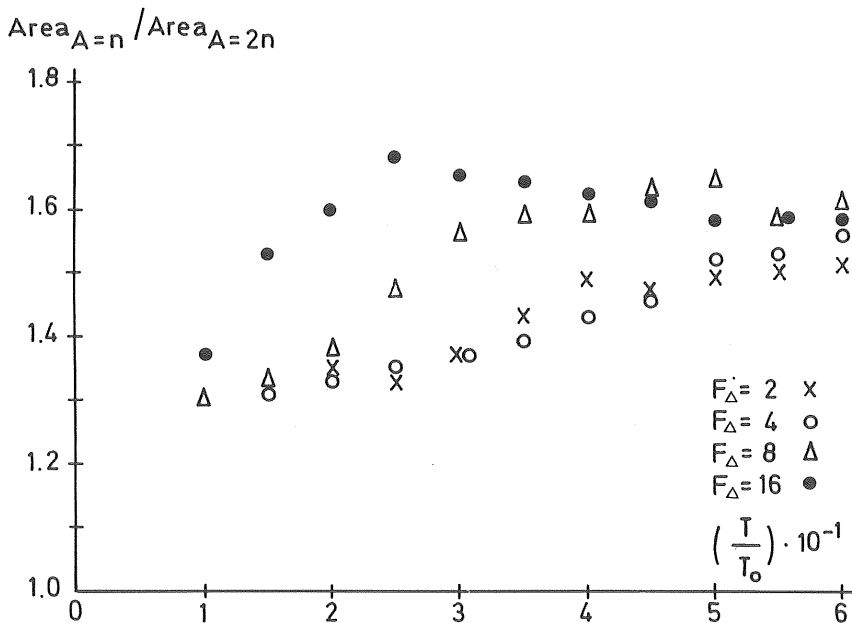


Figure 4.4 Effects of a distortion of two on areas within isotherms as a mean value of aspect ratios $A = 1/4-8$ for different isotherms. Calculation made with the Prych model. Nonbuoyant jet theory gives a corresponding number of 2.0.

The effects of different outlet shapes are shown in Figure 4.5, where the points represent mean values for effects of distortion over the range of 0.2 - 0.6 of excess temperature, T/T_0 . The effects of distortion are greater for low aspect ratios than for high ones, which is especially significant for low densimetric Froude numbers.

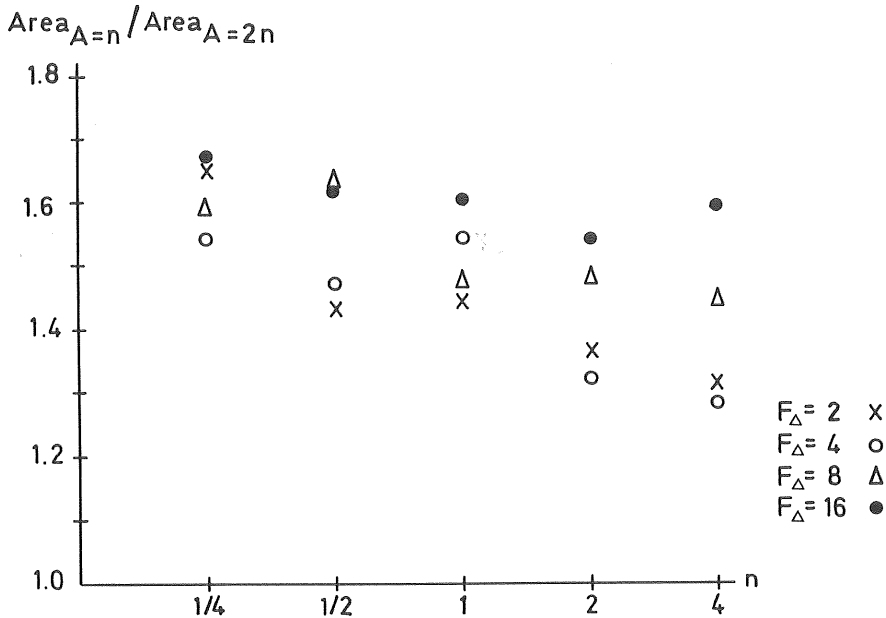


Figure 4.5 Effects of a distortion of two on areas within isotherms as a mean value for the relative excess temperatures $T/T_0 = 0.2-0.6$. Calculation made with the Prych model. Nonbuoyant jet theory gives a corresponding number of 2.0.

Effects of distortion on centre-line excess temperature

The effects of distortion on excess centreline temperature have been examined at different distances from the outlet in Figure 4.6 and for different aspect ratios in Figure 4.7.

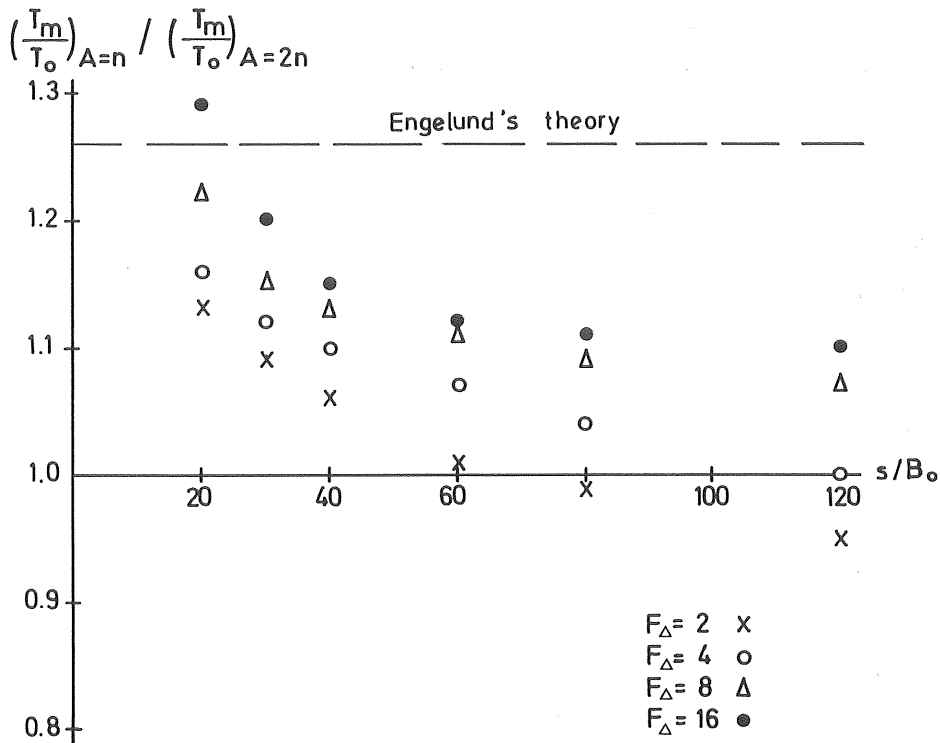


Figure 4.6 Effects of a distortion of two on centre-line excess temperature as a mean value of aspect ratios $A = 1/4-8$ at different distances from outlet. Calculation made with the Prych model. The effects according to Engelund's moderate Richardson number theory are also given.

In Figure 4.6 each point represents a mean value of effects of distortion corresponding to aspect ratios $A = 1/4 - 8$. The figure shows that effects of distortion are greater close to the outlet than far away and that they are greater for high densimetric Froude numbers than for low ones. The latter fact is also shown in Figure 4.7, where the points represent mean values of effects of distortion for distances of 20 to 120 times outlet width. For small numbers of aspect ratio the effects of distortion are greater than for large ones.

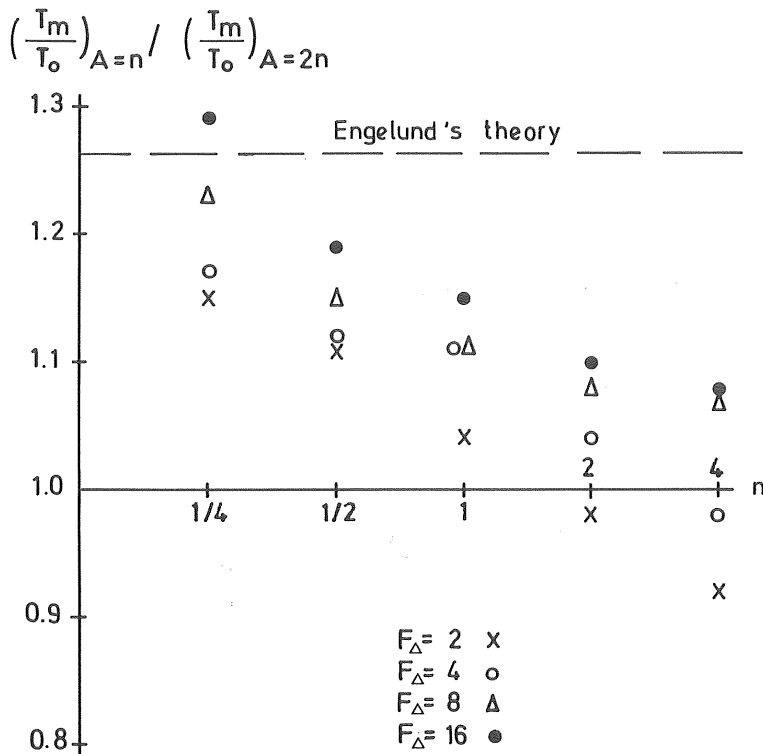


Figure 4.7 Effects of a distortion of two on centre-line excess temperature as a mean value at distances $s/B = 20-120$ for different aspect ratios. Calculation made with the Prych model. The effects according to Engelund's moderate Richardson number theory are also given.

Effects of distortion on thickness of warm-water flow

The effects of distortion on thickness of warm-water flow are given in Figure 4.8 at distances from the outlet of 20, 30, 40, 60, 80, and 120 times outlet width. The points represent mean values for aspect ratios from $1/4$ to 8 and show that the effects of distortion in general are less than unity, thus giving results of measurements in distorted models that are too small. The effects of distortion are most significant close to the discharge. For high densimetric Froude numbers the effects also differ more from unity than for low densimetric Froude numbers.

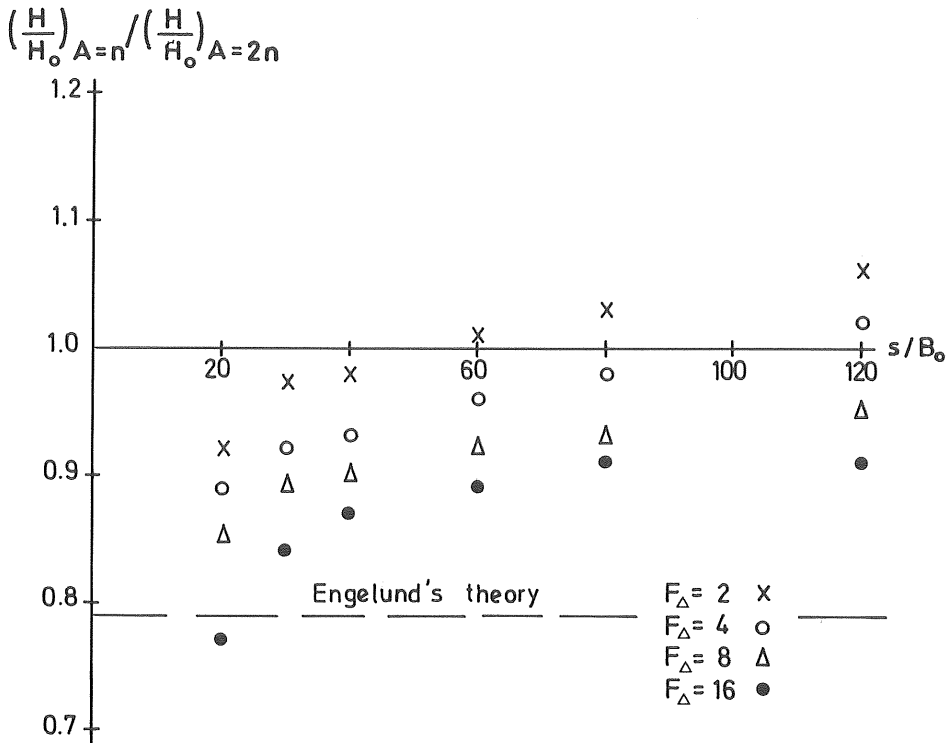


Figure 4.8 Effects of a distortion of two on thickness of warm-water flow as a mean value of aspect ratios $A = 1/4-8$ at different distances from the outlet. Calculation made with the Prych model. The effects according to Engelund's moderate Richardson number theory are also given.

Remarks

Like the PSD-model, the Prych model is basically a jet-type model and since the flow for a densimetric Froude number of 2 hardly can be considered of jet-type the corresponding results are uncertain. The treatment of the jet development zone is a very criticized part of the model. There are thus reasons to be wary of all results close to the discharge, which also means those for high excess temperatures.

Ambient diffusion is important far from the discharge. The effects of distortion are calculated here with consideration only given to

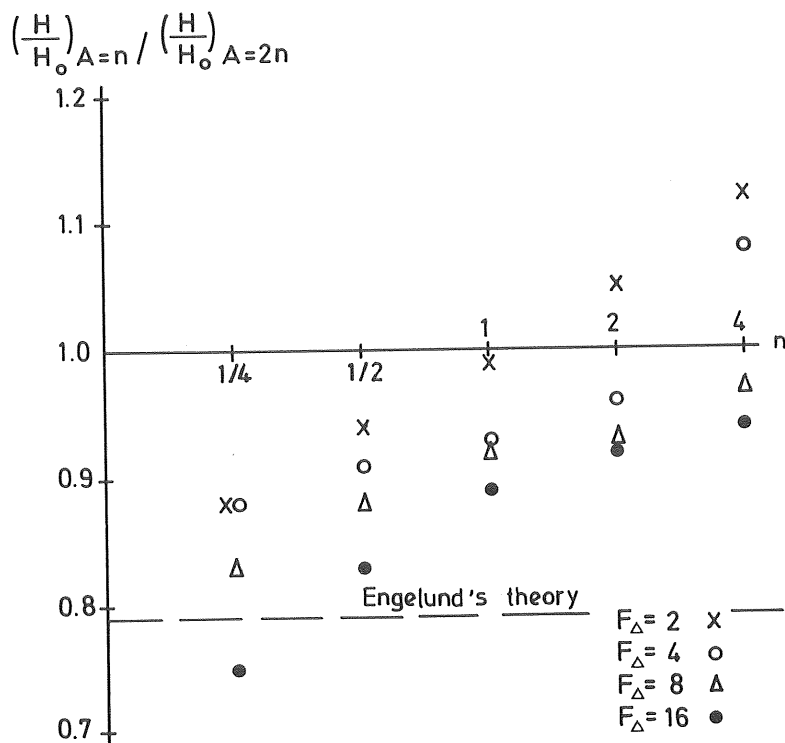


Figure 4.9 Effects of a distortion of two on thickness of warm-water flow as a mean value for distances of 20-120 times outlet width for different aspect ratios. Calculation made with the Prych model. The effects according to Engelund's moderate Richardson number theory are also given.

effects of the jet diffusion and the buoyancy spread. The given diagrams thus give only a rough idea of the effects of distortion.

4.4 Conclusions

The effects of distortion have been calculated by means of numerical models for warm-water discharges. A corresponding analysis was made in Chapter 3, where analytical models were used. The

results of the calculations using different models will be compared here. The parameters that can be compared are those for centre-line excess temperature and warm-water flow depth. Since the results of numerical models show a significant dependence on densimetric Froude number and aspect ratio, the comparison will be made for mean values of a set of data according to Table 4.1.

Table 4.1 Effects of a distortion of two calculated by means of theoretical models.

Theoretical model	Centre-line excess temperature	Thickness of warm-water flow
Nonbuoyant jet	$2^{1/2} = 1.4$	$2^{-1} = 0.5$
Moderate Richardson number flow (Engelund)	$2^{1/3} = 1.26$	$2^{-1/3} = 0.8$
PSD $F_{\Delta} = 2-4$ R=0.1 $A_{\Delta} = 1-16$	0.95 - 1.05	0.87 - 0.97
PSD $F_{\Delta} = 6-10$ R=0.1 $A_{\Delta} = 1-16$	1.0 - 1.25	0.80 - 0.85
Prych $F_{\Delta} = 2-4$ $A_{\Delta} = 1/4-1$	1.04 - 1.17	0.88 - 0.99
Prych $F_{\Delta} = 2-4$ $A_{\Delta} = 2-8$	0.92 - 1.04	0.96 - 1.12
Prych $F_{\Delta} = 8-16$ $A_{\Delta} = 1/4-1$	1.13 - 1.30	0.75 - 0.92
Prych $F_{\Delta} = 8-16$ $A_{\Delta} = 2-8$	1.08 - 1.10	0.91 - 0.97

The nonbuoyant theory gives, as expected, results that show greater effects of distortion than other theories. The theory for moderate Richardson number flow by Engelund and the Prych model for large densimetric Froude numbers and small aspect ratios give results that are quite similar.

For physical modelling of a surface warm-water discharge with a densimetric Froude number of 10-15 and a deep receiving water body it is reasonable to believe that the effects of distortion are of the correct order as given according to the theory by Engelund or to the Prych model. The calculations using the PSD model are, as pointed out earlier, less reliable.

5. EFFECTS OF DISTORTION DETERMINED BY MEANS OF LABORATORY EXPERIMENTS

5.1 Laboratory investigations of surface warm-water jets

During the last decade several investigations of surface buoyant jets have been made, covering different numbers of aspect ratio, outlet densimetric Froude number and relative ambient velocity. In most of the studies the temperature along the jet centre-line has been the main parameter investigated. Most of the data have been collected and presented by Shirazi (1973).

There exist only a few investigations where the aspect ratio is the only parameter varied making it possible to use the data for a determination of effects of distortion in a way similar to what was done in Chapter 4. Besides, the available data are not presented in a form suitable for such a determination. Thus a transformation of the length parameter to the unit outlet width has been done.

The investigations used in this determination are listed in Table 5.1 together with the most important discharge parameters. All data are for a deep receiving body of water with no influence from the bottom.

Table 5.1 Laboratory investigations used for determination of effects of distortion.

Source	Densimetric Froude number	Aspect ratio	Rel ambient current	Fig.	Comment
Stolzenbach and Harleman (1971a)	1.03 1.83 1.42	2.44 2.30 0.46	0 0 0	5.1 " "	} Weighted to give $F_{\Delta}=1.4$ and $A=2.4$
"	4.4 5.22 6.53 6.60	5.8 2.36 1.56 0.51	0 0 0 0	5.2 " " "	
Carter and Regier (1974)	9.90 9.66 11.34	1.94 0.974 0.396	0.32 0.28 0.22	5.3 " "	The ambient current \perp to discharge flow
Wiegel et al. (1964)	22-28 22-28	10 4	0 0	5.4 "	Data from several different measurements

The data are presented in diagrams with log-log scales for relative centre-line excess temperature, T/T_o , versus distance from outlet, s/B_o . Data for the core region of the jet have been excluded. Data points obviously falling outside the normal spread of data have also been neglected. Such points have been marked by a parenthesis. For each group of data a straight line has been fitted using the method of least squares, and these lines are used for the determination of effects of distortion.

The experimental results presented in Figures 5.1 - 5.4 represent different distortions. The effects of distortion determined here are all transformed to hold for a distortion of two so that a comparison with results from Chapter 4 is made possible. An example showing how this is done is taken from Section 5.3. The experiment with $F_{\Delta} = 6.60$ and $A = 0.512$ may be regarded as a reproduction of the experiment with $F_{\Delta} = 6.53$ and $A = 1.56$ at a distortion of $1.56/0.512 \approx 3.1$. For the centre-line excess temperature at a distance of $20 B_o$ from the outlet, the effects of distortion lead to a temperature that is too great by a factor of 1.22. The number of times a distortion of two must be applied to give a distortion of 3.1 is ${}^2\log 3.1$. If the effects of a distortion of two are called x , then the effects of a distortion of 3.1 are given as $x^{2\log 3.1}$, and in this case this number is equal to 1.22. The effects of a distortion of two are accordingly calculated to be 1.13.

5.2 Laboratory data for $F_{\Delta} \approx 1.4$

In Figure 5.1 the data for $F_{\Delta} = 1.03$ and $A = 2.44$ have been plotted with the data for $F_{\Delta} = 1.83$ and $A = 2.30$, and the line fitted to these sets of data is presumed to represent $F_{\Delta} = 1.4$ and $A = 2.4$. The scattering of the data is small enough to justify this approximation. A comparison of this line with the line fitted to the data for $F_{\Delta} = 1.42$ and $A = 0.46$ shows that the centre-line temperatures are almost the same in both cases, although a distortion as large as 5 is present. This also seems likely considering the low value of the densimetric Froude number indicating that buoyancy is important. This means that the vertical entrainment is reduced and relatively unimportant unlike what is the case for a nonbuoyant jet (see Section 2.4).

The agreement is good between this experimental result and that based on calculations using the Prych model. For $F_{\Delta} = 2$ and $A = 0.5-2$ a distortion of two gives a centre-line excess temperature that is too great by a factor of 1.07 (see Figure 4.7). For $F_{\Delta} = 1.4$ this number is probably very close to 1.00. (Nonbuoyant jet theory gives a centre-line excess temperature that is too great by a factor of 1.41.)

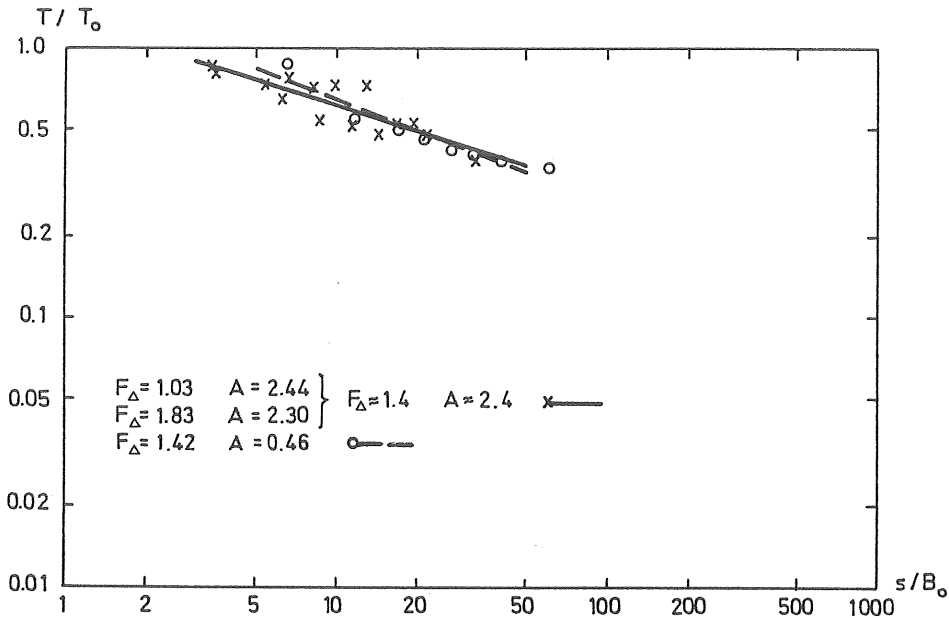


Figure 5.1 Centre-line excess temperature versus distance from outlet for $F_{\Delta} \approx 1.4$, $A = 2.4$, and $F_{\Delta} = 1.42$, $A = 0.46$ comparable to a distortion of 5. Data from Stolzenbach and Harleman (1971 a).

5.3 Laboratory data for $F_{\Delta} \approx 6$

In Figure 5.2 the data for densimetric Froude numbers 4.4, 5.22, 6.53, and 6.60 with the aspect ratios 5.8, 2.36, 1.56, and 0.51, respectively, are presented. As can be seen the temperature decrease for $F_{\Delta} = 4.4$ is quite different from that of the others, which probably is due to the difference, however small, in the densimetric Froude number. This set of data is therefore excluded in the analysis.

The experiment with $F_{\Delta} = 6.53$ and $A = 1.56$ reproduces the experiment with $F_{\Delta} = 5.22$ and $A = 2.36$ at a distortion of $2.36/1.56 \approx 1.5$. This distortion and possibly the variation of F_{Δ} make the centre-line excess temperature too great by a factor of 1.16 - 1.23 at a distance of 10-50 B_0 from the outlet. For a distortion of two this result corresponds to a factor of 1.29 - 1.42.

The experiment with $F_{\Delta} = 6.60$ and $A = 0.51$ reproduces the experiment with $F_{\Delta} = 6.53$ and $A = 1.56$ at a distortion of $1.56/0.51 = 3.1$, which results in a centre-line excess temperature that is too great by a factor of 1.22 - 1.38 at a distance of 20-50 B_0 from the outlet. For a distortion of two the corresponding number is 1.13 - 1.22.

As reported in Chapter 3 nonbuoyant jet theory gives a centre-line excess temperature that is too great by a factor of $2^{1/2} = 1.41$ for a distortion of two, and Engelund's moderate Richardson number theory gives a corresponding number of $2^{1/3} = 1.26$. The results

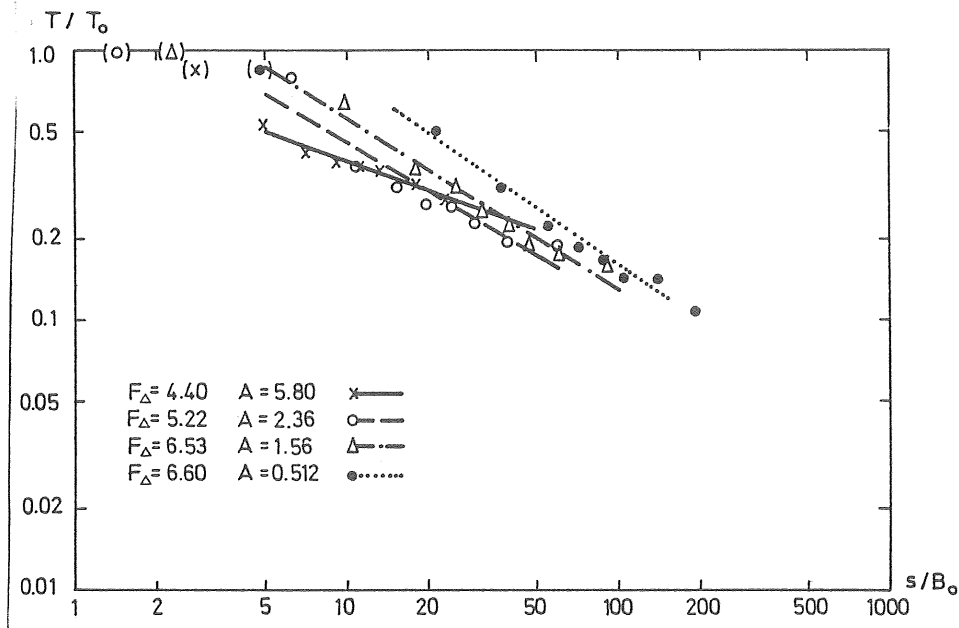


Figure 5.2 Centre-line excess temperature versus distance from outlet for $F_{\Delta}=4.4$, 5.22, 6.53, and 6.60, and $A=5.80$, 2.30, 1.56, and 0.51, respectively. Data from Stolzenbach and Harleman (1971 a).

obtained using the Prych model (Figure 4.7) show for $F_{\Delta} = 6$ and $A = 1/2-2$, a centre-line excess temperature that is too great by a factor of approximately 1.1. The experimental determination of effects of distortion as a mean value agrees very well with the theoretical evaluation using Englund's theory. The nonbuoyant theory gives, as indicated by the low value of the densimetric Froude number, effects that are too large, while the calculations using the Prych model give effects that are too small.

5.4 Laboratory data for $F_{\Delta} \approx 10$

In Figure 5.3 the data for $F_{\Delta} = 9.90, 9.66$ and 11.34 with $A = 1.94, 0.974$, and 0.396 are presented. The experiments are performed with a perpendicular ambient current having a relative velocity, V/u_o , of approximately 0.3.

The experiment with $F_{\Delta} = 9.66$, $A = 0.974$, and $V/u_o = 0.28$ reproduces the experiment with $F_{\Delta} = 9.90$, $A = 1.94$, and $V/u_o = 0.32$ at a distortion of $1.94/0.974 = 2.0$. The distortion leads to a centre-line excess temperature that is too great by a factor of 1.31 - 1.33 at a distance of 5-100 B_o from the outlet.

The experiment with $F_{\Delta} = 11.3$, $A = 0.396$, and $V/u_o = 0.22$ reproduces the experiment with $F_{\Delta} = 9.66$, $A = 0.974$, and $V/u_o = 0.28$ at a distortion of $0.974/0.396 = 2.46$. This distortion leads to a centre-line excess temperature that is too great by a factor of 1.0 - 1.44 at a distance of 10-100 B_o from the outlet. The corresponding factor for a distortion of two is 1.0 - 1.32. As seen in Figure 5.3, the slope of the line representing the data for $F_{\Delta} = 11.3$ is steeper than the slopes of the other lines, which is due to the somewhat higher densimetric Froude number and possibly also the lower relative ambient velocity. Increasing densimetric Froude numbers mean that the slope of the line representing centre-line excess temperature increases until the nonbuoyant case is reached for which the slope is 1:1 (see Figure 2.2). This effect makes the last determination less reliable.

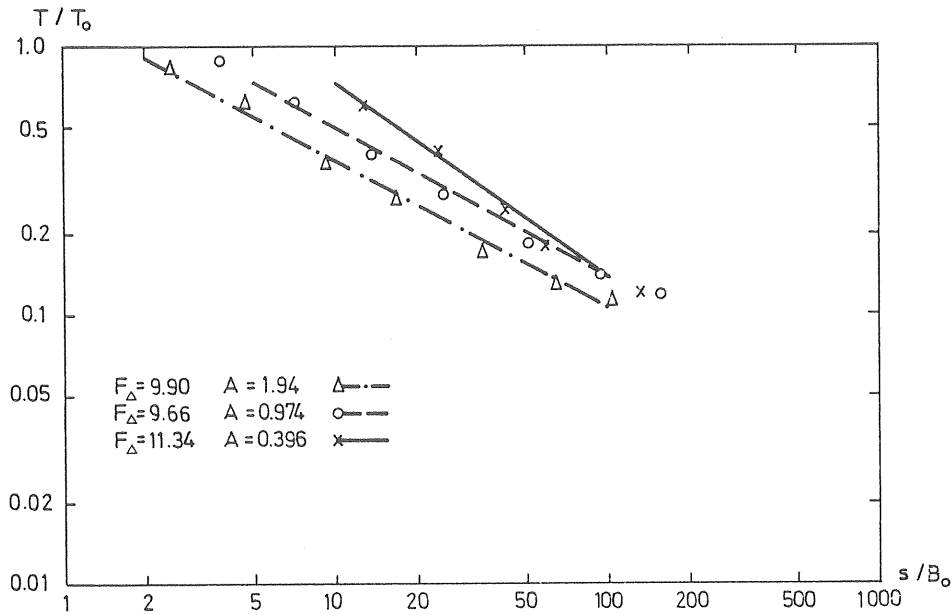


Figure 5.3 Centre-line excess temperature versus distance from outlet for $F_\Delta=9.90$, 9.66 and 11.34 and $A=1.94$, 0.974 and 0.396 respectively, with relative ambient velocity $R \approx 0.3$. Data from Carter and Regier (1974).

The agreement between effects of distortion on centre-line excess temperature as evaluated using Engelund's moderate Richardson number theory and the first experimental determination made here is good, 1.26 compared with 1.31 - 1.33. The relatively high densimetric Froude numbers make the flow more like a nonbuoyant jet, making the evaluation using nonbuoyant jet theory, 1.41, agree better than for discharges with low densimetric Froude numbers. The effects of distortion calculated with the Prych model (Figure 4.7) give a centre-line excess temperature that for $F_\Delta = 10$ and $A = 1$ is too great by a factor of 1.13 taken as a mean value at distances of 20-120 B_0 from the outlet.

5.5 Laboratory data for $F_{\Delta} \approx 25$

In figure 5.4 the data for $F_{\Delta} = 22-28$ and $A = 10$ and the data for $F_{\Delta} = 22-28$ and $A = 4$ are presented. Both sets of data represent several experiments, which explains the spread of the data. The experimental measurements are taken from Shirazi (1973) and not from the original reference, Wiegel et al. (1964). Two points in Figure 5.4 that obviously do not correspond to the others have been excluded. These points have also been excluded by Tamai et al. (1969) in another diagram presentation of the same set of data.

The experiment with $A = 4$ reproduces the experiments with $A = 10$ at a distortion of $10/4 = 2.5$. This distortion leads to a centre-line excess temperature that is too great by a factor of 1.11 - 1.35 at a distance of 10-50 B_o from the outlet. For a distortion of two the corresponding number is 1.08 - 1.25. A diagram representation of the same data by Wiegel et al. (1966) gives a centre-line excess temperature that is 1.15 too great for a distortion of two. The determination made here is uncertain because the spread of data is great compared with the difference between the two lines used for the determination.

The agreement is bad between this determination of effects of distortion, 1.08 - 1.25, and the theoretical evaluations using nonbuoyant jet theory, 1.41, and Engelund's moderate Richardson number theory, 1.26, and also compared with the calculations using the Prych model in Figure 4.7, giving 1.08 for $F_{\Delta} = 16$ and $A = 4$. For $F_{\Delta} = 25$ the calculation with the Prych model should, however, give a greater number. In Figure 4.7 the effects of distortion decrease significantly with increasing aspect ratio, and this relation leads to the nonagreement between the experimental determination and the theoretical evaluations of the effects of distortion. With respect to the large densimetric Froude number, nonbuoyant jet theory is otherwise likely to give a result that agrees well with the experimental determination.

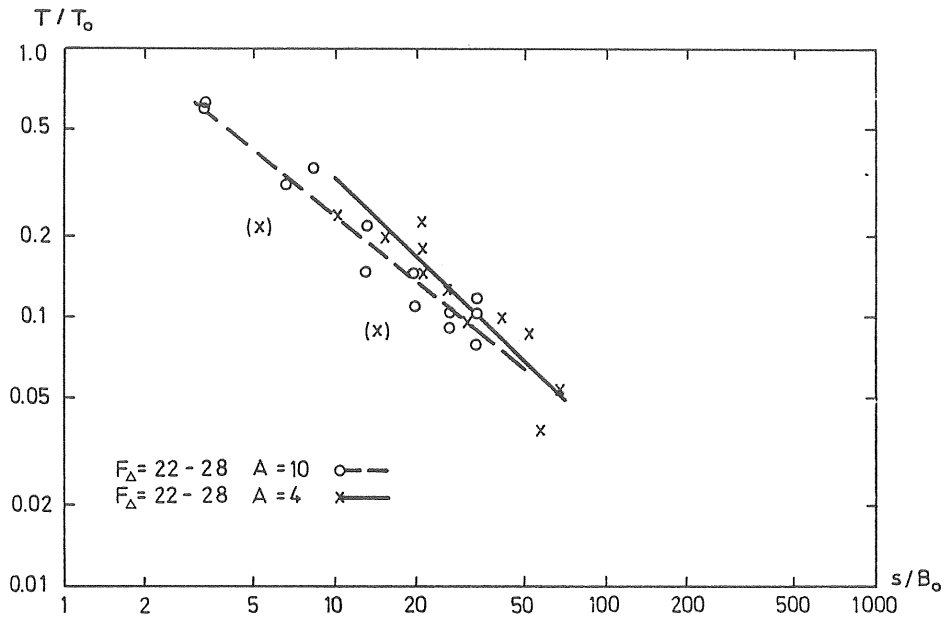


Figure 5.4 Centre-line excess temperature versus distance from outlet for $F_{\Delta}=22-28$ and $A=2.5$ and 10 . Data from Wiegél *et al.* (1964).

5.6 Conclusions

The results of the analysis of laboratory data that has been made in this chapter are shown in the following table together with the corresponding results using nonbuoyant jet theory, Engelund's moderate Richardson number theory, and the Prych model.

For a low densimetric Froude number ($F_{\Delta} \leq 2$) effects of distortion are small or negligible according to the experimental determination as well as the calculations using the Prych model. The evaluations using nonbuoyant jet theory and Engelund's moderate Richardson number theory are not applicable to this case and would give effects of distortion that are far too great.

Table 5.2 Effects of a distortion of two on centre-line
excess temperature T/T_o .

	$F_{\Delta} \quad 1.4$ $A=0.5-2.4$	$F_{\Delta} \quad 6$ $A=0.5-2.4$	$F_{\Delta} \quad 10$ $A=1.0-1.9$	$F_{\Delta} \quad 25$ $A=4-10$
Laboratory	~ 1.0	1.1-1.4	~ 1.3	1.1-1.2
Nonbuoyant jet theory	1.41	1.41	1.41	1.41
Engelund's moderate Richardson number theory	1.26	1.26	1.26	1.26
The Prych model (Figure 4.7 showing (for $F_{\Delta}=2$) mean values for $s/B_o=20-120$)	1.07	1.1	1.13	1.08 (for $F_{\Delta}=16$)

For a densimetric Froude number of 6 to 10 the evaluation using Engelund's theory gives results that agree well with the experimental determination, while the nonbuoyant theory gives too large effects of distortion. The calculations using the Prych model give effects of distortion that are too small.

For a densimetric Froude number of 25 and an aspect ratio of 4 to 10, the experimental determination gives effects of distortion that are smaller than the effects evaluated with nonbuoyant jet theory and Engelund's theory. The calculations using the Prych model, although giving too small effects, indicate that a large aspect ratio decreases the effects of distortion.

6. MODEL-PROTOTYPE COMPARISONS

6.1 Introduction

In this chapter the effects of distortion are studied by comparisons of model and field measurements of cooling-water discharges. Such comparisons do not give the effects of distortion separately but also other effects of incorrect scaling such as influence of laminar flow, incorrect modelling of ambient diffusion, and inconsistent currents of model and prototype. The effects of distortion are unfortunately impossible to separate from the other effects of modelling.

Presentations of model and prototype measurements of warm-water surface discharges are few, and for the available cases the data on discharge conditions are often incomplete. Besides the spread of the measured data is often great in model as well as in prototype, making the comparisons uncertain.

An example showing the difficulties in a model-prototype comparison (Figure 6.1) is taken from an investigation of cooling-water discharges in Hong Kong Harbour (Ackers 1969). The model scales are 1:250 horizontally and 1:50 vertically giving a distortion of 5. Model measurements were made for a stationary cross-current, while the prototype measurements were made during the corresponding tidal phase having similar currents. The discharge from plant A is $2.4 \text{ m}^3/\text{s}$ and from plant B $6.8 \text{ m}^3/\text{s}$.

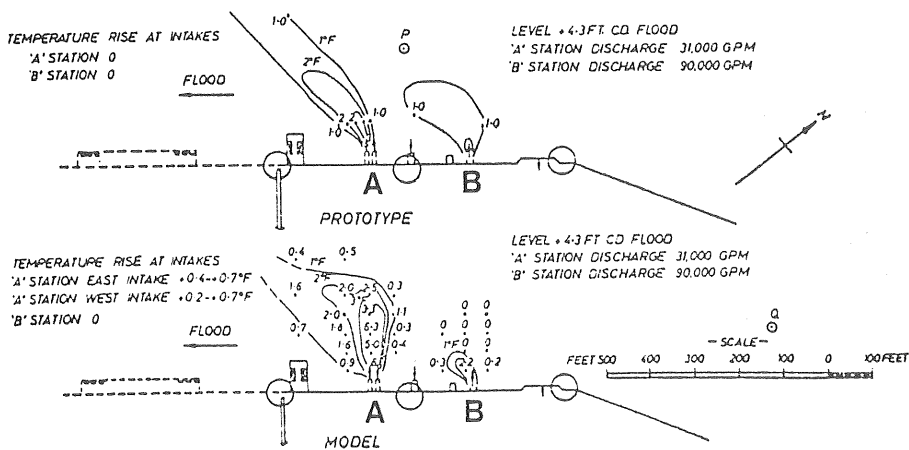


Fig. 6.1 Temperature distribution at Hongkong Harbour according to the prototype and the model measurements. Observe the different reproduction in the model of the two discharges. Adapted from Ackers (1969).

A comparison of model and prototype measurements gives directly the inconsistent result that for one discharge the model gives too large a spread of warm water while for the other discharge it gives a spread that is too small. As no detailed outlet data are given, it is impossible to give an explanation of the phenomenon, but one theory is that outlet B is submerged.

6.2 Model-prototype comparison for Berkeley Power Station

Ackers (1969) and Ackers and Jaffrey (1973) have presented a model-prototype comparison for the discharge from Berkeley Power Station (300 MW) on the Severn Estuary. The discharge of $28 \text{ m}^3/\text{s}$ is situated behind a baffle wall that effectively reduces initial momentum (Figure 6.2). The model scales are 1:480 horizontally and 1:60 vertically, giving a distortion of 8. According to the authors the model reproduces both the currents and the water-level fluctuations of the tidal estuary.

For the area inside the baffle wall the geometry governs to a great extent the flow, which will be of an irregular three-dimensional nature. How the distortion affects this kind of flow is impossible to foresee.

When the warm water leaves the area inside the baffle wall the direction of flow is completely changed, and the initial momentum is lost. The flow is thus in the far-field. The processes governing the spread of the warm water are then heat transfer to the atmosphere, buoyancy spread, convective heat transport, and horizontal and vertical ambient diffusion. The measurements shown in Figure 6.2 indicate that the areas within isotherms are small enough for surface heat transfer to be negligible. Buoyancy spread (Section 2.5) can theoretically be modelled in a distorted model. This is also the case for convective heat transport by ambient currents (Section 2.6) especially after calibration in model against prototype measurements. The modelling of ambient diffusion is on the other hand much affected by a distortion (see Sections 2.7 and 2.8). In the present case the turbulence is probably generated by friction against the bottom. The horizontal ambient diffusion will then be too great in a distorted model, giving too large a lateral spread and too low a centre-line excess temperature of the warm water. The vertical

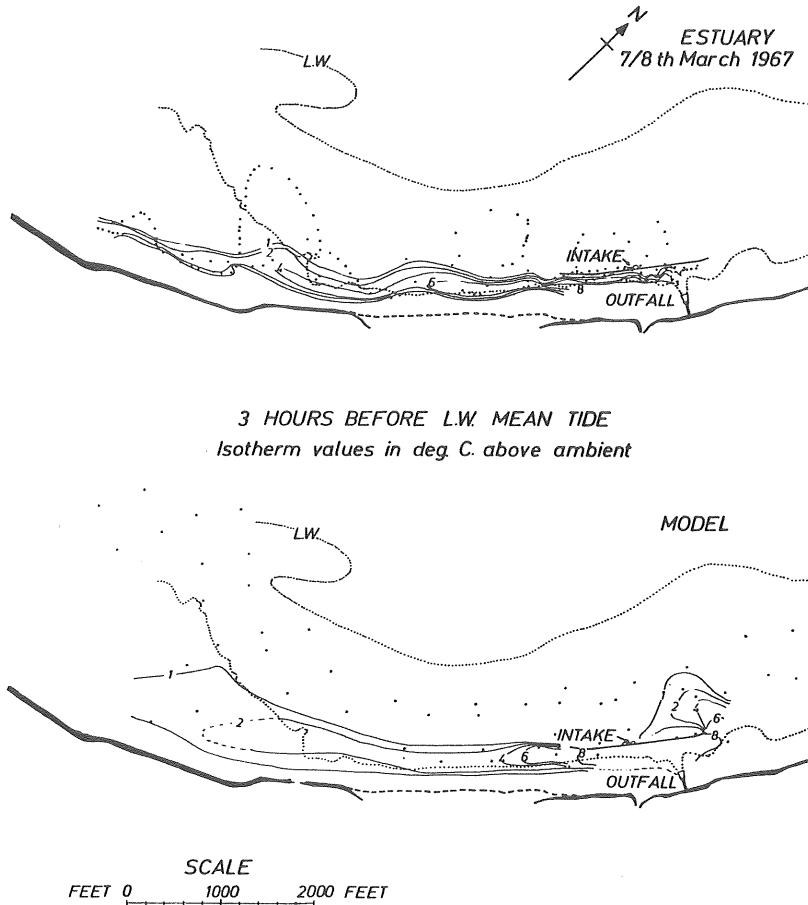


Figure 6.2 Temperature survey at Berkeley Power Station.
Comparison of prototype and model results.
Adapted from Ackers (1969).

ambient diffusion, on the other hand, will be too small in a distorted model, giving too high a centre-line excess temperature. The effects of distortion on the horizontal ambient diffusion are, however, much greater than on the vertical one, which means that the centre-line excess temperature will be too low in the distorted model.

The conclusions that theoretically can be drawn for the far-field are thus:

In the model the warm water will flow in the same way as in the prototype.

In the model the warm water will spread too much in the lateral direction.

In the model the centre-line excess temperature will be too small.

In the model the vertical spread will be too small but this effect is less pronounced.

The conclusions made are mainly based on equations and relations for stationary conditions, while the model-prototype comparison is made for unsteady conditions. In principle, this fact will not change the conclusions. The boundary condition in the form of warm-water flow into the far-field should, however, be the same in the model and in the prototype. This is not the case here, but as can be seen in Figure 6.2, the differences between model and prototype measurements in the far-field are much too great to be caused by only the difference in the spread inside the baffle wall.

The comparison of model and prototype measurements gives the following results:

Near-field

Inside the baffle wall the warm-water flow in the model is wider than it is in the prototype.

Far-field

The main flow pattern is the same in the model and in the prototype.

The centre-line excess temperature is too low in the model.

The lateral spread is too great in the model.

The theoretical conclusions and the model-prototype comparison agree well. The conclusion regarding vertical spread cannot be checked, since the only data that are given are the surface temperatures. Unfortunately, there are insufficient data from the model and the prototype to make a quantitative estimation possible, but as can be seen, the qualitative agreement is good.

6.3 Model-prototype comparisons for Ringsend and Pigeon House Power Stations, Dublin

Ackers (1969) and Ackers and Jaffrey (1972) have presented two model-prototype comparisons for two discharges in Dublin Harbour. The model scales are 1:300 horizontally and 1:50 vertically, giving a distortion of 6. The tide as well as the salinity distribution caused by a river outflow in the harbour is reproduced in the model. The model roughness is adjusted to reproduce measured vertical and horizontal salinity gradients in the harbour. The capacity of the power stations is 35 and 88 MW, respectively, probably giving discharges of $1.5 \text{ m}^3/\text{s}$ and $3.5 \text{ m}^3/\text{s}$. Unfortunately, no details of the discharge structures are given. However, the outlet of the Pigeon House Power Station is situated in a local basin and the inflow velocity into the main harbour basin is low, thus making the densimetric Froude number low. As indicated by the temperature measurements shown in Figure 6.3, the densimetric Froude number for the other discharge should also be low, since the lateral spread is large close to the discharge.

If the outlet conditions are as assumed, the near-field for each discharge can be modelled accurately in a distorted model as discussed in Section 5.2 for the laboratory experiments with $F_{\Delta} \approx 1.4$. The near-field is, however, small. In the far-field the agreement between the model and the prototype very much depends on how ambient diffusion is reproduced, while, like in the preceding Section, the buoyancy spread is assumed to be correctly reproduced and the heat transfer to the atmosphere is considered of minor importance. In this case the model has been adjusted to reproduce both the tidal currents and the salinity gradients. Therefore, both currents and vertical and horizontal ambient diffusion are correctly reproduced. The agreement between the model and the prototype is therefore expected to be good.

The model and prototype measurements are given in Figure 6.3. The temperature spread is measured at a depth of 1.2 m below the water surface at two different tidal stages. The areas within isotherms are determined, and the relation between the model and the prototype measurements are given in Table 6.1.

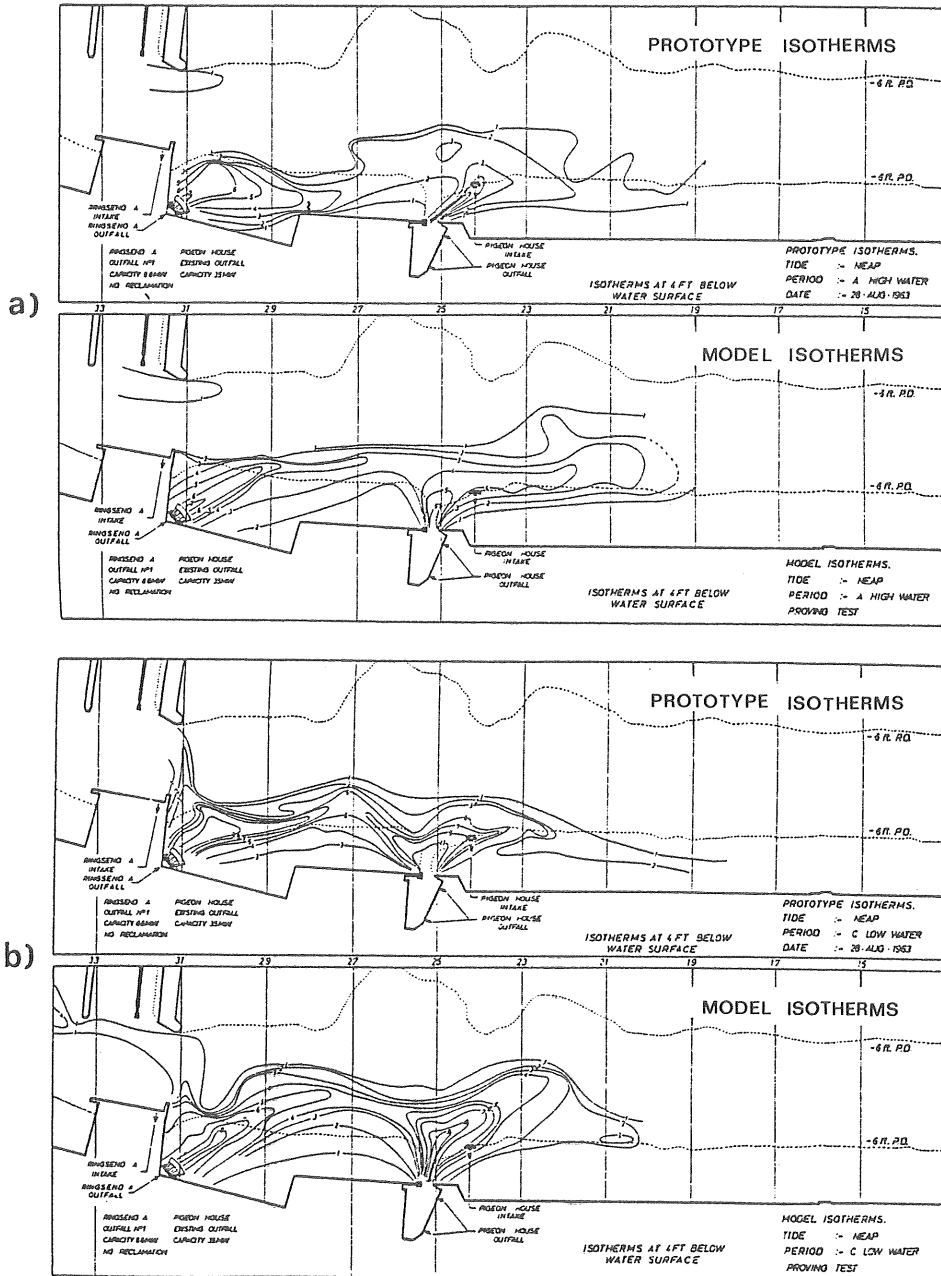


Figure 6.3 Comparison of model and prototype measurements with the temperature rise in $^{\circ}\text{F}$ above background. Temperature measured at a depth of 1.2 m. a) High water, b) Low water. Adapted from Ackers (1969).

Table 6.1 Model-prototype comparison of areas within isotherms, Dublin Harbour.

Excess temperature °F	<u>Area in model</u>	<u>Area in model</u>
	Area in prototype	Area in prototype
	Figure 6.3 a	Figure 6.3 b
9	-	0.16
8	-	0.36
7	-	0.58
6	1.02	0.70
5	0.91	-
4	1.53	-
3	2.13	1.17
2	1.56	0.88

The model-prototype comparisons of areas within isotherms can be summarized as follows:

The main flow pattern in the model agrees well with that of the prototype.

The areas within isotherms in the model agree well with those of the prototype for excess temperatures of 2-6°F.

The areas within isotherms in the model do not agree with those of the prototype for excess temperatures higher than 6°F, which give too small areas in the model.

The theoretical estimation of the accuracy of the model results agree well with the model-prototype comparisons, except close to the outlets. More information about the outlet structures must, however, be available before this disagreement can be explained.

The model-prototype comparisons show that a good picture of the warm-water spread can be achieved in a distorted model if the model is calibrated to reproduce the ambient diffusion correctly. It may also be pointed out that the warm-water spread cannot be calculated by any of the numerical models recommended by Dunn et al. (1975). A problem with two interacting warm-water plumes is so far too complex to be solved theoretically.

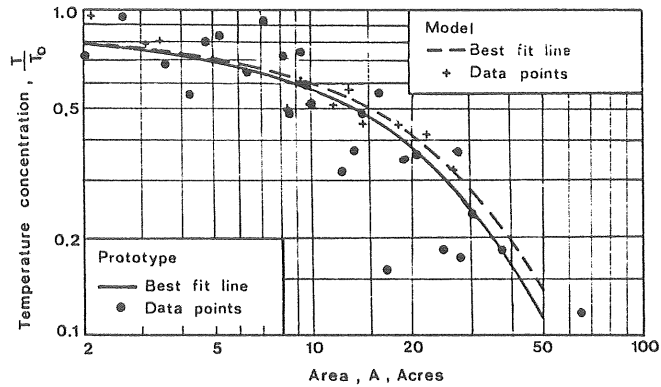
6.4 Model-prototype comparison for Pacific Gas and Electric Company's Pittsburg Power Plant

Hindley et al. (1971) have presented a model-prototype comparison for a discharge from a 1320 MW power plant in Pittsburg, just below the confluence of the Sacramento and the San Joaquin rivers.

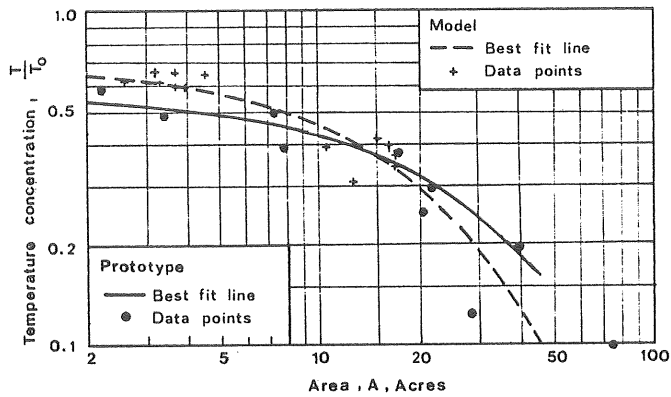
The model scales are 1:1000 horizontally and 1:100 vertically, giving a distortion of 10. The warm water is in the prototype discharged through several pipes of 0.6 - 2.5 m diameter spread over 30 m of the shore. In the model, however, the discharge structure consists of one single pipe, giving a densimetric Froude number of 5 for the prototype discharge of $30 \text{ m}^3/\text{s}$. A shallow area close to the outlet and a wooden barrier 200 m out from the shore-line are not modelled in detail. By calibrating the model against prototype measurements the tidal currents as well as the salinity distribution are accurately modelled according to the authors.

The modelling of the near-field is as explained made in a very rough way. The near-field is probably small because the river currents influenced by the tide are strong. According to the measurements the areas influenced by increased temperatures within the modelled area are so small that the rate of heat transfer to the atmosphere is just a few percent of the discharged heat rate. As before, the buoyancy spread is assumed to be correctly modelled. By the calibration the currents as well as the ambient diffusion are well reproduced. If the warm-water spread is correctly modelled where the far-field starts, the warm-water spread in the far-field will be accurately modelled.

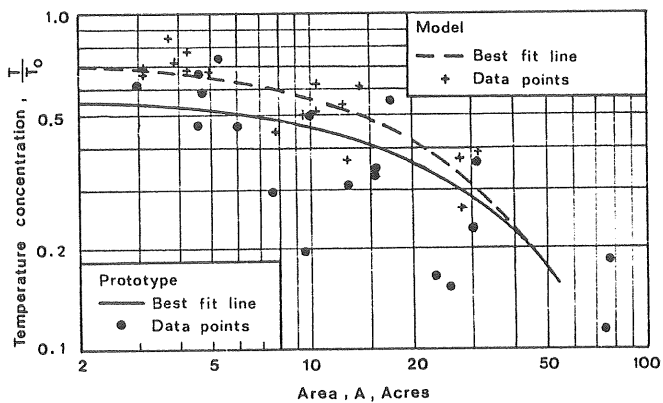
The model-prototype comparisons are made separately for ebb, flood, and slack tide. The measuring technique is infrared photography in model as well as in prototype with a possible inaccuracy of $0.5 - 1.0^\circ\text{F}$ of the surface temperatures. Areas within isotherms for the relative excess temperature are plotted for several measurements in model and in prototype, and a best fit line is computed and drawn for each set of points by the authors (Figure 6.4). These lines are used for the model-prototype comparison of the areas within isotherms shown in Table 6.2. The model data cover only relative excess temperatures of 0.3 or greater, limiting the comparison to this range.



a) Ebb tide



b) Flood tide



c) Slack water

Figure 6.4

Model-prototype comparison of areas within isotherms for discharge from Pacific Gas and Electric Company's Pittsburg Power Plant. Adapted from Hindley *et al.* (1971).

Table 6.2 Model-prototype comparison of areas within isotherms, Pittsburg Power Plant.

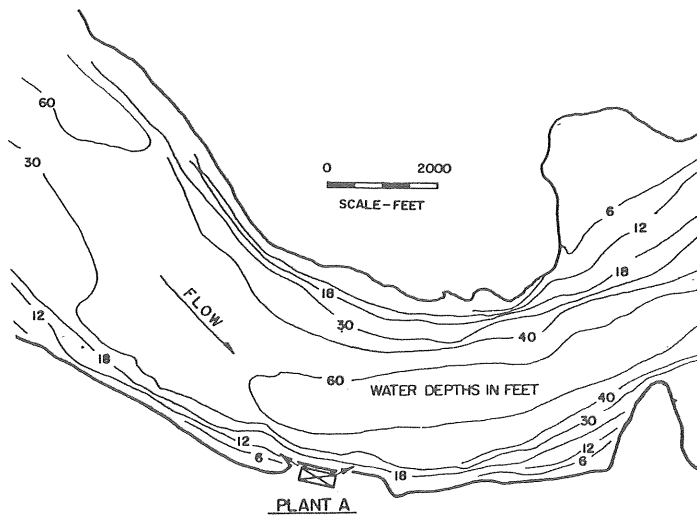
Relative temperature T/T_o	Area in model/Area in prototype		
	Ebb tide Fig. 6.4a	Flood tide Fig. 6.4b	Slack tide Fig. 6.4c
0.7	1.14		
0.6	1.12		
0.5	1.12	1.88	2.25
0.4	1.10	1.05	1.38
0.3	1.11	0.88	1.12

As an average, the agreement between the model and the prototype measurement is good. The spread of the data is, however, great. The good agreement for large excess temperatures is surprising considering the rough way of modelling the outlet conditions and the bottom topography. The modelling of the far-field is good, taking the great distortion of 10 into consideration.

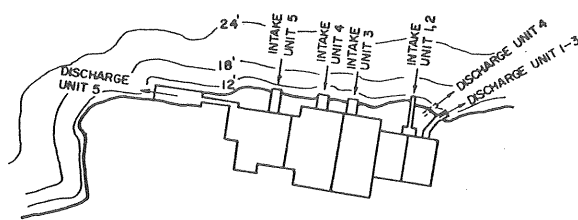
6.5 Model-prototype comparison for Power Plant at the US East Coast

Neale and Hecker (1972) have presented a model-prototype comparison for a discharge from a 510 MW power plant in a tidal river at the US East Coast. The warm water is discharged through three different pipes with orientation according to Figure 6.5 and with a flux of 6-7 m³/s each. The outlet velocities are approximately 0.9 m/s. Two of the outlets are submerged 2-3 m. The water depth is given by Figure 6.5. The river flow is predominantly tidal with an amplitude of 1 m. River velocities reach 0.6 m/s as maximum flood or ebb current.

The model is constructed using a horizontal scale of 1:400 and a vertical scale of 1:80, giving a distortion of 5. The heat transfer to the atmosphere considering the model and prototype weather conditions is well reproduced with this scaling according to the authors. Because an excessive dilution of the warm water is obtained with the normal scaling of the outlets, the outlet velocities are reduced. It is very likely that this phenomenon is due to the submergence of



RIVER BOTTOM TOPOGRAPHY AND SITE OF PLANT A



ARRANGEMENT OF COOLING WATER STRUCTURES
PLANT A

Figure 6.5 Bottom topography and arrangement of cooling-water structures of power plant A.
Adapted from Neale and Hecker (1972).

the outlets, which, however, is not treated in this investigation. According to the authors excessive dilution in the near-field has been observed during studies in distorted models of both surface and submerged discharges.

The adjustments of the outlet conditions and the submergence make a theoretical estimation of the effects of distortion for the near-field of little interest. The disagreement between model and prototype for this region is just stated as a fact.

The model thus reproduces the warm-water spread in the far-field. The heat transfer to the atmosphere is correctly modelled as is the buoyancy spread. The tidal currents are calibrated in the model against prototype measurements and are thus correctly reproduced. The modelling of ambient diffusion and the roughly modelled spread in the near-field will thus be the causes of non-agreement between the model and the prototype. The ambient diffusion is probably caused by friction against the bottom since the tidal currents are strong. According to Section 2.7, the lateral ambient diffusion in this case will be overestimated in a distorted model. The vertical ambient diffusion will be underestimated according to Section 2.8. The lateral spread of the warm water will therefore be too great in a distorted model and the vertical spread too small. The incorrectness of the warm-water spread in the near-field will propagate into the far-field.

At different tidal stages model and prototype measurements are made. In general, the model gives excessive dilution close to the discharge, in spite of the reduced discharge velocities, and gives too great a lateral spread for the low excess temperatures. An average picture for the whole tidal cycle is given in Figure 6.6, where the increased dilution close to the outlet is seen as well as the overestimated lateral spread for low temperatures. The areas within isotherms are determined and compared for the model and the prototype measurements in Table 6.3.

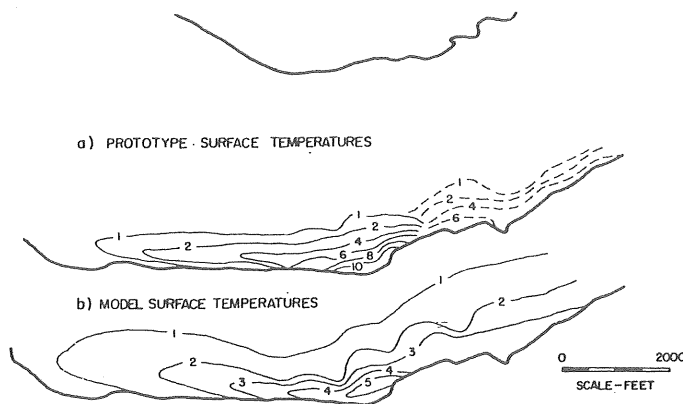


Figure 6.6

Comparison of average tidal temperature rise ($^{\circ}\text{F}$)-plant A. Adapted from Neale and Hecker (1972).

Table 6.3 Comparison of average tidal temperature rise
($^{\circ}\text{F}$)-plant A, US East Const.

Excess-temperature $^{\circ}\text{F}$	Area in model/Area in prototype
4	0.3
2	1.3
1	1.8

The qualitative estimation of the effects of distortion agree well with the result from the model and the prototype measurements. In spite of the too small area within the 4°F -isotherm in the model, the lateral spread is increased to be of the order two times too great for the 1°F -isotherm. The lateral ambient diffusion is obviously too great in the distorted model. Unfortunately, no information on the vertical spread is given.

6.6 Model-prototype comparison for Madison Gas and Electric Company Plant, Lake Monona

Silberman and Stefan (1970) have presented data of Niemeyer (1969) on model-prototype comparisons of centre-line velocities for a warm-water discharge from a 190 MW fossil fuel power plant. The cooling water is discharged through two separated channels. The water depth is of the order of 1 m out to 90 m from the shoreline, where the depth increases rapidly. Ambient currents are wind-driven and weak. The model scales are 1:100 horizontally and 1:15 vertically, giving a distortion of 6.7.

The measured centre-line velocities are of the order of 0.1 m/s compared with the ambient velocity of 0.06 m/s. The model-prototype comparisons are thus for the near-field. If the outlet conditions are known, it is possible to estimate the effects of distortion. This is not the case here, but still some theoretical conclusions can be drawn.

For the shallow area out to 90 m from the outlet the warm-water flow will probably be of a two-dimensional nature. The effects of

distortion will therefore be very small according to Section 2.3. For the area outside this region the flow will change to a three-dimensional character. How the effects of distortion affect the flow in the model are according to Chapters 4 and 5 depending on the outlet conditions (see Section 5.6).

If the outlet densimetric Froude number is low ($F_{\Delta} \leq 2$) the effects of distortion are small.

If the outlet densimetric Froude number is high but still finite ($F_{\Delta} = 6 - 25$), the estimation using Engelund's moderate Richardson number theory is good. In this case the theory gives $6.7^{1/3} = 1.9$ too high centre-line velocities in the distorted model.

If the outlet densimetric Froude number is infinite, i.e. the discharge is nonbuoyant, the three-dimensional jet theory (Section 2.2) is applicable, giving centre-line velocities that are $6.7^{1/2} = 2.6$ times too high.

The estimations discussed above are, of course, not applicable immediately after the warm water leaves the shallow area. There will instead be a successive transition from the effects of distortion of the shallow area to one of the estimations given above.

The model-prototype comparisons are made for measurements of centre-line velocities from both discharge channels at two different occasions in the prototype. The prototype conditions were reproduced in the model and two sets of model measurements were made for each prototype situation. The total data set is here given in Table 6.4 with model data transformed into prototype conditions.

The velocity decay along the centre-line is also represented graphically in Figure 6.7. For each of the prototype cases and for the corresponding two model tests, regression lines are drawn on log-log paper and these lines are used for the model-prototype comparison. As can be seen, the two model tests for each prototype test differ remarkably. It is, however, evident that the velocity is too high in the model. As an average, the centre-line velocities in the model are 1.3 - 1.7 times too high with the low number 60 m from the outlet.

Table 6.4 Model-prototype comparisons of centre-line
velocity, Lake Monona

Simulations of 1966 07 08 field data									
Livingston discharge $2.8 \text{ m}^3/\text{s}$					Blount discharge $2.6 \text{ m}^3/\text{s}$				
Field	Model	1	2		Field	Model	1	2	
Dist. Vel.	Dist. Vel.	Vel.	Vel.	Vel.	Dist. Vel.	Dist. Vel.	Vel.	Vel.	Vel.
m m/s	m m/s	m/s	m/s	m/s	m m/s	m m/s	m m/s	m/s	m/s
62	0.141	61	0.16	0.18	57	0.257	61	0.24	0.24
93	0.107	91	0.13	0.16	86	0.135	91	0.18	0.22
125	0.089	122	0.11	0.14	113	0.097	122	0.08	0.19
155	0.083	152	0.10	0.14	177	0.083	183	0.08	0.12
		183	0.08	0.09	240	0.076	244		0.08

Simulations of 1966 08 30 field data									
Livingston discharge $2.7 \text{ m}^3/\text{s}$					Blount discharge $1.1 \text{ m}^3/\text{s}$				
Field	Model	1	2		Field	Model	1	2	
Dist. Vel.	Dist. Vel.	Vel.	Vel.	Vel.	Dist. Vel.	Dist. Vel.	Vel.	Vel.	Vel.
m m/s	m m/s	m/s	m/s	m/s	m m/s	m m/s	m m/s	m/s	m/s
61	0.187	61	0.12	0.23	61	0.110	61	0.17	0.21
91	0.143	91	0.10	0.21	91	0.051	91	0.13	0.20
120	0.105	122	0.09	0.18	122	0.048	122	0.10	0.19
147	0.091	152	0.09	0.16	152	0.046	152	0.08	0.14
173	0.088	183	0.08	0.12	183	0.030	183		

As pointed out earlier the outlet conditions must be characterized before a theoretical estimation of effects of distortion on centre-line velocity can be made. It is also assumed that the centre-line velocity and the centre-line excess temperature behave in the same way. Then the slopes of the regression lines in Figure 5.1 - 5.4 can be compared with the slopes of the lines in Figure 6.7. These comparisons give the result that the slopes in Figure 6.7 agree well with the slopes in Figure 5.2 and 5.3, indicating that the outlet densimetric Froude number is of the order of 6-10. The estimation of effects of distortion using Engelund's theory should therefore be applied.

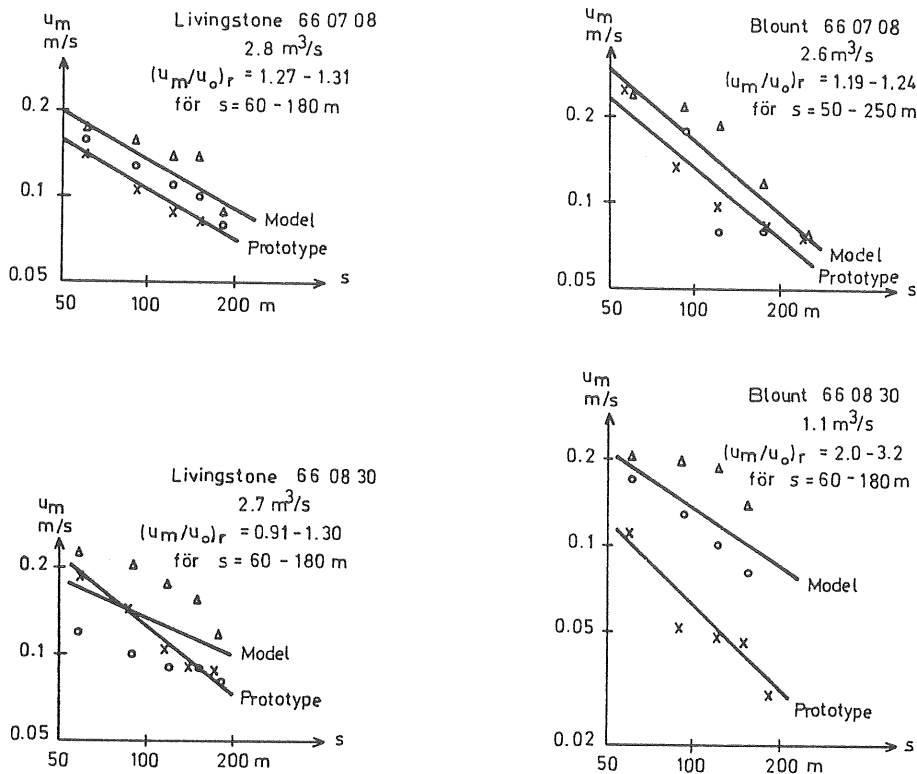


Figure 6.7 Model (Δ) and prototype (x) comparison of centre-line velocity. The straight lines are fitted to data by the method of least squares.

In the shallow area the agreement between the model and the prototype is fair giving a centre-line velocity that is too high by a factor of 1.3. According to the theoretical estimation, no effects of distortion should occur. The disagreement is, however, not too great. Outside the shallow area, the centre-line velocity should successively increase to be too high by a factor of 1.9 according to the estimation using Engelund's theory. The agreement is good with the model-prototype comparison giving a successive increase up to the number 1.7.

6.7 Model-prototype comparison for Ingå Power Plant

Kuuskoski (1974) has presented investigations of cooling-water discharges in model and prototype from Ingå Power Plant, Finland. The 250 MW power plant discharge is $8 \text{ m}^3/\text{s}$. The plant is situated in a nontidal bay. The water depth close to the outlet is 4 m and increases rapidly to 14 m. No information on outlet velocity is given, but the velocity seems to be low. The ambient currents are small and mainly wind-driven in the prototype, while no ambient currents are present in the model test. The model has a horizontal scale of 1:450 and a vertical scale of 1:60, giving a distortion of 7.5.

With a low outlet velocity the warm-water spread will mainly be governed by ambient currents and ambient diffusion but also by the heat transfer to the atmosphere. In the model tests no ambient currents and no ambient diffusion are present. The warm water will then flow over the ambient water in a thin surface layer that is laminar except close to the outlet.

The dilution with ambient water will be drastically reduced by the flow being laminar and by the absence of ambient diffusion. These effects are so strong that they will overshadow the effects of distortion. The areas within isotherms are thus expected to be much too great in the model.

One model and two prototype measurements of surface temperatures are given in Figure 6.8. As can be seen from the prototype measurements, the influence of the wind and consequently the wind-driven currents is great. The lack of ambient currents in the model thus makes a correct reproduction of the warm-water spread impossible. This fact is clearly demonstrated in Figure 6.8.

6.8 Model-prototype comparison for Oskarshamn Nuclear Power Plant, Sweden

A model investigation of cooling water spread from the Oskarshamn Nuclear Power Plant has been presented by Rahm and Häggström (1976). The investigation treats discharges from the present values of $22\text{--}50 \text{ m}^3/\text{s}$ up to a possible future value of $250 \text{ m}^3/\text{s}$. Prototype measurements have been performed by the Swedish Meteorological

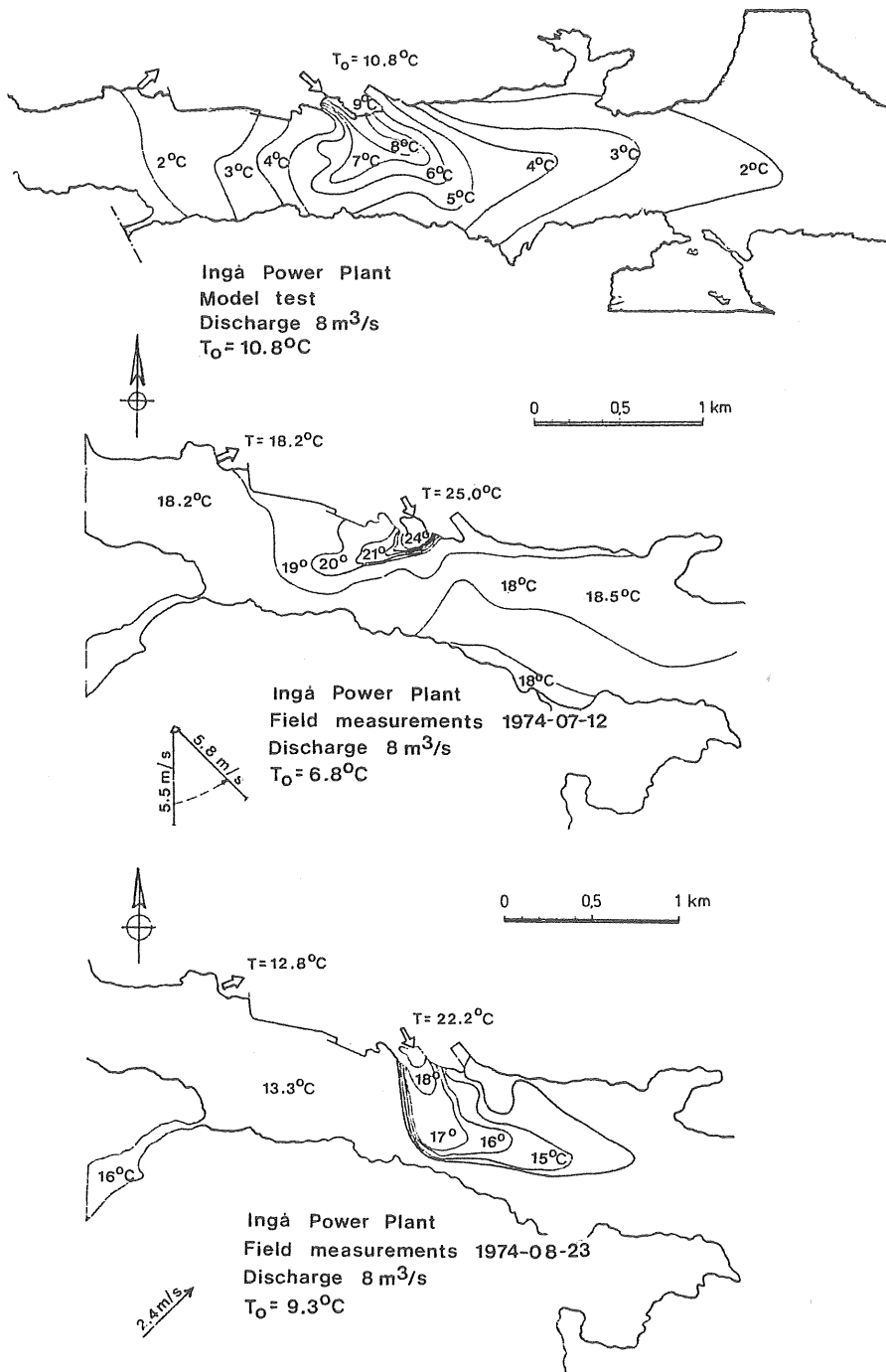


Figure 6.8 Comparison of model and prototype measurements of surface temperatures. Ingå Power Plant (Finland). Adapted from Kuuskoski (1974).

and Hydrological Institute (Bergstrand, 1972-1977) for discharges of $22 \text{ m}^3/\text{s}$ and $50 \text{ m}^3/\text{s}$ with a temperature increase of 10°C .

The cooling water is led into a small bay with a sound slowly expanding towards the sea. When the warm water flow leaves the sound, the width is approximately 60 m and the densimetric Froude number is close to one. The area is nontidal, and currents are predominantly wind-driven with velocities of the order of $0.1 - 0.2 \text{ m/s}$. During the summer period the upper 10-15 m of the sea has almost uniform temperature and salinity distributions, however, the shallow areas in the archipelago can have a higher temperature. Outside the archipelago the water depth is 10 m or more.

The physical model is constructed with a 1:400 horizontal scale and a 1:50 vertical scale, giving a distortion of 8. The bottom roughness is increased by gluing 0.005 m stones on the bottom. Ambient currents parallel to the shore-line are reproduced, but density stratifications are not considered.

Close to the sound, where the densimetric Froude number is one the physical model can reproduce the warm water spread with accuracy according to the theoretical and experimental results summarized in Section 5.6. Because the outflow velocity is small ($\sim 0.3 \text{ m/s}$), the ambient currents, the ambient diffusion, and the buoyancy spread will soon govern the spread of the warm water. Heat transfer to the atmosphere is for the area studied just a few percent of the rate of discharged heat. Assuming as before that buoyancy spread is correctly modelled the agreement between model and prototype will depend on the reproduction of the ambient currents and the ambient diffusion. The ambient currents are wind-driven and the velocities as well as the directions of the currents can therefore vary. At a depth of 10 m the velocities were in 40 % of the measurements less than 0.03 m/s . The surface currents parallel to the shore-line are, however, predominant and reproduced in a roughly correct way. The ambient diffusion is in the prototype generated by the wind, while it in the model is generated by bottom friction. There are, however, no determinations available of the diffusion characteristics of the ambient water in the prototype. Therefore no estimations can be made of the effects of distortion in the far-field.

Model-prototype comparisons are available for discharges of $22 \text{ m}^3/\text{s}$ and $50 \text{ m}^3/\text{s}$. For the $22 \text{ m}^3/\text{s}$ discharge the prototype conditions only rarely were the same as those reproducible in the model. Comparisons for these cases have been presented by Rahm and Häggström (1976). The results are similar to the results for $50 \text{ m}^3/\text{s}$ presented here but based on fewer prototype measurements. For the discharge of $50 \text{ m}^3/\text{s}$ the prototype conditions during several measurements have been similar to the conditions reproduced in the model. No detailed current measurements were, however, made in the prototype. Therefore, the comparisons have been made for situations in the model and in the prototype where the main ambient current has had the same direction. Thus two prototype and three model measurements for NE ambient current have been averaged and compared and also seven prototype and two model measurements for SW ambient current. The averaging has been done by fitting a straight line to the data on a log-log paper using the method of least squares. The parameter studied is the areas within isotherms represented in Figure 6.9.

In Figure 6.10 one model and two prototype measurements are shown as examples of a discharge of $50 \text{ m}^3/\text{s}$. The somewhat higher temperatures naturally occurring in the shallow archipelago of the prototype make it difficult to distinguish the temperature pattern caused by the warm-water discharge from that of the natural temperature.

For a SW ambient current the model gives areas within isotherms that are 1.5 - 3 times the prototype areas in the relative temperature range 0.5 - 0.2 and for a NE ambient current 1 - 5 times the prototype areas in the same temperature range. The spread of data is large, but still the tendency seems clear.

Since the reproduction of ambient diffusion is not made properly and is not even determined in the prototype, it is impossible to estimate the effects of the modelling. Very close to the sound the agreement between the model and the prototype measurements is good, which is due to the fact that the outlet conditions are correctly modelled.

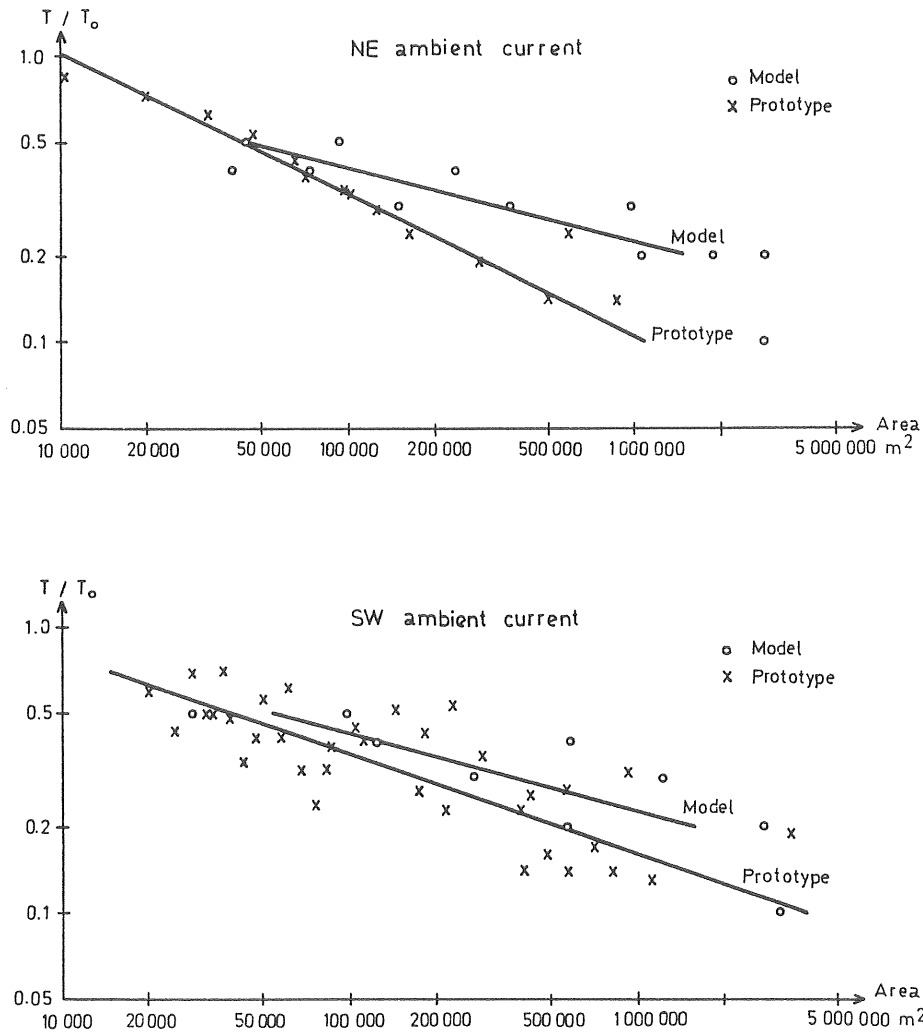


Figure 6.9

Comparison of model (o) and prototype (x) measurements of areas within isotherms for NE and SW ambient currents. The straight lines are fitted to data by the method of least squares.

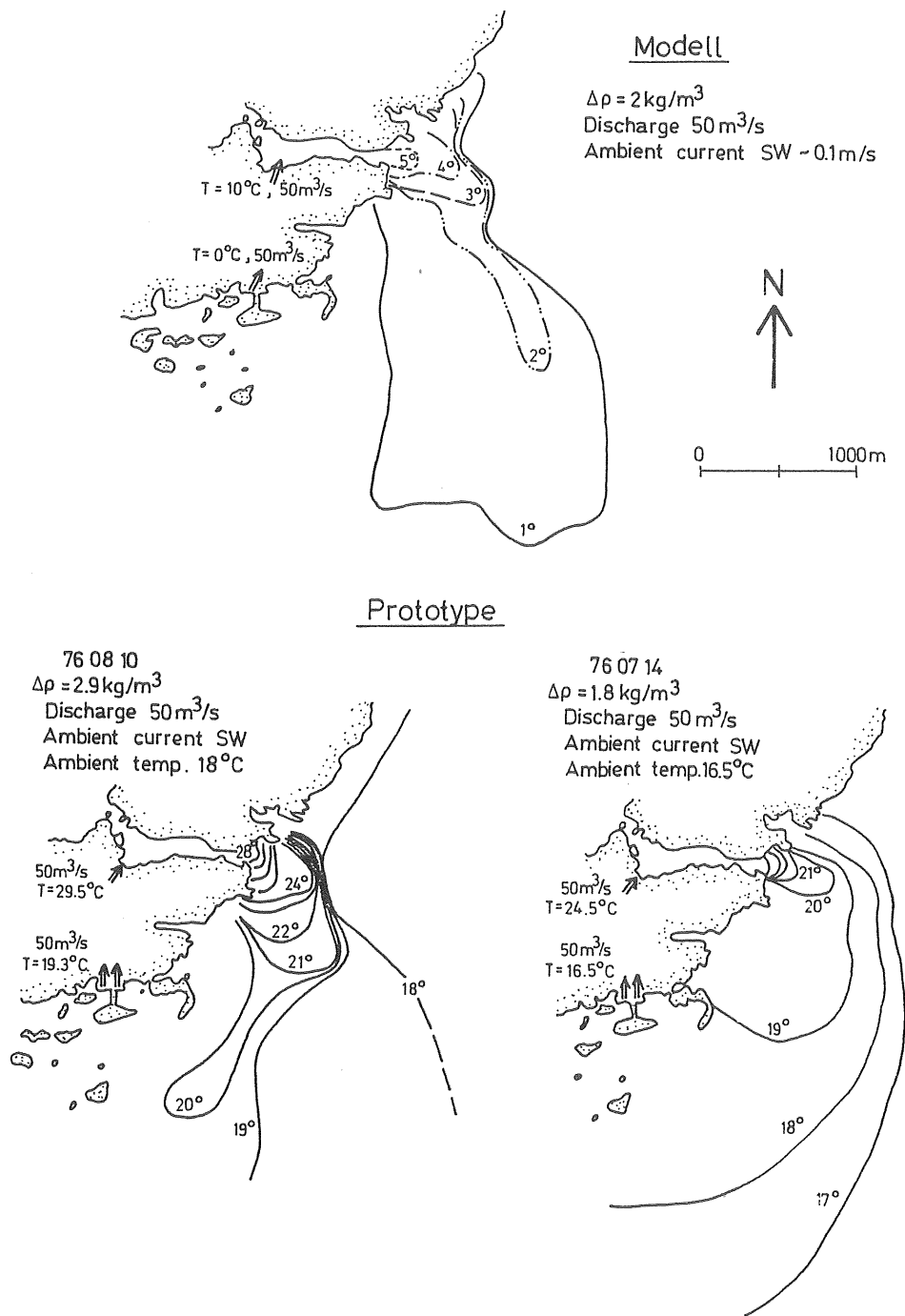


Figure 6.10 Model and prototype measurements of surface temperatures for a discharge of $50 \text{ m}^3/\text{s}$. Oskarshamn Nuclear Power Plant.

7. DISCUSSION OF RESULTS

7.1 Effects of distortion in summary

In the present investigation effects of distortion in physical models of warm-water discharges are obtained by theoretical and numerical analyses and by determination from laboratory experiments. The results are also discussed and applied to some model-prototype comparisons. The different methods of obtaining the effects of distortion have their specific limitations:

In Chapter 2 the most important processes affecting the warm water spread are studied. The effects of distortion are evaluated for each process separately, which is important and increases the understanding of the problem of physical modelling. Direct applications of these results are, however, rarely possible.

In Chapter 3 the effects of distortion are obtained using analytical solutions to surface warm-water discharge problems. In these theories the ambient water is assumed to be quiescent and deep. Ambient diffusion is neglected.

In Chapter 4 the effects of distortion are calculated using numerical models. These models are only applicable to discharges in deep receiving bodies of water but both ambient currents and ambient diffusion are included in the models. In the calculations using the Prych model the effects of ambient diffusion have, however, been excluded.

In Chapter 5 the effects of distortion have been determined from laboratory experiments with surface discharges of warm water. The ambient water has been deep and in most of the experiments stagnant.

In Chapter 6 the results obtained in Chapters 2-5 have been discussed and applied to model-prototype comparisons of cooling-water discharges, including all processes normally affecting a warm-water flow.

Each of the methods of investigating effects of distortion has thus a limited application. The different methods give, however, results that point in the same direction and taking the investigation as a whole, some conclusions can be drawn with confidence. This is done

for two separate cases:

One where jet diffusion is the most important process, i.e. studies of the near-field.

One where ambient diffusion and convective transport with ambient currents are the most important processes, i.e. studies of the far-field.

As in earlier chapters, the effects of distortion are in general discussed for a distortion of two.

Modelling of the near-field

Most of the theoretical estimations of effects of distortion in this investigation are for application in the near-field of a surface warm-water discharge in a deep receiving body of water.

The parameter for which the best theoretical and experimental base is present is the centre-line excess temperature. For the parameters areas within isotherms and thickness of warm-water flow, the effects of distortion are to a great extent obtained from the calculations using the Prych model. The parameter centre-line velocity is here as in most theories of surface jets assumed in principle to behave in the same way as the centre-line excess temperature (see Chapters 3 and 4).

For discharges with a small outlet densimetric Froude number ($F_{\Delta} \leq 2$) the effects of distortion on centre-line excess temperature (and centre-line velocity) are small. This is shown by the laboratory experiments in Figure 5.1 and by the calculations using the Prych model in Figures 4.6 and 4.7. An explanation of this result is given in a very simplified way. In the near field the spread of the warm water is governed by jet diffusion, which can be divided into vertical and horizontal entrainment, and by buoyancy spread. Of these processes the horizontal entrainment (Section 2.3) and the buoyancy spread (Section 2.5) can theoretically be reproduced correctly in a distorted model. The effects of distortion in the near field are thus dependent on the reproduction of the vertical entrainment. A small densimetric Froude number indicates that the buoyancy effects are strong compared with inertia forces. For this case the vertical en-

trainment is small and the reproduction good according to the Summary of Section 2.4. Thus for a discharge with a small densimetric Froude number, the near-field can be modelled with accuracy in a distorted model.

For discharges with a large outlet densimetric Froude number, the buoyancy effects are less pronounced, and therefore the vertical entrainment will be incorrectly reproduced in a distorted model. The effects of distortion on the centre-line excess temperature (and centre-line velocity) will thus be significant and will increase with increasing outlet densimetric Froude number until the nonbuoyant case ($F_{\Delta} = \infty$) is reached. For this case the effects of distortion on centre-line excess temperature (and centre-line velocity) give values that are too great by a factor of $2^{1/2} = 1.41$ according to Section 3.2. In the intermediate case ($\sim 6 < F_{\Delta} < \sim 25$) the experimental results of Chapter 5 agree with the analysis using Engelund's moderate Richardson number theory (Section 3.4), giving a centre-line excess temperature (and centre-line velocity) that is too great by a factor of $2^{1/3} = 1.26$. This agreement is good for an aspect ratio of the outlet of approximately one. The calculations using the Prych model indicate that the effects of distortion decrease with increasing aspect ratio (Figure 4.7).

Of the model-prototype comparisons presented in Chapter 6, only the investigation from Lake Monona (Section 6.6) is applicable to the near-field. The comparison is made for centre-line velocity. Close to the outlet the ambient water is shallow, and after 90 m, the depth increases rapidly. In the shallow area the vertical entrainment is reduced compared with deep-water conditions. The warm-water flow will therefore have a two-dimensional character and can thus be reproduced in a distorted model (Section 2.3). The model-prototype comparison gives for this area a centre-line velocity that is too large by a factor of 1.3, which for a distortion of 6.7, is a good agreement. In the deeper part the centre-line velocity should be as much as $6.7^{1/3} = 1.9$ too great according to the analysis using Engelund's moderate Richardson number theory. The model-prototype comparison gives a number increasing from 1.3 to 1.7 in this area, showing that the theoretical estimation using Engelund's theory is reasonably good.

For discharges with a small outlet densimetric Froude number ($F_{\Delta} \leq 4$) the effects of distortion on the areas within isotherms are of the order of 1.3 too large in a model with a distortion of two according to the Prych model calculations. The isotherms considered are for excess temperatures, T/T_O , 0.3 or less (Figure 4.4). For discharges with an outlet densimetric Froude number close to one, the agreement between model and prototype can be expected to be better. However, ambient diffusion will affect the results for low excess temperatures, and this effect is not included in the calculations. For discharges with a large outlet densimetric Froude number ($F_{\Delta} = 8-16$), the calculations using the Prych model give areas within isotherms that are too great by a factor of 1.5. The Prych model gives results of centre-line excess temperatures that under the same outlet conditions underestimate the effects of distortion. This is also likely to be the case here. However, the analysis using nonbuoyant jet theory (Section 2.2) gives areas within isotherms that are too great by a factor of 2.0. Because the buoyancy effects are not included the effects of distortion are overestimated. Therefore, it is reasonable to expect the effects of distortion on the areas within isotherms to give a factor of 1.6 - 1.8 too great values.

The thickness of warm-water flow can for discharges with a small densimetric Froude number ($F_{\Delta} \leq 4$) be expected to be almost correctly reproduced in a distorted model like the other parameters. This holds also as an average according to the calculations using the Prych model (Figures 4.8 and 4.9).

For discharges with a large outlet densimetric Froude number ($F_{\Delta} = 8-16$), the thickness is wrong by a factor of $2^{-1/3} = 0.8$ according to the evaluation using Engelund's moderate Richardson number theory (Section 3.4). This result is in agreement with the calculations using the Prych model for $F_{\Delta} = 8-16$ and aspect ratios of the order of one or less (Figure 4.9). For a larger aspect ratio the corresponding number is closer to one. For the non-buoyant case the thickness of the warm water flow will be one half of the correctly modelled value.

The flow path of the warm water has not been treated earlier in this study. This can easily be done by using the numerical models, but no general figures can be obtained in this way because the curvature depends on the outlet conditions as well as on the ambient current velocity. Some qualitative estimations can, however, be made. A change of the direction of the warm-water flow is caused by entrainment of ambient water having another direction of flow. If the centre-line excess temperature is too high the entrainment of ambient water is too small. Therefore the change of direction of flow will be too slow and the warm water will flow out too far from the shore. This is the case for discharges with a large densimetric Froude number. If, on the other hand the entrainment is correctly modelled, the direction of flow is correct.

The influence of the bottom on the effects of distortion has been discussed in Sections 2.3, 2.6 and 6.6. In general, the influence of bottom geometry will increase the reproducibility of the warm-water spread in the model. Special effects such as separation of the flow from the bottom can because of increased slopes occur in a distorted model and may not be present in the prototype.

Modelling of the far field

In the far-field the most important processes affecting the warm-water spread are ambient diffusion, convective transport with ambient currents, and heat transfer to the atmosphere. The effects of distortion on these processes are evaluated in Sections 2.6 - 2.9. The physical modelling of the far-field as a whole has also been treated in the model-prototype comparisons presented in Sections 6.2, 6.3, 6.4, 6.5, 6.7, and 6.8. In the comparisons of Sections 6.2 - 6.5 the ambient currents are tidal and thus nonstationary. This does not, however, in principle change the conclusions drawn even if these are based on theories for stationary conditions.

The reproduction of ambient currents in the models has been done properly except for the Ingå investigation (Section 6.7). In this investigation the weak ambient currents were not modelled, which made the agreement between the main temperature spread in the model and in the prototype very poor. In the other cases where am-

bient currents were modelled, the main flow pattern of the warm water was fairly well reproduced even if the excess temperature of the warm water was incorrect.

The physical models of Dublin Harbour (Section 6.3) and Pittsburg Power Plant (Section 6.4) were adjusted to reproduce the tidal currents as well as measured salinity profiles. The ambient diffusion was thus correctly modelled. The agreement between the model and the prototype measurements was therefore good in these cases in spite of a distortion as large as 6 and 10, respectively. In the physical models of the Severn Estuary (Section 6.2) and a river at the U.S. East Coast (Section 6.5), the bottom roughness was adjusted so that the tidal currents were correctly reproduced. The ambient diffusion was in these cases caused by bottom friction, and according to Sections 2.7 and 2.8, the lateral spread will be overestimated and the vertical spread underestimated under this condition. The model-prototype comparisons show clearly that the lateral spread was overestimated. The available data permitted no determination of the vertical spread giving no possibility to control the evaluation of Section 2.8. In the model-prototype comparison in the Oskarshamn investigation (Section 6.8) the ambient diffusion of the prototype was due to wind effects, while the ambient diffusion in the model was due to bottom friction. Unfortunately, no measurements of the ambient diffusion were made in the prototype. Too large a lateral spread of the warm water occurred in the model.

The heat transfer to the atmosphere has in most of the model-prototype comparisons been considered of little importance for the warm-water spread, but in one case (Section 6.5) it has been correctly modelled according to the theories of Section 2.9. Incorrect reproduction of heat transfer to the atmosphere can, however, be treated by estimating the heat transfer under both model and prototype conditions and by correcting the model results accordingly. In this case the difference in temperature caused by the incorrect modelling must be small enough for the difference in buoyancy to be negligible.

7.2 Recommendations for physical model investigations

For prediction of the spread of warm water from a thermal power plant different numerical models as well as physical models are available. According to Dunn et al. the best numerical models give excess temperature areas which are up to five times too large or too small. Of course, the accuracy will increase with greater experience and improvements of existing numerical models and also when future, more correct models are available.

According to the present study, a near-field physical model with, as an example, a distortion of eight gives excess temperature areas which at worst are four to six times too large for a discharge with a high outlet densimetric Froude number and a deep receiving body of water. An even better agreement between a physical model and the prototype is obtained for discharges with low outlet densimetric Froude numbers and for shallow receiving bodies of water, where the bottom affects the flow, which so far is impossible to reproduce practically in a numerical model. Of course, the effects of distortion can be reduced by decreasing the distortion. However, this possibility is limited by the fact that the modelling must be done under turbulent conditions as pointed out in Chapter 1.4.

For the far-field the agreement between the physical model and the prototype depends very much on the reproduction of ambient diffusion. Much more attention must be paid to this problem than has been done so far. Thus the agreement between the model and the prototype spread of warm water can be improved significantly if the diffusion in the prototype is measured and the model is calibrated against these data. The agreement between numerical model calculations and the prototype will probably also be improved if "correct" ambient diffusion coefficients are used in the calculations. As pointed out in Section 1.3 the most reliable numerical models are based on the entrainment theory and are thus mainly applicable to the near-field even if ambient diffusion is included in the models.

The predictions of the spread of warm water using a physical model seem to give results that are much more accurate than results obtained by numerical model calculations even if the physical model is heavily distorted. In cases where the bottom will affect the warm-water flow significantly, a physical model is necessary. The

disadvantages with a physical model are, that it is more expensive and time-consuming than a numerical model. However, the costs are as a rule, small compared to the costs of field measurements, which are necessary irrespective of which type of model is used.

For the choice between a physical or a numerical model a thorough study of the aims of the prediction is necessary. Who are the users of the results? How are the results to be used? What are the problems of the receiving body of water? How accurate a result is necessary? etc. If with this background a physical model is chosen, it should be in combination with a numerical model. To form a basis for the design work of the physical model, predictions of the warm-water spread should be made with the numerical model. Calculations of effects of distortion can be done before the model is designed as well as afterwards for transformation of physical model data into prototype conditions. Extreme situations can also be calculated as a supplement to the tests in the physical model.

The effects of distortion can in the specific case be calculated more carefully than was done in Chapter 4 where the presentation had a general character. An example how this is done and how the physical model data are transformed into prototype conditions is taken from the Oskarshamn investigation (Rahm and Häggström 1976).

A proposed outlet construction for a discharge of $130 \text{ m}^3/\text{s}$ gave an outlet velocity of 2 m/s and a water depth at the outlet of 6 m . This gave an outlet densimetric Froude number of 6. The water depth outside the outlet increased rapidly to 10 m or more. The spread of the warm water was studied in a physical model with the horizontal scale of 1:400 and the vertical scale of 1:50, giving a distortion of 8.

In the model the warm water had a thickness corresponding to 4-5 m a few hundred metres from the outlet and was thus unaffected by the bottom. The Prych model was chosen for calculating the effects of the physical modelling because it was considered as one of the best numerical models at that time (1974) and also was verified by Weil (1974). The outlet conditions given above were similar to the basic conditions for the Prych model, i. e. jet-like flow ($F_{\Delta} \sim 6$) and a deep receiving body of water. The calculation of the warm-water

spread was done with model data as well as with prototype data as input. A comparison of the results gave the effects of the distortion. For the most important variables, areas within isotherms, thickness of the warm-water flow, and the curvature of the warm-water centre-line the following results were obtained:

Areas within isotherms were as an average 3-4 times too great in the physical model (Figure 7.1).

Thickness of warm-water flow was in the physical model too small by a factor of $2/3$.

The warm water will flow at a distance from the shoreline, which was 1.3 - 1.4 times too great in the physical model.

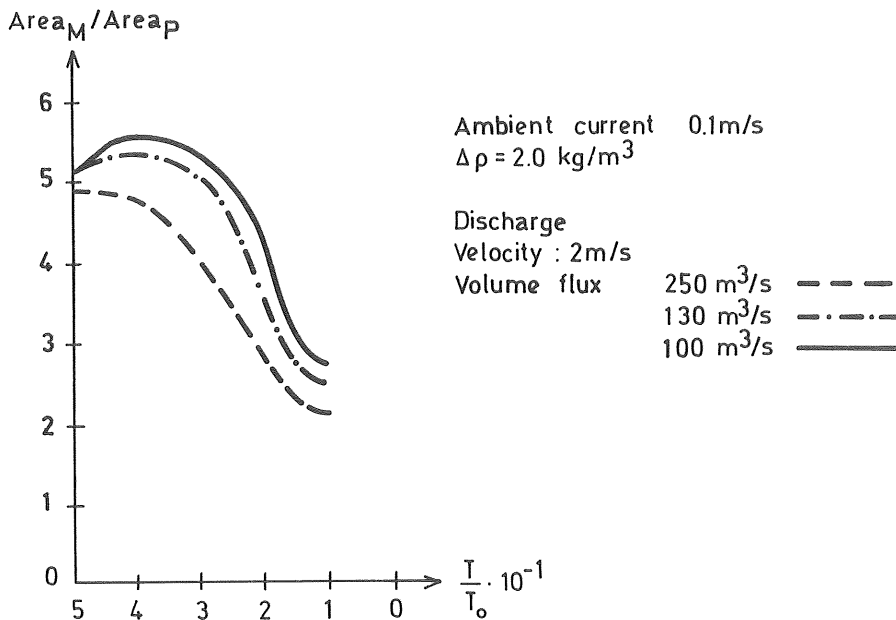


Figure 7.1 Model-prototype comparison of areas within isotherms for different discharges as calculated by the Prych model. Adapted from Rahm and Häggström (1976).

A widened basis for the transformation of the physical model results into prototype conditions was achieved by a comparison of model and prototype results for a discharge of $22 \text{ m}^3/\text{s}$. In this case the outlet densimetric Froude number was one and the outlet velocity

of the order of 0.3 m/s compared with the ambient currents of 0.1 m/s. The most important governing processes for the over-all spread of warm water were convective transport with ambient currents and ambient diffusion. The ambient currents were modelled in a roughly correct way, while no estimation of the modelling of ambient diffusion was present. The model-prototype comparisons gave results that were similar to those presented in Section 6.8 for a discharge of 50 m³/s. As an average the areas within isotherms were 3-4 times too great in the model. The thickness of the warm-water flow could not be determined in the prototype because there was a small natural temperature gradient. Also, the positions of the surface isotherms were uncertain because of the natural horizontal temperature gradients in the prototype.

The scale effects estimated by the two methods gave approximately the same result. The calculated effects of distortion were therefore used for a transformation of the temperature spread for the discharge of 130 m³/s with the proposed outlet structure. The surface isotherms are shown in Figure 7.2 both as measured in the model and after transformation into prototype conditions.

The transformed temperature pattern is, of course, not correct in detail but gives a result that is better than both the direct model measurement and calculations using a numerical model. Considering the spread of data that is present for prototype measurements (Figure 6.9), the accuracy of the transformation seems sufficient.

In the reported example the influence of the bottom was negligible. In cases where the bottom significantly affects the warm water flow the numerical models will not be of much help since they cannot reproduce such effects. The bottom effects will, however, as a rule increase the agreement between the spread in the distorted model and in the prototype. Thus the agreement between model and prototype is probably better for the Forsmark investigation (Swedish State Power Board 1971) than for the Oskarshamn investigation (Rahm and Häggström 1976), since the former site is in a shallow archipelago where the bottom configuration is very important for the flow of warm water as well as for ambient currents.

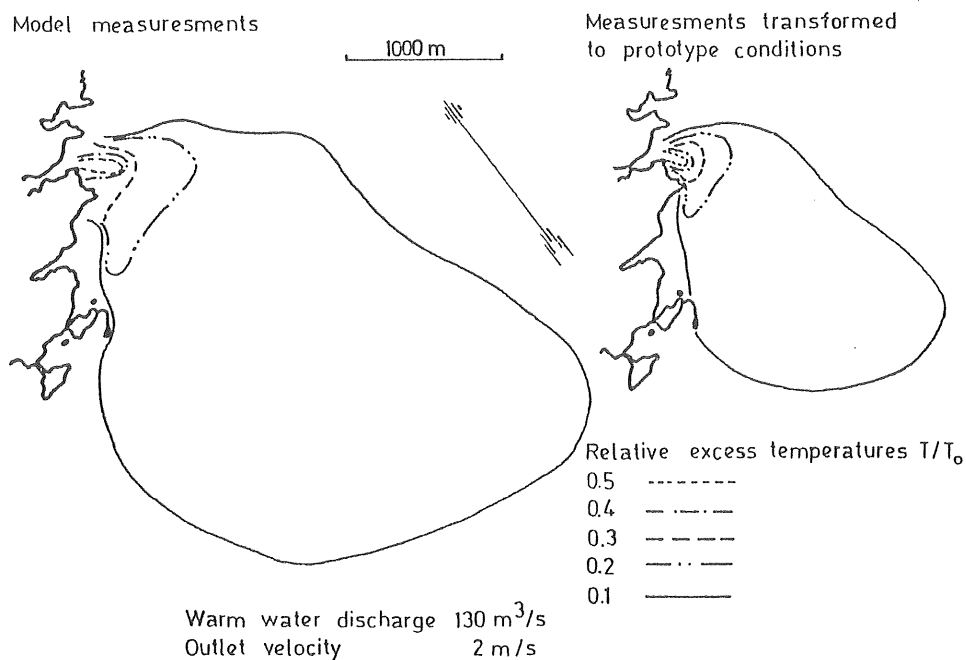


Figure 7.2 Excess temperature T/T_0 as measured in model and after transformation into prototype conditions for a discharge of $130 \text{ m}^3/\text{s}$.

7.3 Further research

The physical modelling technique of surface warm-water discharges fails mostly in the reproduction of the ambient diffusion but also in the reproduction of the near-field for discharges with high densimetric Froude numbers. Improvement of the physical modelling technique can be made mainly by paying special attention to the modelling of ambient diffusion as discussed earlier. For better results in the near-field undistorted models are necessary.

A better evaluation of the effects of distortion and the whole problem of modelling warm-water surface discharges can be done in the following ways

By comparing more results from model and prototype measurements.

By improving the numerical model technique making possible better estimations than those in Chapter 4.

The number of model investigations is great, but the follow-up with prototype measurements is bad. Thus the model-prototype comparisons that are presented in the available literature are few, and they also give incomplete information on outlet conditions. Therefore, more model-prototype comparisons for different conditions of outlet and ambient bodies of water can give a much better understanding of the distortion problems.

By improving the numerical model technique, one could also improve the predictions of warm water spread in physical models. The calculations of effects of distortion could be done more accurately but still in the same way as in Chapter 4. It seems, however, that the possibility to calculate complex prototype situations with the bottom affecting the warm-water flow lies in the distant future. Therefore, judgement based on the results and methods presented in this investigation is necessary when predictions of warm-water spread from surface discharges are made from measurements in physical distorted models.

REFERENCES

- Abbot, M., B., (1961): On the Spreading of One Fluid over Another. *La Houille Blanche* No 5-6, Dec. 1961.
- Abraham, G., (1963): Jet Diffusion in Stagnant Ambient Fluid. Delft Hydraulics Laboratory, Publication No 29, 1963.
- Abraham, G., (1975): Hydraulic Near-Field Modeling, Chapter 10.A and Hydraulic Far-Field Modeling, Chapter 10.B of European Course on Heat Disposal from Power Generation in the Water Environment. Delft Hydraulics Laboratory, Delft, The Netherlands, June 1975.
- Abramovich, G., N., (1963): The Theory of Turbulent Jets. The M.I.T. Press, M.I.T. Cambridge, Massachusetts, 1963.
- Ackers, P., (1969): Modeling of Heated-Water Discharges, Chapter 6 of Engineering Aspects of Thermal Pollution. Proc. of the National Symposium on Thermal Pollution, 1968, ed. by F.L. Parker and P.A. Krenkel, Vanderbilt University, Press 1969.
- Ackers, P., and Joffrey, L., J., (1973): The Applicability of Hydraulic Models to Pollution Studies. Paper 16 of Mathematical and Hydraulic Modelling of Estuarine Problems, Proceedings of Symposium held at the Water Pollution Research Laboratory 1972. Ed. by A.L.H. Gameson, London 1973.
- Adams, E., E., and Stolzenbach, K., D., (1975): Zone Models for the Near-Field: Surface Discharges. Chapt. 7 of European Course on Heat Disposal from Power Generation in the Water Environment. Delft Hydraulics Laboratory, Delft, The Netherlands, June 1975.
- Albertson, M., L., Dai, Y., B., Jensen, R., A., and Rouse, H., (1950): Diffusion of Submerged Jets. Transactions, ASCE, Vol. 115, 1950.
- Barr, D., I., H., (1967): Densimetric Exchange Flow in Rectangular Channels. *La Houille Blanche* No 6, 1967.
- Barry, R., E., and Hoffmann, D., P., (1972): Computer Model for Thermal Plume. *Journal of the Power Div. ASCE*, PO 1. (June 1972).
- Bergstrand, E.; Personal Communication. 1972-1977. Swedish Meteorological and Hydrological Institute.
- Borque, C., and Newman, B., G., (1960): Reattachment of a Two-Dimensional, Incompressible Jet to an Adjacent Flat Plate. *The Aeronautical Quarterly*, Vol. XI, August 1960.
- Brooks, N., H., (1960): Diffusion of Sewage Effluent in an Ocean Current. Proc. of First Intern. Conf. on Waste Disposal in the Marine Environment, Pergamon Press, 1960.

- Carter, H., H., (1969): A Preliminary Report on the Characteristics of a Heated Jet Discharged Horizontally into a Transverse Current. Part I Constant Depth. Technical Report No. 61. Chesapeake Bay Institute. The Johns Hopkins University, Baltimore, Md. (Nov. 1969).
- Carter, H., H., and Regier, R., (1974): The Three Dimensional Heated Surface Jet in a Cross Flow. Technical Report 88, Chesapeake Bay Institute, The John Hopkins University, Baltimore, Md. 1974.
- Cederwall, K., (1968): Hydraulics of Marine Waste Water Disposal. Report No. 42, Hydraulic Division, Chalmers Institute of Technology, Göteborg, Sweden, Jan. 1968.
- Csanady, G., T., (1973): Turbulent Diffusion in the Environment. D. Reidel Publishing Co., Dordrecht, Holland, 1973.
- Daily, J., W., and Harleman, D., R., F., (1966): Fluid Dynamics, Addison-Wesley Publishing Company, Inc., Reading, Massachusetts, U.S.A. 1966.
- Ditmars, J., D., (1971): Chapter 9: Temperature Distributions in the Far-Field Region. Partial Mixing. Engineering Aspects of Heat Disposal from Power Generation, (D.R.F. Harleman, Ed.), R.M. Parsons Laboratory for Water Resources and Hydrodynamics, Department of Civil Engineering, M.I.T., Cambridge, Massachusetts, June 1971.
- Dunn, W., E., Policastro, A., J., and Paddock, R., A., (1975): Surface Thermal Plumes: Evaluation of Mathematical Models for the Near and Complete Field. ANR/WR-75-3, Argonne National Laboratory, Argonne, Illinois, May 1975.
- Ehlin, U., (1974): Spread and Cooling of Cooling Water in Cooling Water. Effects on the Environment. National Swedish Environment Protection Board, Stockholm 1974:25 (in Swedish).
- Ellison, T., H., and Turner, I., S., (1959): Turbulent Entrainment in Stratified Flows, Journal of Fluid Mech., Vol. 6, part 3. Oct. 1959.
- Engelund, F., A., (1976): Hydraulics of Surface Buoyant Jet. ASCE Journal of the Hydraulics Divisions, Vol. 102, No. HY9, Sept. 1976.
- Engelund, F., A., and Pedersen, F., B., (1973): Surface Jet at Small Richardson Numbers. ASCE, Journal of the Hydraulics Division, Vol. 99. No. HY3, March 1973.
- Frazer, W., Barr, D., I., H., and Smith, A., A., (1968): A Hydraulic Model Study of Heat Dissipation at Longannet Power Station. Proc., Institute of Civil Engineering. 39. Jan. 1968.
- Grimås, U., (1974): Heat Effects in Different Levels of the Ecosystem in Cooling Water. Effects on the Environment. National Swedish Environment Protection Board. Stockholm 1974:25 (in Swedish).

- Hayashi, T., and Shuto, N., (1967): Diffusion of Warm Water Jets Discharged Horizontally at the Water Surface. Proceedings of the 12th Congress of the International Association for Hydraulics Research, Vol. 4, Colorado State University, Fort Collins, Colorado, Sept. 1967, pp 47-59.
- Hindley, P., D., Miner, R., M., and Cayot, R.F., (1971): Thermal Discharge. A Model-Prototype Comparison. Journal of the Power Division, ASCE, Vol. 97, No. PO4, Dec. 1971.
- Holley, E., R., and Abraham, G., (1973): Laboratory Studies on Transverse Mixing in Rivers, Journal of Hydraulic Research, Vol. 11, 1973, No. 3.
- Holley, E., R., and Karelse, M., (1974): Model-Prototype Comparisons for Transverse Mixing in Rivers. Delft Hydraulics Laboratory, Purbl. No. 116, March 1974.
- Hoopes, J., A., Zeller, R., W., and Rohlich, G., A., (1968): Heat Dissipation and Induced Circulations from Condenser Cooling Water Discharges into Lake Monona. Univ. of Wisconsin. Eng. Exp. Stations Report No. 35. Feb. 1968.
- Häggström, S., (1973): Scale Effects in Laboratory Models for Warm Water Discharge. Bulletin 72, Department of Hydraulics, Chalmers University of Technology. Göteborg 1973 (in Swedish).
- Kullenberg, G., (1974): An Experimental and Theoretical Investigation of the Turbulent Diffusion in the Upper Layer of the Sea. Univ. of Copenhagen, Inst. phys. oceanography, Rept. No. 25, Jan. 1974.
- Kuuskoski, M., (1974): Finnish Experiences of Cooling Water Discharges from Thermal Power Plants. Lecture held at the Symposium on Cooling Water Discharges. The Environmental Foundation of the Swedish State Power Board. Stockholm, dec. 1974.
- Larsen, I., and Sörensen, T., (1968): Buoyancy Spread of Waste Water in Coastal Regions. 11th Conference on Coastal Engineering, London, Sept. 1968.
- Mikhail, R., Chu, V., H., and Savage, S.B., (1975): The Reattachment of a Two-Dimensional Turbulent Jet in a Confined Cross Flow. Proc. Vol. 3, XVI IAHR Congress, Sao Paulo, Brazil, 1975.
- Milanov, T., (1969): Problems of Cooling in Receiving Bodies of Water at Discharges of Cooling Water, Swedish Meteorological and Hydrological Institute, Series Hydrology. No. 6, Stockholm, Sweden 1969, (in Swedish).

- Motz, L., H., and Benedict, B., H., (1970): Heated Surface Jet Discharged into a Flowing Ambient Stream. National Center for Research and Training in the Hydrologic and Hydraulics Aspects of Water Pollution Control, Report No. 4, Dep. of Environmental and Water Resources Engineering, Vanderbilt University, Northville, Tennessee, Aug. 1970.
- Neale, L., C., and Hecker, G., E., (1972): Model versus Field Data on Thermal Plumes from Power Stations. Paper 18 of International Symposium on Stratified Flows, IAHR, Novosibirsk, 1972.
- Niemeyer, I., A., (1969): Modelling of Power Plant Cooling Water Discharges into Lake Monona", M.S. Thesis, Department of Civil Engineering, University of Wisconsin. 1969.
- Nyman, L., (1974): Temperature Effects on Fishes in Cooling Water. Effects on the Environment. National Swedish Environment Protection Board Stockholm 1974:25.
- Odgaard, J., (1975): Parameter Sensitivity in the Estimation of Excess Temperatures in Natural Water Bodies. Paper C23, Proc. of the XVIth Congress of IAHR, Sao Paulo. 1975.
- Okoye, J., K., (1970): Characteristics of Transverse Mixing in Open-Channel Flows. Report No. KH-R-23, W.M. Keck Laboratory of Hydraulics and Water Resources, California Institute of Technology, Pasadena, California, 1970.
- Okubo, A., (1971): Oceanic Diffusion Diagrams, Deep-Sea Research, 1971, Vol. 18, pp 789-802.
- Okubo, A., and Ozmidov, R., V., (1970): Empirical Dependence of the Coefficient of Horizontal Turbulent Diffusion in the Ocean on the Scale of the Phenomenon in Question. Izv., Atmospheric and Oceanic Physics, Vol. 6, No. 5, 1970, pp 534-536.
- Ottesen Hansen, N.-E., (1973 a): Calculation of the Surface Buoyant Jet. Prog. Rep. 28, pp. 9-18. Institute of Hydrodynamics and Hydraulics Engineering. Technical University of Denmark, April 1973.
- Ottesen Hansen, N.-E., (1973 b): The Surface Jet in Shallow Water. Progr. Rep. 29, pp. 29-38. Institute of Hydrodynamics and Hydraulic Engineering. Technical University of Denmark. Aug. 1973.
- Ottesen Hansen, N.-E., (1975): Entrainment in Two-Layered Flows, Series Paper 7, Institute of Hydrodynamics and Hydraulic Engineering, Technical University of Denmark, 1975.
- Paily, P., P., Macagno, E., O., and Kennedy, J., F., (1974): Winter-Regime Surface Heat Loss from Heated Streams. IIHR, Report No. 155, Institute of Hydraulic Research, The University of Iowa, Iowa City, Iowa. March 1974.

- Pande, B., B., L., and Rajaratnam, N., (1975 a): A Similarity Analysis of Heated Surface Discharges into Quiescent Ambients. Report No. HY-1975-TPR1. Department of Civil Engineering. The University of Alberta. Edmonton, Canada, May 1975.
- Pande, B., B., L., and Rajaratnam, N., (1975 b): An Experimental Study of Heated Surface Discharges into Quiescent Ambients. Department of Civil Engineering. The University of Alberta, Edmonton, Canada. Sept. 1975.
- Pearce, A., F., (1966): Critical Reynolds Number for Fully-Developed Turbulence in Circular Submerged Water Jets, National Mechanical Engineering Res. Inst., Council for Scientific and Industrial Res., CSIR Report MEG 475, Pretoria, South Africa (1966).
- Prych, E., A., (1970): Effects of Density Difference on Lateral Mixing in Open-Channel Flows. W.M. Keck Lab. of Hyd. and Wat. Res. Report No. KH-R-21. Calif. Institute of Tech. Pasadena, California May 1970.
- Prych, E., A., (1972 a): A Warm Water Effluent Analyzed as a Buoyant Surface Jet, Swedish Meteorological and Hydrlogical Institute, Series Hydrology, No. 21, Stockholm, Sweden. 1972.
- Prych, E., A., (1972 b): An Analysis of a Jet into a Turbulent Ambient Fluid. Int. Council for the Exploration of the Sea, Symposium on the Physical Processes Responsible for the Dispersal of Pollutants in the Sea with Special References to the Near-Shore Zone, Aarhus, Denmark, May 1972.
- Rahm, L., and Häggström, S., (1976): Oskarshamn's Nuclear Power Plant. Model Studies of Cooling Water Spread at Future Expansion. Part I - Main Report. Part II- Appendices. Bulletin 86, Department of Hydraulics, Chalmers University of Technology, Gothenburg 1976. (in Swedish).
- Sawyer, R., A., (1963): Two-Dimensional Reattaching Jet Flows Including the Effects of Curvature on Entrainment. Journal of Fluid Mechanics. 17. (1963).
- Shirazi, M., (1973): Some Results for Experimental Data on Surface Jet Discharge of Heated Water, paper presented at the First World Conference on Water Resources, Chicago, Illinois (1973).
- Shirazi, M., and Davis, L., (1974): Workbook of Thermal Plume Prediction, Volume 2, Surface Discharge, Pacific Northwest Environmental Research Laboratory Report, EPA-R2-72-005 b, Corvallis, Ore. May 1974.
- Silberman, E., and Stefan, H., (1970): Physical (Hydraulic) Modeling of Heat Dispersion in Large Lakes. A Review of the State of the Art. Project Report No. 115, St. Anthony Falls Hydraulic Laboratory, University of Minnesota (1970).

- Stefan, H., and Schiebe, F., R., (1970): Heated Water Flow from Channels into Impoundments. Meeting Preprint 1135. ASCE National Water Resources Engineering Meeting, Memphis, Tenn. 1970.
- Stolzenbach, K., D., (1971), Chapter 1: Environmental Heat Transfer. Engineering Aspects of Heat Disposal from Power Generation, (D.R.F. Harleman, Ed.), R.M. Parsons Laboratory for Water Resources and Hydrodynamics, Dep. of Civil Eng., M.I.T., Cambridge, Massachusetts, June 1971.
- Stolzenbach, K., D., and Harleman, D., R., F., (1971 a): An Analytical and Experimental Investigation of Surface Discharges of Heated Water, Report 135, Ralph M. Parsons Lab. for Water Res. and Hyd., M.I.T., Feb. 1971.
- Stolzenbach, K., D., and Harleman, D., R., F., (1971 b): Physical Modeling of Heated Discharges, Chapter 6, Engineering Aspects of Heat Disposal from Power Generations, (D.R.F. Harleman, Ed.), R.M. Parsons Laboratory for Water Resources and Hydrodynamics, Department of Civil Engineering, M.I.T., Cambridge, Massachusetts, June 1971.
- Swedish State Power Board: (1971), Forsmark Power Plant. Spread of Cooling Water in the Öregrundsgrepen, Swedish State Power Board, The Hydraulics Laboratory, Älvkarleby, Sweden 1971. (in Swedish).
- Swedish State Power Board, (1972), Forsmark Nuclear Power Stations. Spread and Dilution of Cooling Water in the Near-Field Region. Swedish State Power Board. The Hydraulics Laboratory. Älvkarleby. Sweden. 1972. (in Swedish).
- Tamai, N., Wiegel, R., L., and Tornberg, G., F., (1969): Horizontal Surface Discharge of Warm Water Jets, Proc. ASCE Journal of the Power Div., Oct. 1969.
- Ungate, C., D., (1974): Temperature Reduction in a Submerged Vertical Jet in the Laminar-Turbulent Transition, M.S. Thesis, Department of Civil Engineering, M.I.T., Cambridge, Massachusetts (1974).
- Weil, J., G., (1974): Verification of Heated Water Jet Numerical Model, H B Report Nr 5, Swedish Meteorological and Hydrological Institute, Stockholm. 1974.
- Wiegel, R., L., Mobarek, I., and Jen, Y., (1964): Discharge of Warm Water Jet over Sloping Bottom, Hydraulic Engineering Lab., University of California, Berkeley, California, Report HGL 3-4, 1964.
- Wiegel, R., L., Mobarek, I., and Jen, Y., (1966): Discharge of Warm Water Jet over Sloping Bottom, Modern Trends in Hydraulic Engineering Research. Golden Jubilee Symposia. Vol. 2. Central Water and Power Research Station, Poona, India (1966).

Yevdjovich, V., M., (1966): Diffusion of Slot Jets with Finite Length-Width Ratios, Hydraulic Papers, Colorado State University, Ft. Collins, Colorado, No. 2, 1966.

LIST OF FIGURES

Page

Figure 1.1	Surface discharge of cooling water. Adapted from Ehlin (1974).	12
Figure 1.2	Spreading pattern of warm-water discharge. The lines shown are dye patterns at different times after marking the flow at the outlet. The flow and outlet are the same, and the densimetric Froude number is changed by different heating, and thus different buoyancy is received. From Hayashi and Shuto (1967).	13
Figure 2.1	Definition sketch of three-dimensional jet. The flow has a rotational symmetry. After Albertson <u>et al.</u> (1950).	26
Figure 2.2	Velocity and concentration decay along centre-line of a three-dimensional jet.	26
Figure 2.3	Centre-line velocity decrease for nonbuoyant jets with rectangular outlets, according to Stolzenbach and Harleman (1971 a) with experimental data from Yevdjovich (1966), where $1.0 \leq B_0/H_0 \leq 94$.	28
Figure 2.4	Velocity and concentration decay along centre-line of a two-dimensional jet.	35
Figure 2.5	Velocity and concentration decay along centreline of a two-dimensional jet.	36
Figure 2.6	Definition sketch of reattachment of a two-dimensional jet to an adjacent wall, adapted from Borque and Newman (1960).	37
Figure 2.7	Reattachment distance for a two-dimensional jet reattaching to an adjacent wall, adapted from Borque and Newman (1960). Variables are defined by Figure 2.6.	37
Figure 2.8	Definition sketch of reattachment of a two-dimensional jet caused by a crossflow, adapted from Mikhail <u>et al.</u> (1975).	38
Figure 2.9	Eddy height as defined by Figure 2.8 for a two-dimensional jet in a crossflow, adapted from Mikhail <u>et al.</u> (1975).	39
Figure 2.10	The two-dimensional flow of the prototype can change character in a distorted model with exaggerated slopes.	40
Figure 2.11	Definition sketch of vertical entrainment in stratified flow.	41
Figure 2.12	Entrainment coefficient as a function of $F_{\Delta}^2 = \frac{1}{Ri}$ from Ottesen Hansen (1975).	42

Figure 2.13	Definition sketch of unidirectional surface buoyant flow.	47
Figure 2.14	Definition sketch of lock exchange flow.	48
Figure 2.15	Spread of buoyant layer, with notation from Figure 2.14 after Frazer et al. (1968). The horizontal lines indicate a relationship $L_f/T_f = \text{constant} \cdot (H_f \cdot g(\rho_s - \rho)/\rho)^{1/2}$.	49
Figure 2.16	Flow separation can occur due to exaggerated slopes in distorted models.	57
Figure 2.17	Velocity distribution in prototype and in a distorted model, after Stolzenbach and Harleman (1971 b).	58
Figure 2.18	Dimensionless lateral mixing coefficient as a function of channel geometry (Okoye 1970).	61
Figure 2.19	Horizontal diffusion coefficient for large lakes and oceans as a function of scale of diffusion (Okubo 1971).	62
Figure 2.20	Definition sketch of the lateral diffusion problem solved by Brooks (1960) - plan view.	63
Figure 2.21	Temperature decay according to Equations (2.82), $K_y = K_{y0}$ and (2.84), $K_y = K_{y0} \cdot (b/b_0)^{4/3}$ (Brooks 1960).	65
Figure 2.22	Lateral plume spread according to Equations (2.83), $K_y = K_{y0}$, and (2.85), $K_y = K_{y0} (b/b_0)^{4/3}$ (Brooks 1960).	65
Figure 2.23	Rate of heat exchange between a water surface and the atmosphere.	73
Figure 4.1a-c	Effects of a distortion of two on areas within isotherms. Calculation made with the PSD model data. The corresponding effects according to nonbuoyant jet theory are also given.	96-98
Figure 4.2a-c	Effects of a distortion of two on centre-line excess temperature at given distances from discharge. Calculation made with the PSD model data. The corresponding effects according to Engelund's moderate Richardson number theory are also given.	99
Figure 4.3	Effects of distortion of two on thickness of warm-water flow. Calculation made with the PSD model data. The corresponding effects according to Engelund's moderate Richardson number theory are also given.	100

		163.
Figure 4.4	Effects of a distortion of two on areas within isotherms as a mean value of aspect ratios $A = 1/4-8$ for different isotherms. Calculation made with the Prych model. Nonbuoyant jet theory gives a corresponding number of 2.0.	102
Figure 4.5	Effects of a distortion of two on areas within isotherms as a mean value for the relative excess temperatures $T/T_o = 0.2-0.6$. Calculation made with the Prych model. Nonbuoyant jet theory gives a corresponding number of 2.0.	103
Figure 4.6	Effects of a distortion of two on centre-line excess temperature as a mean value of aspect ratios $A = 1/4-8$ at different distances from outlet. Calculation made with the Prych model. The effects according to Engelund's moderate Richardson number theory are also given.	104
Figure 4.7	Effects of a distortion of two on centre-line excess temperature as a mean value at distances $s/B = 20-120$ for different aspect ratios. Calculation made with the Prych model. The effects according to Engelund's moderate Richardson number theory are also given.	105
Figure 4.8	Effects of a distortion of two on thickness of warm-water flow as a mean value of aspect ratios $A = 1/4-8$ at different distances from outlet. Calculation made with the Prych model. The effects according to Engelund's moderate Richardson number theory are also given.	106
Figure 4.9	Effects of a distortion of two on thickness of warm-water flow as a mean value for distances of 20-120 times outlet width for different aspect ratios. Calculation made with the Prych model. The effects according to Engelund's moderate Richardson number theory are also given.	107
Figure 5.1	Centre-line excess temperature versus distance from outlet for $F_{\Delta} \approx 1.4$, $A=2.4$, and $F_{\Delta} = 1.42$, $A=0.46$ comparable to a distortion of 5. Data from Stolzenbach and Harleman (1971 a).	112
Figure 5.2	Centre-line excess temperature versus distance from outlet for $F_{\Delta} = 4.4$, 5.22, 6.53, and 6.60, and $A = 5.80$, 2.30, 1.56, and 0.51, respectively. Data from Stolzenbach and Harleman (1971 a).	113
Figure 5.3	Centre-line excess temperature versus distance from outlet for $F_{\Delta} = 9.90$, 9.66 and 11.34 and $A = 1.94$, 0.974 and 0.396 respectively, with relative ambient velocity $R \approx 0.3$. Data from Carter and Regier (1974).	115

Figure 5.4	Centre-line excess temperature versus distance from outlet for $F = 22-28$ and $A = 2.5$ and 10 . Data from Wiegel <u>et al.</u> (1964).	117
Figure 6.1	Temperature distribution at Hongkong Harbour according to the prototype and the model measurements. Observe the different reproduction in the model of the two discharges. Adapted from Ackers (1969).	119
Figure 6.2	Temperature survey at Berkeley Power Station. Comparison of prototype and model results. Adapted from Ackers (1969).	121
Figure 6.3	Comparison of model and prototype measurements with the temperature rise in $^{\circ}\text{F}$ above background. Temperature measured at a depth of 1.2 m. a) High water, b) Low water. Adapted from Ackers (1969).	124
Figure 6.4	Model-prototype comparison of areas within isotherms for discharge from Pacific Gas and Electric Company's Pittsburg Power Plant. Adapted from Hindley <u>et al.</u> (1971).	127
Figure 6.5	Bottom topography and arrangement of cooling-water structures of power plant A. Adapted from Neale and Hecker (1972).	129
Figure 6.6	Comparison of average tidal temperature rise ($^{\circ}\text{F}$)-plant A. Adapted from Neale and Hecker (1972).	130
Figure 6.7	Model (Δo) and prototype (x) comparison of centre-line velocity. The straight lines are fitted to data by the method of least squares.	134
Figure 6.8	Comparison of model and prototype measurements of surface temperatures. Ingå Power Plant (Finland). Adapted from Kuuskoski (1974).	136
Figure 6.9	Comparison of model (o) and prototype (x) measurements of areas within isotherms for NE and SW ambient currents. The straight lines are fitted to data by the method of least squares.	139
Figure 6.10	Model and prototype measurements of surface temperatures for a discharge of $50 \text{ m}^3/\text{s}$. Oskarshamn Nuclear Power Plant.	140
Figure 7.1	Model-prototype comparison of areas within isotherms for different discharges as calculated by the Prych model. Adapted from Rahm and Haggström (1976).	149
Figure 7.2	Excess temperature T/T_o as measured in model and after transformation into prototype conditions for a discharge of $130 \text{ m}^3/\text{s}$.	151

LIST OF TABLES

2.1	Summary of effects of distortion on a nonbuoyant surface jet	33
2.2	Summary of effects of distortion on vertical entrainment	46
3.1	Analytical solutions of warm-water flow problems	79
4.1	Effects of a distortion of two calculated by means of theoretical models	108
5.1	Laboratory investigations used for determination of effects of distortion	110
5.2	Effects of a distortion of two on centre-line excess temperature T/T_o	118
6.1	Model-prototype comparison of areas within isotherms, Dublin Harbour.	125
6.2	Model-prototype comparison of areas within isotherms, Pittsburg Power Plant	128
6.3	Comparison of average tidal temperature rise ($^{\circ}\text{F}$)-plant A, US East Coast	131
6.4	Model-prototype comparisons of centre-line velocity, Lake Monona	133

LIST OF NOTATION

A	(= B_o/H_o) aspect ratio of outlet
A_{c/c_o}	area limited by the isoconcentration line for c/c_o (for two- and three-dimensional jets)
B	width of warm-water flow
B_o	width of outlet (slot)
B_c	width of crossflow for reattaching two-dimensional jet
B_c	width of warm-water flow at control section
b	width of plume
b_o	width of line source
C	Bowen's constant
C_{1-15}	unknown constants
c	local concentration of tracer or discharged fluid
c	index indicating property of control section
\bar{c}	(= $\int_{-\infty}^{\infty} \int_{-\infty}^{\infty} c \, dx \, dy$) concentration integrated over the horizontal plane
c_{1-2}	unknown constants
c_m	concentration on centreline of jet
c_o	concentration at outlet
c_p	specific heat of water
D	constant, vertical, characteristic length
D_a	distance from slot to adjacent wall for two-dimensional jet
$D_{\text{equivalent}}$	diameter of a circle having the same area as a rectangular outlet
D_o	outlet diameter for jet
d	water depth of prismatic channel
d_1	local water depth
E	volumetric evaporation rate per unit area
e	entrainment factor
e_a	vapour pressure of air

168.

e_{az}	air vapour pressure at level z above water surface
e_o	entrainment factor corresponding to $Ri = 1$
e_s	saturation vapour pressure corresponding to water surface temperature T_s
F	$(= \frac{u}{\sqrt{gh}})$ Froude number
F_M	Froude number in model
F_P	Froude number in prototype
F_Δ	$(= \frac{u}{g \frac{\Delta\rho}{\rho} h})$ Froude densimetric number
$F_{\Delta M}$	Froude densimetric number in model
$F_{\Delta P}$	Froude densimetric number in prototype
f	friction factor
g	gravitational acceleration
H	thickness of warm water flow
H_a	heat content above some datum of undisturbed ambient fluid
H_f	water depth of channel for lock exchange flow
H_i	eddy height for two-dimensional jet
H_o	height of rectangular outlet
H_t	heat content above some datum
h	water depth or height of upper layer for stratified flow
h	index indicating horizontal property
K	heat exchange coefficient
K^x	$(= \frac{K}{\rho c_p u_o})$ dimensionless heat exchange coefficient
$K_{x, y, z}$	eddy diffusion coefficient in $x, y,$ and z -directions, respectively
k	equivalent sand roughness
L	constant representative length (can be restricted to horizontal length)
$L(T)$	latent heat of vapourization
L_f	travelling distance for buoyant front in lock exchange flow

l	dimension of plume or marked cloud
M	index indicating model property
N	evaporation coefficient (can be a function of wind velocity)
P	index indicating prototype property
p_a	air pressure (in mb)
q	volume flux (for two-dimensional jet volume flux per unit height)
q_c	volume flux at control section
q_o	volume flux of discharge
R	($= \frac{V}{u_o}$) relative ambient velocity
R	Bowen's ratio
Re	($= \frac{u \cdot D}{\nu}$ or $= \frac{U \cdot 4 R_h}{\nu}$) Reynolds number
Re_{cr}	critical Reynolds number
R_h	hydraulic radius
Ri	($= \frac{g \cdot \Delta \rho / \rho \cdot h}{U^2}$) gross Richardson number
r	coordinate perpendicular to centre-line of three-dimensional jet
r	index indicating model-to-prototype ratio of parameter
S	bottom or head slope
S_f	friction slope
s	coordinate along centre-line of jet
s	index indicating surface property
T	excess temperature
T_{air}	air temperature
T_f	time coordinate for buoyant front in lock exchange flow
T_m	centre-line excess temperature
T_o	outlet excess temperature
T_s	temperature at water surface
t	time coordinate

170.

U	constant representative velocity
\bar{U}	mean velocity of section or upper layer of stratified flow
U_f	front velocity for buoyancy spread
u	local velocity (often in x- or s-direction)
u_m	velocity at centreline of jet
u_o	outlet velocity
u_s	velocity at water surface
u_x	($= \sqrt{gdD}$) shear velocity
V	crossflow or ambient velocity
V_{az}	wind velocity at level z above water surface
v	velocity in y-direction
v	index indicating vertical property
W	constant representative vertical velocity
w	velocity in z-direction
x	horizontal Cartesian coordinate
x_R	reattachment distance for two-dimensional jet
y	horizontal Cartesian coordinate or coordinate perpendicular to jet axis for two-dimensional jet
Z_P	depth to a given fraction of surface velocity or excess temperature
z	Cartesian coordinate directed vertically upwards
α	entrainment coefficient
$\alpha_{1, 2, 3}$	constants
λ	geometric length scale (model length/prototype length)
λ_h	horizontal length scale
λ_v	vertical length scale
η	dynamic viscosity
ν	kinematic viscosity
ρ	density

$\Delta\rho$	density deficit compared to ambient water density
$\overline{\Delta\rho}$	mean density deficit of upper layer of stratified flow
σ	variance of temperature or concentration distribution
σ	Stefan-Boltzmann's constant
ϕ^x	net heat loss to the atmosphere
ϕ_{ba}	atmospheric long wave radiation
ϕ_{br}	reflected long wave radiation
ϕ_{bw}	long wave radiation emitted by water surface
ϕ_E	heat loss due to evaporation
ϕ_H	heat loss due to conduction
ϕ_{ri}	infalling short wave radiation
ϕ_{rr}	reflected short wave radiation

Institutionen för Vattenbyggnad
CHALMERS TEKNISKA HÖGSKOLA

Meddelanden

78. Cederwall, K.: Havet som recipient. Hydrodynamiska synpunkter.
Föredrag vid Sv. Havsforskningsföreningens årsmöte i Stockholm, mars 1975.
79. Sellgren, A.: Hydraulisk transport av fasta material i rör. 1975.
80. Andreasson, L. och Cederwall, K.: Rubbningar av grundvattenbalansen i urbana områden.
Hydrologisk konferens, Sarpsborg, 1975.
81. Cederwall, K.: Bräddning av avloppsvatten och effekten av utjämningsbassänger. "Världen, Vattnet och vi", Elmia 1975.
82. Cederwall, K.: Gross Parameter Solutions of Jets and Plumes. ASCE, HY5, May 1975.
83. Larsson, Sören och Lindquist, Per: Kalkning av försurade sjöar. Del I: Problembeskrivning samt utvärdering av kalkningen av Östra Nedsjön. Ex.arb. 1974:5.
84. Cederwall, K. och Svensson, T.: "Sediment flusing after dredging in tidal bays". 1975.
85. Göransson, C-G. och Svensson, T.: Strömkorsmätningar. Datorprogram för utvärdering inkl. korrektion för avdrift. Mars 1976.
86. Rahm, L. och Häggström, S.: Oskarshamns Kärnkraftverk. Modellstudier avseende kylvattenspridning vid framtida utbyggnad. Maj 1976. Del I Huvudrapport. Del II Bilagedel.
87. Sjöberg, A.: Beräkning av icke stationära flödesförlopp i reglerade vattendrag och dagvattensystem. Aug. 1976.

Slut på Meddelande-serien.